AD-A086 482 DAVID W TAYLOR NAVAL SHIP RESEARCH AND DEVELOPMENT CE--ETC F/G 20/4
VIBRATIONS OF A MARINE PROPELLER OPERATING IN A NONUNIFORM INFL--ETC(U)
APR 80 J E BROOKS
UNCLASSIFIED DTNSRDC-80/056 NL

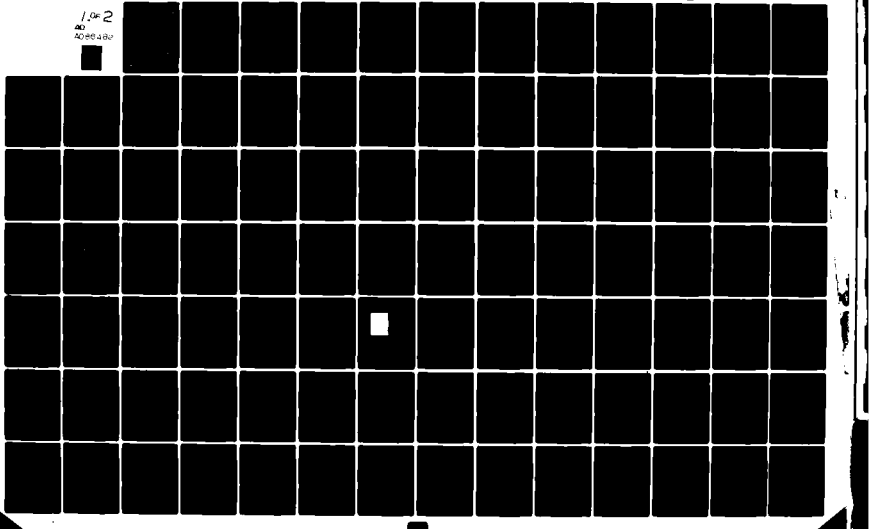

DAVID W. TAYLOR NAVAL SHIP RESEARCH AND DEVELOPMENT CENTER

Bethesda, Maryland 20084

VIBRATIONS OF A MARINE PROPELLER OPERATING IN A NONUNIFORM INFLOW

by

James Emmert Brooks

APPROVED FOR PUBLIC RELEASE: DISTRIBUTION UNLIMITED

Reprint of Dissertation Submitted to the Faculty of The School of Engineering and Architecture of the Catholic University of America

SHIP ACOUSTICS DEPARTMENT
RESEARCH AND DEVELOPMENT REPORT

April 1980

DTNSRDC-80/056

MAJOR DTNSRDC ORGANIZATIONAL COMPONENTS

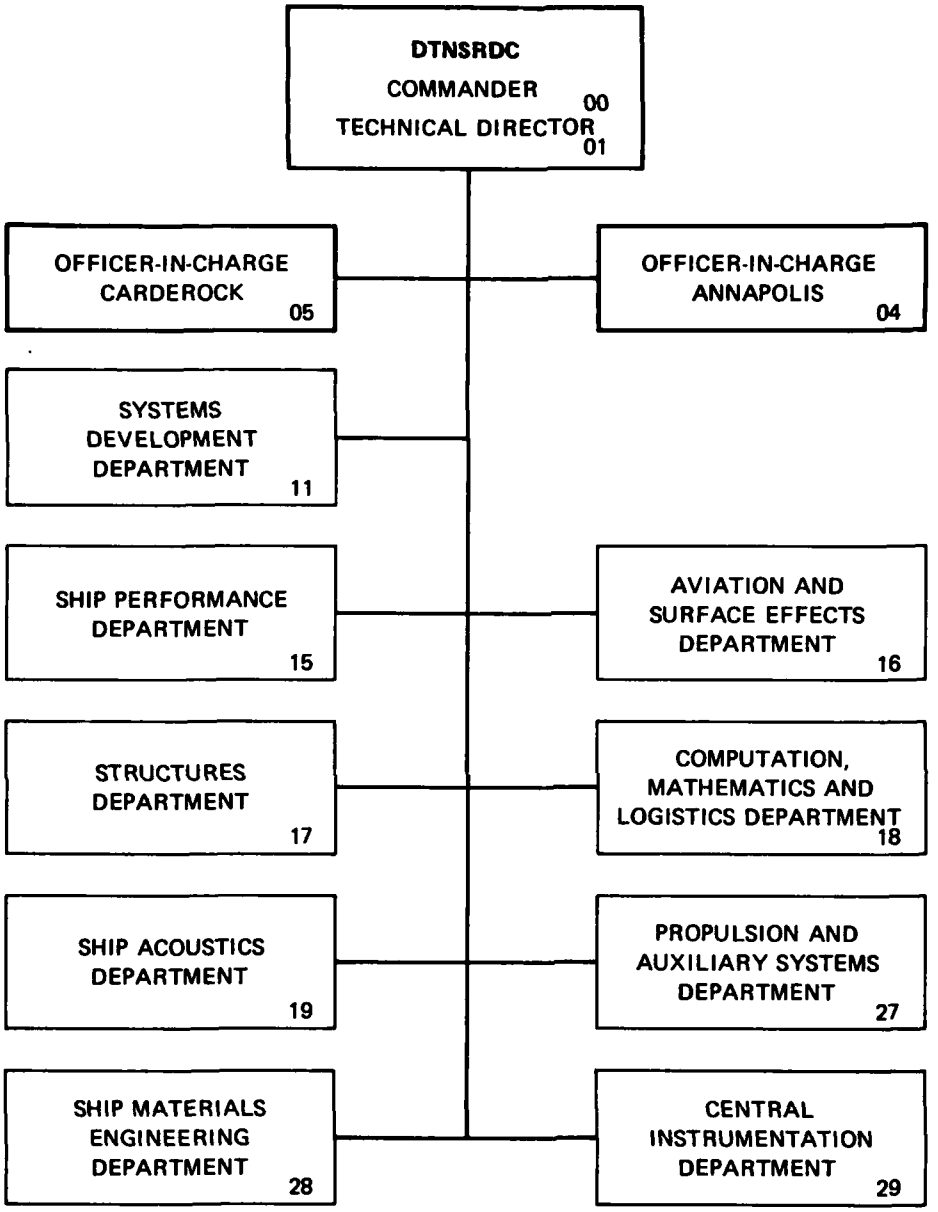

UNCLASSIFIED

SECURITY CLASSIFICATION OF THIS PAGE (When Data Entered)

REPORT DOCUMENTATION PAGE

READ INSTRUCTIONS BEFORE COMPLETING FORM

1. REPORT NUMBER: DTNSRDC-80/056	2. GOVT ACCESSION NO.: AD-A086482
3. RECIPIENT'S CATALOG NUMBER:	
4. TITLE (and Subtitle): VIBRATIONS OF A MARINE PROPELLER OPERATING IN A NONUNIFORM INFLOW	5. TYPE OF REPORT & PERIOD COVERED: Formal
	6. PERFORMING ORG. REPORT NUMBER:
7. AUTHOR(s): James Emmert Brooks	8. CONTRACT OR GRANT NUMBER(s):
9. PERFORMING ORGANIZATION NAME AND ADDRESS: David W. Taylor Naval Ship Research and Development Center, Bethesda, Maryland 20084	10. PROGRAM ELEMENT, PROJECT, TASK AREA & WORK UNIT NUMBERS: Task Area SF43452702, Work Units 1960-010 and 1960-020
11. CONTROLLING OFFICE NAME AND ADDRESS: F43452	12. REPORT DATE: April 1980
	13. NUMBER OF PAGES: 139
14. MONITORING AGENCY NAME & ADDRESS (if different from Controlling Office): Naval Sea Systems Command, Washington, D.C. 20360	15. SECURITY CLASS. (of this report): UNCLASSIFIED
	15a. DECLASSIFICATION/DOWNGRADING SCHEDULE:

16. DISTRIBUTION STATEMENT (of this Report)

APPROVED FOR PUBLIC RELEASE: DISTRIBUTION UNLIMITED

17. DISTRIBUTION STATEMENT (of the abstract entered in Block 20, if different from Report)

18. SUPPLEMENTARY NOTES

research and development report

19. KEY WORDS (Continue on reverse side if necessary and identify by block number)

Propeller	Blade Vibrations
Marine Propeller	Unsteady Flow
Nonuniform Inflow	Water Tunnel
Vibrations	Unsteady Lifting Surface Theory

20. ABSTRACT (Continue on reverse side if necessary and identify by block number)

The effect of blade vibration on the unsteady forces developed by an elastic marine propeller is investigated for a controlled laboratory situation. The study involves the development of a theory for a flexible propeller operating in a spatially nonuniform inflow velocity field and a series of experimental tests. Measurements of unsteady propeller forces in a 24-inch water tunnel are presented for two model propellers whose fundamental resonance frequencies are excited by a nonuniform

(Continued on reverse side)

DD FORM 1 JAN 73 1473 EDITION OF 1 NOV 65 IS OBSOLETE S/N 0102-LF-014-6601

UNCLASSIFIED

SECURITY CLASSIFICATION OF THIS PAGE (When Data Entered)

391682

(Block 20 continued)

inflow field. Measured unsteady thrust and torque, presented as a function of excitation frequency, show distinctly different elastic effects--one propeller demonstrates a large force amplification near its resonance frequency while the other did not. The simple theoretical model explains the difference as being due to differing amounts of induced hydrodynamic damping; there is a large hydrodynamic damping in one case and a small amount in the other case. Another result of the study is that blade vibration can significantly reduce the unsteady forces transmitted to the propeller shaft over a certain range of excitation frequencies. Calculated forces are in general agreement with the experimental measurements.

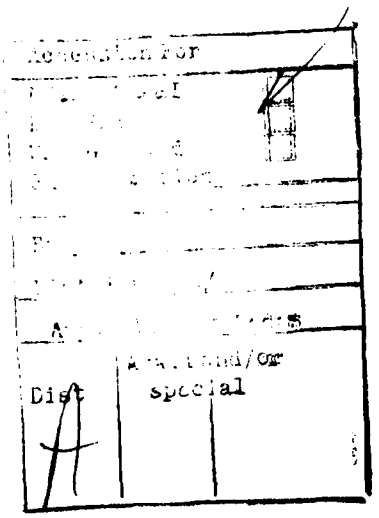

TABLE OF CONTENTS

LIST OF FIGURES

LIST OF TABLES

ABSTRACT

The effect of blade vibration on the unsteady forces developed by an elastic marine propeller is investigated for a controlled laboratory situation. The study involves the development of a theory for a flexible propeller operating in a spatially non-uniform inflow velocity field and a series of experimental tests. Measurements of unsteady propeller forces in a 24-inch water tunnel are presented for two model propellers whose fundamental resonance frequencies are excited by a non-uniform inflow field. Measured unsteady thrust and torque, presented as a function of excitation frequency, show distinctly different elastic effects--one propeller demonstrates a large force amplification near its resonance frequency while the other did not. The simple theoretical model explains the difference as being due to differing amounts of induced hydrodynamic damping; there is a large hydrodynamic damping in one case and a small amount in the other case. Another result of the study is that blade vibration can significantly reduce the unsteady forces transmitted to the propeller shaft over a certain range of excitation frequencies. Calculated forces are in general agreement with the experimental measurements.

ADMINISTRATIVE INFORMATION

The investigation presented in this report was initiated under the Independent Research Program and completed under funding from the Naval Sea Systems Command (05H) under Task Area SF 43452702, Task 18185, Work Units 1960-010 and 1960-020.

ACKNOWLEDGMENT

I would like to thank Dr. Murray Strasberg for his assistance throughout the formulation, execution and documentation of this work.

INTRODUCTION

The study of the unsteady forces developed by a marine propeller as it operates and interacts with a nonuniform inflow velocity field, has given us an enormous body of research over the past fifty years or so (for example, references 1-6).* For the most part, the recent, more sophisticated theories agree with the existing, albeit small, set of reliable experimental measurements. Almost all of the studies, however, assume that the blades do not respond elastically to the fluctuating pressure field. The assumption is valid provided the excitation frequency is much below the propeller's fundamental resonance frequency, but it is certainly not true at or near resonance. It is the nature of the resulting unsteady forces near blade resonance that is the subject of the present study.

One of the early researchers in this area was Sears [2]. He applied a two-dimensional unsteady wing theory, developed by von Karman and Sears [7], to the problem of a fan operating in a nonuniform inflow. The frequency of loading was such as to excite the fundamental torsional mode on each blade. In addition to providing a forcing mechanism, he showed that the fluid adds damping to the response and adds "mass" to the blades.

A more recent study of a marine propeller by Tsushima [8], using the complicated three-dimensional lifting theory developed by Tsakonas and company [4] and the water tunnel facilities at the now Applied Research Laboratory of the Pennsylvania State University, showed the potentially pernicious effect of resonant blade vibration on propeller forces. The

---

A complete listing of references is given on page 125.

propeller was excited into vibration by operating it in a nonuniform inflow. For loading frequencies near the blade's fundamental resonance frequency, the propeller developed significantly larger forces than if the blades were perfectly rigid. He successfully predicted the propeller's resonance frequency in water, and he had some success in predicting the peak magnitude of the unsteady force produced by the blade vibration.

Tsushima's study, however, was limited to one type of propeller geometry, and he studied the propeller's forced response only over a limited range of exciting frequencies about the propeller's fundamental resonance frequency. He also left the impression that blade vibration near resonance is a condition which should be avoided.

In this report we present a separate, more extensive study of the effect of blade vibration on unsteady propeller forces. We explore the effect blade width can have on the vibration by considering propellers with two different blade geometries, one with narrow blades and one with wide blades, and measure the unsteady forces and moments transmitted to the propeller shaft over a wide range of exciting frequencies, including a range beyond the resonance frequency of each. We show that radically different responses are possible for the two geometries, and that blade vibration can in some instances actually reduce the unsteady propeller forces. This result is significantly different from that obtained by Tsushima.

In the following sections we describe a general theory for propeller-blade vibration and summarize a computational scheme for calculating blade vibration amplitudes and propeller forces. We also report the results of a series of experimental tests designed to measure the effect of blade vibrations on unsteady propeller forces and moments. And, finally, we compare calculations with experiment.

THEORY FOR BLADE VIBRATION AND RESULTING PROPELLER FORCES

As a marine propeller moves through a nonuniform fluid velocity field, it develops an unsteady pressure distribution on its blade surfaces. Since the blades are not rigid their surfaces respond by vibrating, thereby inducing a pressure distribution that can be quite different than the one produced by a rigid propeller. Whether or not this elastic effect is significant in contributing to ship vibrations or propeller fatigue depends on the magnitude of the induced blade motion which, in turn, is controlled by the fluid inflow conditions and the elastic characteristics of the blade.

We focus attention on an elastic propeller operating in a spatially nonuniform flow field where the resulting blade vibration is steady. The analysis could also be adapted to other steady state vibration situations such as the case of an elastic propeller operating in close proximity to a rudder or other ship appendage, where steady blade oscillations are produced through an interference effect. Excluded from the analysis is the often important situation of the transient vibration brought about by a ship executing a sudden turn or change in shaft speed.

The blade-vibration theory described below assumes that a great deal is known already about the propeller. We assume the pressure distribution is known on each blade surface and that the pressure is the sum of the induced pressure caused by blade vibration only and that caused by rigid blades in the absence of blade vibration. We also assume that a propeller blade's in-air mode shapes and resonance frequencies are known and,

moreover, are the same for each blade. Later we will describe a procedure for calculating the pressure distribution and a technique for measuring the blade's mode shapes and resonance frequencies.

The general theory developed here accounts for the contributions from all the vibrational modes. In the last section we give approximations for the resulting propeller forces when the fundamental mode is the dominant contributor to the vibration of the blades.

KINEMATICS OF BLADE AND FLUID MOTION

It is convenient to measure the blade motion from a nonoscillating surface which rotates and advances with the propeller. The time-averaged (averaged over one blade oscillation) mid-surface of the blade is taken for this purpose. This surface is identical to the mid-surface of a rigid propeller blade provided there is no static elastic deformation of the blades, as we will assume in this study. If the ship advances with steady velocity $\vec{V}_a$ and the propeller rotates with steady angular velocity $\vec{\Omega}$, then a point on this reference surface, located a vector distance $\vec{S}$ from the center of the propeller hub, has velocity $\vec{V}_a + \vec{\Omega} \times \vec{S}$, when measured from a fixed inertial frame. The vector vibration displacement of a point on the mid-surface is taken as $\vec{d}(\vec{S},t)$, and the instantaneous velocity of that point at time t is then

$$\vec{V}_a + \vec{\Omega} \times \vec{S} + \frac{\delta \vec{d}}{\delta t} \tag{1}$$

where $\delta/\delta t$ denotes time differentiation in an advancing and rotating coordinate system fixed to the reference surface; and $\vec{d}$ is reckoned positive when the displacement has an axial component directed towards the ship.

We assume that the oscillatory motion of the blade's mid-surface can be written as a superposition of its in vacuo or in-air (and not rotating) normal modes,

$$\vec{d}(\vec{S},t) = \Sigma\, q_i(t)\, \psi_i(\vec{S})\, \hat{\delta}_i(\vec{S}), \tag{2}$$

where $q_i(t)$ is a set of normal displacement amplitudes which measures the amount mode i is excited, $\psi_i(\vec{S})$ is a set of modal patterns and $\hat{\delta}_i(\vec{S})$ is a unit vector giving the local direction of motion for mode i at point $\vec{S}$. And for each modal pattern ψ_i there is a characteristic in-air resonance frequency of vibration $\omega_{a,i}$.

For most propellers the modal pattern for the fundamental or lowest characteristic frequency probably resembles a one-noded cantilever mode with some twisting motion--i.e., its modal displacement is almost zero near the hub, increases radially towards the tip, and is nonuniform along a chord of constant radius. The next mode would probably resemble a two-noded cantilever mode or a one-noded twisting mode, depending on the width-to-length ratio of the blade.

The modes are orthogonal to one another and are taken to be normalized as

$$\rho_B \iiint \psi_i \psi_j\, (\hat{\delta}_i \cdot \hat{\delta}_j)\, dV = \begin{cases} M_B & i=j \\ 0 & i \neq j \end{cases} \tag{3a}$$

where

$$M_B = \rho_B \iiint dV \tag{3b}$$

and where dV is a local differential element of blade volume, the blade is of homogeneous density ρ_B, and the modal patterns are normalized by the blade's total mass M_B .

Take $\vec{u}$ as the time-independent fluid velocity which would be at the propeller disk if the propeller were removed and the ship were constrained to maintain its advance speed. This velocity is made up of two parts: a part $\vec{u}_o$ which is spatially uniform or at most a function of radial position, and a part $\vec{u}_m$ which is a function of both radial position r and angular position φ. By the rules of Fourier Series we can decompose $\vec{u}_m$ into an infinite summation of circumferential wake harmonics m,

$$\vec{u}_m(r,\varphi) = \sum_{m=1}^{\infty} \vec{u}_m(r) \cos [m\varphi + \epsilon_m(r)] \tag{4}$$

where ϵ_m is the phase angle for the m(th) harmonic of the inflow. This decomposition is important since it allows us, because of the assumption of linearity which follows, to examine the effect of one wake harmonic at a time. And therefore we can consider only one circumferential harmonic m to be present in the inflow.

The additional velocity induced by the presence and motion of the elastic propeller is denoted by $\vec{v}$. Then the velocity of a fluid particle is $\vec{u} + \vec{v}$ relative to a fixed inertial frame and $\vec{u} + \vec{v} - \vec{V}_a - \vec{\Omega} \times \vec{S}$ relative to a frame fixed to the blade's reference surface.

The component of fluid velocity normal to the blade's surface is equal to the normal component of blade velocity. If $\vec{n}'_{inst}(\vec{S}',t)$ is an instantaneous outward normal at a point $\vec{S}'$ on the blade's surface, then this condition at the boundary is expressed as

$$\vec{n}'_{inst} \cdot (\vec{u} + \vec{v} - \vec{V}_a - \vec{\Omega} \times \vec{S}' - \dot{\vec{d}}) = 0 \tag{5a}$$

where the dot over the displacement vector is shorthand notation for $\delta/\delta t$. Consider only one modal component, then the boundary condition is linearized by first approximating the instantaneous surface normal by

$$\vec{n}'_{inst}(\vec{S}',t) \simeq \hat{n}'(\vec{S}') - q_i(t)\, \nabla_{tan}\psi_i(\hat{n}'\cdot\hat{\delta}_i) \qquad (6)$$

$$+ q_i(t)\, \hat{n}'\, \nabla_{tan}\cdot(\psi_i\hat{\delta}_i)$$

where $\hat{n}'$ is the time-averaged unit surface normal (or unit normal for a rigid blade) at point $\vec{S}'$ and ∇_{tan} stands for the tangential gradient taken along the reference surface (see Appendix A for a detailed derivation of equation (6)). The first gradient term in expression (6) gives a gradient contribution to the instantaneous normal vector from the normal component of displacement and the second gradient term gives the contribution from the tangential displacement.

Now replace the surface normal in the boundary condition by this approximation. Expanding and retaining only those terms which are at least linear in q_i we get a linearized boundary condition

$$\hat{n}'\cdot\vec{v} \simeq \hat{n}'\cdot(\vec{V}_a + \vec{\Omega}\times\vec{S}' - \vec{u}) + \dot{q}_i\psi_i(\hat{n}'\cdot\hat{\delta}_i)$$

$$- q_i\,(\vec{V}_a + \vec{\Omega}\times\vec{S}' - \vec{u})\cdot\left[\nabla_{tan}\,\psi_i(\hat{n}'\cdot\hat{\delta}_i) - \hat{n}'\,\nabla_{tan}\cdot(\psi_i\hat{\delta}_i)\right] \qquad (5b)$$

We now separate the fluid velocity $\vec{v}$ into a velocity $\vec{v}_R$, which is induced by a propeller with no blade vibration, and an additional velocity $\vec{v}_V$ induced by the vibrating blades. Consistent with the linearized boundary condition of equation (5b) we assume

$$\vec{v} = \vec{v}_R + \vec{v}_V \qquad (7)$$

with boundary conditions

$$\hat{n}' \cdot \vec{v}_R = \hat{n}' \cdot (\vec{V}_a + \vec{\Omega} \times \vec{S}' - \vec{u}_o - \vec{u}_m) \tag{8}$$

and (assuming small spatial variations so that $|\vec{u}_m|$ is small compared with $|\vec{V}_a + \vec{\Omega} \times \vec{S}' - \vec{u}_o|$)

$$\hat{n}' \cdot \vec{v}_V = \dot{q}_i \psi_i \, (\hat{n}' \cdot \hat{\delta}_i) - q_i \, (\vec{V}_a + \vec{\Omega} \times \vec{S}' - \vec{u}_o) \cdot \nabla_{tan} \, \psi_i \, (\hat{n}' \cdot \hat{\delta}_i)$$

$$+ q_i \, (\vec{V}_a + \vec{\Omega} \times \vec{S}' - \vec{u}_o) \cdot \hat{n}' \, \nabla_{tan} \, (\psi_i \hat{\delta}_i) \tag{9}$$

The assumption leading to equations (7-9) allows the total induced fluid velocity to be considered as a sum of the induced velocities resulting from two independent propeller problems. The first is the standard problem of a rigid propeller operating in a spatially nonuniform fluid velocity field. The $(\vec{V}_a + \vec{\Omega} \times \vec{S}' - \vec{u}_o) \, \hat{n}'$ portion of the normal fluid velocity is steady in time and results in a steady thrust and torque on the propeller. (This steady portion is suppressed in the subsequent analysis since we are mainly interested in time-dependent velocities and pressures.) The $\hat{n}' \cdot \vec{u}_m$ portion is time varying (in a coordinate system fixed to the blades) and results in unsteady forces and moments on the blade.

The second problem is that of an elastic propeller, operating in a fluid velocity field with no circumferential variations (i.e., $\vec{u}_m = 0$), whose surface is constrained to vibrate with a prescribed pattern and amplitude. It has the alternative interpretation of a rigid propeller operating in a flow field which is both time varying and spatially nonuniform; the variations being exactly those that give the boundary condition of equation (9). Also, with some slight rearrangement of terms, equation (9)

can be reinterpreted as a rigid propeller operating in a particular time independent, spatially nonuniform flow field; so that a solution scheme which solves problems of the type given in equation (8) could be used to give solutions to the boundary conditions posed in equation (9).

EQUILIBRIUM EQUATION OF BLADE MOTION

We make several assumptions about the equilibrium state of the vibrating propeller blade and its surrounding fluid. We ignore the blade's rotational acceleration compared to its local acceleration.* The fluid is idealized as being inviscid and of constant density ρ, and is assumed to be irrotational except on propeller surfaces and on infinitesimally thick regions of fluid vorticity which trails each of the blades. Energy losses by structural damping (and boundary layer shear stresses) are neglected compared to the energy lost by the blades shedding fluid vorticity. We will show later that the losses due to structural damping are small enough to be neglected compared to the losses due to hydrodynamically induced damping.

Using the orthogonality properties of the modes, the normal coordinate q_i obeys the equation of motion of a simple, forced oscillator

$$M_B \left(\ddot{q}_i + \omega_{a,i}^2 q_i\right) = -\iint d\sigma' \; p\psi_i \; \hat{n}'\cdot\hat{\delta}_i \tag{10}$$

where $\omega_{a,i}$ is the circular resonance frequency, in air, for mode i, $\ddot{q}_i$ is the acceleration amplitude of the mode relative to a coordinate system

*The centrifugal force makes the blades behave stiffer than when they are not rotating. This increases the fundamental frequency in air from $\omega_{a,1}^2$ to approximately $\sqrt{\omega_{a,1}^2+\Omega^2}$ [9], less than a 0.5 percent change for the propellers tested in this study.

fixed to the reference surface, p is the local surface pressure due to water loading, $d\sigma'$ is an element of surface area with outward normal $\hat{n}'_i$, and the integration extends over both the forward and rear faces of a single blade. Note that we need only specify the component of the modal pattern normal to the surface of the blade.

The surface pressure is set up by the circumferentially varying inflow $\vec{u}_m$ buffeting the propeller blade. This results in a time-dependent pressure, even though the inflow itself is not time dependent. Because of the assumption of linearity, each wake harmonic m of the inflow results in an independent surface pressure which has a frequency of loading $\omega = m\Omega$. The total pressure field is determined by adding contributions from all wake harmonics.

Expression (10) is the motion equation for a single blade; to get the vibration on all blades, we need to see how blade motion on one blade is related to that on another. For vibration with single frequency $\omega = m\Omega$ produced by the interaction of the propeller with a single wake harmonic, the surface pressure on blade k, at position $\vec{S}_k$ and time t, is the same as that on blade 1 earlier when it occupied the position of blade k, i.e.,

$$p\ (\vec{S}_k, t) = p\ (\vec{S}_1, t-\Delta t) \tag{11a}$$

$$\Delta t = \frac{2\pi}{\Omega} \frac{k-1}{N_B}$$

where N_B is the total number of propeller blades. Moreover, if the pressure on blade 1 is of the form

$$p\ (\vec{S}_1, t) = p_o\ (\vec{S}_1) \cos\ (\omega t + \phi_p) \tag{12}$$

where ϕ_p is a phase angle in the reference coordinate system and $\omega = m\Omega$, then the pressure on blade k is

$$p(\vec{S}_k,t) = p_o(\vec{S}_1) \cos\left(\omega t + \phi_p - 2\pi\,(k-1)\,\frac{m}{N_B}\right) \tag{13}$$

We see that the normal coordinate describing the motion of mode i of blade k is similarly related, provided all blades have identical elastic properties, by

$$q_{i,k}(t) = q_{i,1}\,(t - \Delta t) \tag{14}$$

and

$$q_{i,k}\,(t) = q_{o,i} \cos\left(\omega t + \phi - 2\pi\,(k-1)\,\frac{m}{N_B}\right) \tag{15}$$

where $q_{o,i}$ is the amplitude of the normal coordinate for mode i on blade 1, and ϕ is its phase angle. This means that we need specify only the pressure on a single blade and need solve only for the normal coordinate pertaining to that blade. The pressures, normal coordinates and blade displacements on all other blades are then obtained using the simple time transformation.

Consistent with the field decomposition represented by equations (7-9), the local surface pressure on any one blade is caused by all propeller blades interacting with both a spatially nonuniform inflow, which is present whether or not the blades vibrate, and a time varying velocity field created by the induced blade vibrations. We assume that the total unsteady pressure is a sum of the pressures induced by each of these two effect--i.e., we assume

$$p = p_R + p_V \tag{16}$$

where p_R is the unsteady pressure distribution that would be present on the blade surfaces if the blades were perfectly rigid, and p_V is the pressure set up on the blade surface if there were no circumferential nonuniformities ($\vec{u}_m = 0$) in the inflow and the blades were constrained to vibrate with a prescribed velocity $\dot{\vec{d}}$.

We now introduce this decomposition of pressure into equation (10) to get

$$M_B \left(\ddot{q}_i + \omega_{a,i}^2 q_i\right) = Q_{R,i} + Q_{V,i} \tag{17a}$$

where p_R excites mode i with a modal force

$$Q_{R,i} = -\iint d\sigma' \; p_R \; \psi_i \; (\hat{n}' \cdot \hat{\delta}_i), \tag{17b}$$

which is independent of the normal coordinate q_i, and p_V excites mode i with a modal force

$$Q_{V,i} = -\iint d\sigma' \; p_V \; \psi_i \; (\hat{n}' \cdot \hat{\delta}_i) \tag{17c}$$

Since p_V is the pressure induced by blade vibration composed of all modes, the resulting modal force $Q_{V,i}$ is a function of all the normal coordinates, and, consequently, the differential equation of motion is not uncoupled in the normal coordinate q_i. In principle, there exists a new set of mode shapes ψ'_i and frequencies ω'_i which are characteristic of the blade vibration of an advancing and rotating propeller and which lead to a set of uncoupled equations of motion, provided the damping is of a particular form.* But if these new mode shapes are nearly the same as the in-air

*If the vibration were conservative, then both the mode shape ψ'_i and frequency ω'_i are real and can be expressed in terms of the in-air mode shape ψ_i and frequency ω_i [10]. But ours is not a conservative system and what we mean by the mode shape ψ'_i and frequency ω'_i needs careful examination. Following an idea of Rayleigh [11], a real set of mode shapes will

ones, then the induced pressure from mode i is the major contributor to the modal force $Q_{V,i}$. The other modes induce pressures that would result in much smaller contributions to $Q_{V,i}$ and could be neglected. This simplification is followed here, but neglecting contribution from the remaining modes is probably a better approximation for the first few modes, where the mode shapes are fairly simple and water loading only alters the patterns slightly, than for the more complicated patterns of the higher modes.

In making the assumption that $Q_{V,i}$ arises only from blade motion contribution from mode i, we have introduced a great simplification in that analysis, for now the equation of motion becomes uncoupled in the normal coordinate q_i. It remains still to specify the functional dependence of $Q_{V,i}$ on the blade motion.

Let $p_{V,i}$ be the local induced pressure on the blade caused by each blade vibrating with velocity $\dot{q}_{i,k}(t)\,\psi_i(\vec{S}_k)\,\hat{\delta}_i(\vec{S}_k)$, where $q_{i,k}$ is given by equation (15). Since pressures are assumed to behave linearly, $p_{V,i}$ is directly proportional to $q_{o,i}$, the amplitude of the normal mode coordinate. Furthermore, in the most general case, $p_{V,i}$ has a time dependent part in phase with the local blade acceleration and a part in phase with the local velocity. So if

$$q_i(t) = q_{o,i} \cos(\omega t + \phi), \tag{18a}$$

$$\omega = m\Omega, \tag{18b}$$

---

exist if the two phase components of the pressure distribution p_V form a ratio which is constant over the entire blade surface; then the mode shapes are real and the characteristic frequencies are complex. However, in the more general case, the classical modal description breaks down and the equations of motion are only approximately uncoupled [12].

this pressure can be split into two parts

$$p_{V,i}(\vec{S},t) = p^{c}_{V,i}(\vec{S}) \cos(\omega t + \phi) - p^{s}_{V,i}(\vec{S}) \sin(\omega t + \phi), \tag{19}$$

and consequently the modal force $Q_{V,i}$ is rewritten in the form

$$Q_{V,i}(t) = - M_i \ddot{q}_i - \omega D_i \dot{q}_i, \tag{20}$$

where

$$M_i = -\iint d\sigma' \; p_{V,i} (\omega^2 q_{o,i})^{-1} \psi_i (\hat{n}' \cdot \hat{\delta}_i) \tag{21}$$

$$D_i = +\iint d\sigma' \; p^{s}_{V,i} (\omega^2 q_{o,i})^{-1} \psi_i (\hat{n}' \cdot \hat{\delta}_i) \tag{22}$$

The quantities M_i and D_i are independent of the absolute amplitude of motion and are easily shown to be independent of the frequency of vibration $\omega = m\Omega$ as well, provided the advance ratio

$$J = 2\pi \frac{V_a + \bar{u}_o}{\Omega D} \tag{23}$$

--where V_a is the advance speed of the ship, $V_a + \bar{u}_o$ is the amplitude of the mean volume velocity which flows through the propeller disk (if the propeller were removed and the ship constrained to advance with speed V_a), Ω is the shaft's angular frequency, and D is the propeller's diameter--is kept constant as the vibration frequency changes. M_i can be interpreted as an induced modal mass or added mass of the propeller vibrating in its i(th) mode; D_i has the interpretation of an induced modal hydrodynamic damping (with units of mass) of the propeller vibrating in the same mode. The pressure distribution $p_{V,i}$ (for a unit $q_{o,i}$) is a function only of the

propeller geometry, mode shape, shaft harmonic m and advance ratio. Likewise, the hydrodynamic quantities M_i and D_i are intrinsic or characteristic quantities of the propeller itself. These characteristic quantities are independent of mean speed (for a fixed advance ratio) provided viscous effects are negligible, as we assume to be the case.

If the propeller vibrated without generating an unsteady circulation about the blade surface--the so-called "non-lifting" or no circulation problem--the modal force $Q_{V,i}$ would be in phase with the acceleration $\ddot{q}_i$, and the hydrodynamic damping D_i would be zero. But the presence of a sharp trailing edge in a well-designed propeller sets up circulation about the blade. And the vorticity, generated in the fluid boundary layer, is shed by the blades into a "wake" region and subsequently convected downstream away from the propeller. This process results in vibrational energy dissipation, accounted for in the analysis by D_i, and results in an added mass contribution M_i which is generally different than that for the solution for no circulation.

Equations (17a) and (20) give the final form of the equation for the steady state motion for the i(th) normal mode

$$(M_B + M_i)\,[\ddot{q}_i + \omega\beta_i\dot{q}_i + \omega_{w,i}^2\, q_i] = Q_{R,i} \tag{24}$$

where the water loading increases the apparent mass from its in-air value of M_B to $M_B + M_i$, thereby decreasing the blade's resonance frequency from $\omega_{a,i}$ to

$$\omega_{w,i} = \sqrt{\frac{M_B}{M_B + M_i}}\;\omega_{a,i} \tag{25}$$

and the ratio of modal dissipative force to modal inertial force is given by the modal hydrodynamic damping factor*

$$\beta_i = \frac{D_i}{M_B + M_i} \tag{26}$$

Enough is now known about the motion to enable us to solve for q_i. The relevant propeller characteristics--M_B, M_i, β_i, ψ_i, $\omega_{a,i}$--can all be specified independently from the forcing field p_R by either a calculation or measurement or a combination of both. Mode shapes and resonance frequencies are easily measured, as was done in this analysis, or calculated [13,8]. But the hydrodynamic quantities M_i and β_i are more difficult to measure and are possibly best estimated using an appropriate propeller theory.

If we let $Q_{R,i}$ be of the form

$$Q_{R,i}(t) = Q_{oR,i} \cos (\omega t - \phi_{oR,i}) \tag{27}$$

where $Q_{oR,i}$ is the amplitude of the modal driving force and $\phi_{oR,i}$ is its phase angle (measured relative to the coordinate system fixed to the reference system), then the normal mode has the solution

$$q_i(t) = q_{o,i} \cos (\omega t - \phi_{oR,i} + \phi_{q,i}) \tag{28}$$

---

*The value of β_i depends on the distribution of vorticity in the propeller's wake region. Since this distribution pattern is not the same for the transient as for the steady state vibration, the hydrodynamic damping factor for the two cases are generally different. This means that β_i is in general different from a hydrodynamic damping factor obtained by observing the free, exponential decay of blade vibration while the propeller operates in the uniform inflow.

where the modal displacement amplitude is given by

$$q_{o,i} = \frac{Q_{oR,i}}{\omega^2 (M_B + M_i)} \sqrt{\frac{1}{(\omega_{w,i}^2/\omega^2 - 1)^2 + \beta_i^2}} \tag{29}$$

and the phase angle is

$$\phi_{q,i} = \tan^{-1}\left(\frac{-\beta_i}{\omega_{w,i}^2/\omega^2 - 1}\right) \tag{30}$$

Since the modal force $Q_{oR,i}$ is proportional to the square of frequency for a constant advance ratio, the ratio $Q_{oR,i}/\omega^2$ is independent of frequency, and the frequency dependence of the displacement is determined entirely by the quantity under the radical in equation (29). We see that the amplitude of displacement is near zero when ω is much below $\omega_{w,i}$; it reaches a maximum at resonance (defined when $\omega = \omega_{w,i}$); and has a non-zero asymptotic value for frequencies much above resonance. Likewise, the phase angle $\phi_{q,i}$ is zero or slightly negative much below resonance; has a value $-\pi/2$ at resonance; and reaches an asymptotic value $\tan^{-1}(-\beta_i/-1)$ above resonance.

PROPELLER FORCES AND MOMENTS

Take $q_{o,i}$, momentarily, to be unity, then we can define a characteristic quantity $\tilde{p}_{V,i}$ (with units of pressure per unit displacement) which is independent of the amplitude of vibration

$$\tilde{p}_{V,i} = p_{V,i}/q_{o,i} \tag{31}$$

The total pressure field, accounting for all modes of motion, is then

$$p = p_R + \sum q_{o,i}\, \tilde{p}_{V,i} \tag{32}$$

The net vector force exerted by the water on the blade surfaces, accounting for the induced pressure contributions from all the modes of vibration, is then

$$\vec{F}_B(t) = \iint p\, \hat{n}'\, d\sigma'_{all} = \vec{F}_R + \vec{F}_V \tag{33}$$

where

$$\vec{F}_R = \iint p_R\, \hat{n}'\, d\sigma'_{all} \tag{34a}$$

and

$$\vec{F}_V = \sum q_{o,i} \iint \tilde{p}_{V,i}\, \hat{n}'\, d\sigma'_{all} \tag{34b}$$

and where the intergration extends over the surfaces of all blades. $\vec{F}_R$ is the force exerted on the blades by the water loading if the blades were rigid; this is also the force transmitted to the propeller's hub or shaft for a rigid propeller. $\vec{F}_V$ is the additional force exerted on the blades by the water because of the vibration of the blades.

The net vector force transmitted to the propeller's hub or shaft is given by

$$\vec{F}(t) = \vec{F}_B + \vec{F}_I \tag{35}$$

where

$$\vec{F}_I = -\sum \rho_B \iiint \ddot{q}_i\, \psi_i\, \hat{\delta}_i\, dV_{all} \tag{36}$$

The transmitted force $\vec{F}$ differs from the force $\vec{F}_B$ exerted by the water on the blades, the difference being the inertial reaction of the blades $\vec{F}_I$. It is important to make this distinction between $\vec{F}$ and $\vec{F}_B$ since in the subsequent experiments we measure the unsteady forces acting on the propeller shaft, not the blade surfaces.

Likewise, the net vector moment exerted by the water on the blade surfaces is

$$\vec{M}_B(t) = \iint p\ \vec{S}'\times\hat{n}'\ d\sigma'_{all} = \vec{M}_R + \vec{M}_V \tag{37}$$

where

$$\vec{M}_R = \iint p_R\ \vec{S}'\times\hat{n}'\, d\sigma'_{all} \tag{38a}$$

and

$$\vec{M}_V = \sum q_{o,i} \iint \tilde{p}_{V,i}\ \vec{S}'\times\hat{n}'\ d\sigma'_{all} \tag{38b}$$

and the net vector moment transmitted to the hub is

$$\vec{M}(t) = \vec{M}_B + \vec{M}_I \tag{39}$$

where

$$\vec{M}_I = -\sum \rho_B \iint \ddot{q}_i\ \psi_i\ \vec{S}\times\hat{\delta}_i\ dV_{all} \tag{40}$$

Because of the rotational symmetries of blade geometry and the rotational symmetries of pressure distribution [cf. equation (13)], only certain harmonics of shaft frequency result in noncancelling forces and moments on the blade surfaces [1]. Similar arguments limit the shaft harmonics which result in noncancelling propeller forces and moments transmitted to the hub. For wake or shaft harmonics where m/N_B is an integer, there is a net axial force or alternating thrust and a net alternating torque about the axial direction whose amplitudes are N_B times that force and moment acting on any one blade. When $(m\pm1)/N_B$ is an integer, there are net sidwise forces and moments whose amplitudes are $N_B/2$ times those of any single blade. Although the other wake harmonics can result in forces and moments on individual blades--and even destructively large

forces and moments near resonance--they produce cancelling or near cancelling transmitted propeller forces and moments when they are summed at the hub or propeller shaft.

It is conventional to nondimensionalize each component of force and moment by a force or moment characteristic of the size and operating speed of the propeller. Then a typical alternating component of force F is represented by a force coefficient

$$\tilde{K}_F = \frac{4\pi^2 F}{\rho\Omega^2 D^4} \tag{41a}$$

and a typical alternating moment component M by a moment coefficient

$$\tilde{K}_M = \frac{4\pi^2 M}{\rho\Omega^2 D^5} \tag{41b}$$

The notable thing about these coefficients is that they are independent of rotation frequency provided the blades behave rigidly, i.e., the alternating forces and moments increase with the square of shaft rotation speed as long as the advance ratio is maintained constant and the relative inflow variations do not change. This is not the case when the propeller responds elastically since the amplitude of blade vibration, and consequently the resulting forces and moments, are a function of shaft rotation speed.

ONE-MODE APPROXIMATION

For the calculations which follow of unsteady thrust and unsteady torque, we make a simplifying assumption to the general theory for the resulting propeller forces developed in equations (1) through (40). We assume that the vibration pattern over the blades does not change with excitation frequency, that is, only the fundamental mode of vibration is excited by the $m = N_B$ harmonic of the nonuniform inflow. This one-mode

approximation is strictly valid only if the impressed pressure field on the blade surface is proportional to the fundamental mode shape, i.e., $p_R/\hat{n}'\cdot\hat{\delta}\ d\sigma'/dV)$ is orthogonal to all modes except the first one [cf. equations (17b) and 3b)]. We would expect it to be a good approximation for excitation frequencies near the fundamental resonance, particularly if p_R on the blade resembles the fundamental mode shape. We will reexamine this approximation in light of the calculated and experimental results in a later section.

Neglecting the induced pressure field contributions as well as the inertial blade reactions from all but the first mode in equations (35) and (39) we get the transmitted unsteady thrust at the hub to be

$$F_z(t) = \vec{F}\cdot\hat{z} \approx \iint p_R\ \hat{n}'\cdot\hat{z}\ d\sigma'_{all} + \iint p_{V,1}\ \hat{n}'\cdot\hat{z}\ d\sigma'_{all} - \rho_B\ \ddot{q}_1 \iiint \psi_1\ \hat{\delta}_1\cdot\hat{z}\ dV_{all} \qquad (42)$$

and the unsteady torque transmitted to the hub to be

$$M_z(t) = \vec{M}\cdot\hat{z} \approx \iint p_R(\vec{S}'\times\hat{n}')\cdot\hat{z}\ d\sigma'_{all} + \iint p_{V,1}(\vec{S}'\times\hat{n}')\cdot\hat{z}\ d\sigma'_{all} - \rho_B\ \ddot{q}_1 \iiint \psi_1(\vec{S}'\times\hat{\delta}_1)\cdot\hat{z}\ dV_{all} \qquad (43)$$

We see that a calculation of the transmitted force requires the addition of three separate quantities, taking proper account of phase and amplitude of each as the excitation frequency varies.

The quantities given by equations (42) and (43) can be interpreted as a modal force and a modal moment which correspond to the first mode of

vibration. These two expressions, which we will refer to as the "inertial approximations", would be exact--within the assumptions of the theory--if only the first mode is excited into vibration.

There is another, much simpler, one-mode approximation which can be derived and which is also exact if only the first mode is excited. The expressions above are a statement that the transmitted force (or moment) is equal to the applied force less the inertial reaction of the blades. The transmitted force, however, is also proportional to the blade motion. If only one mode is excited and the shaft and hub are rigid, then the transmitted thrust amplitude F_z is given by

$$F_z = \kappa\, q_{o,1} \tag{44}$$

where κ can be interpreted as a dynamic stiffness constant, which for simple, linear vibrations would be independent of excitation frequency. (In the general case where more than one mode is excited, κ would be a function of excitation frequency and $q_{o,1}$ would be replaced by a weighted average of modal displacements.) Since κ is independent of loading frequency, we can take

$$\kappa = \left(\frac{F_z}{q_{o,1}}\right)_{\substack{\omega \to 0 \\ J=\text{const}}} \tag{45}$$

Then from equations (29), (35), (45), and (44) we get the simple and useful relationship

$$\left(\frac{F_z}{F_{z,R}}\right) = \left(\frac{\omega_{w,1}}{\omega}\right)^2 \sqrt{\frac{1}{(\omega_{w,1}^2/\omega^2 - 1)^2 + \beta_1^2}} \tag{46}$$

Equation (46) says that the ratio of the transmitted thrust F_z to the force $F_{z,R}$, which would be transmitted were the blades rigid, is a function only of the hydrodynamic damping factor β_1 and the ratio of excitation

frequency to the fundamental resonance frequency in water. If more than one mode is excited, the equation would be an approximation whose validity depends on the dominance of the fundamental mode to the vibration.

The approximation given by equation (46) suggests some interesting properties about the forces transmitted to a propeller hub when the fundamental mode dominates the vibration. First we see that the transmitted force can be smaller when the blades vibrate than when they do not. This would occur for excitation frequencies

$$\omega > \omega_{w,1} \sqrt{\frac{2}{1 + \beta_1^2}} \tag{47}$$

We can also show that the maximum force magnification brought on by blade vibration is

$$\left(\frac{F_z}{F_{z,R}}\right)_{max} \approx \sqrt{1 + \frac{1}{\beta_1^2}} \tag{48}$$

which occurs when

$$\left(\frac{\omega_{w,1}}{\omega}\right) \approx \sqrt{1 + \beta_1^2} \tag{49}$$

After a derivation similar to that given above, we get the identical relationship for the transmitted unsteady torque ratio

$$\left(\frac{M_z}{M_{z,R}}\right) = \left(\frac{\omega_{w,1}}{\omega}\right)^2 \sqrt{\frac{1}{(\omega_{w,1}^2/\omega^2 - 1)^2 + \beta_1^2}} \tag{50}$$

We will refer to equations (46) and (50) as the "stiffness approximation."

The two sets of expressions, given in equations (42) and (43) and equations (46) and (50), although different in appearance, give identical results if only the fundamental mode is excited into vibration. The blade

then acts as a simple oscillator which causes the unsteady force ratio to diminish to zero as the excitation frequency is increased beyond the fundamental resonance frequency. In the real situation where many modes are excited, the two sets of equations are only approximations and they give different results. The stiffness approximation indicates that the force ratios always go to zero for a sufficiently large exciting frequency. There is no such requirement inherent in the inertial approximations and, in general, their high-frequency asymptotic values will approach some constant. In the real situation, the higher modes begin to dominate as the exciting frequency is increased, causing multiple resonances to be observed, and both sets of approximations break down.

Nevertheless, of the two sets of approximations, we can argue that the first one should give marginally better results than the second. In the first set of approximations we neglected the inertial reaction of the higher modes. Examination of the second set of equations suggests that we neglected the stiffness contributions of the higher modes in arriving at this set of one-mode approximations. The contributions of the higher modes would be expected to be smaller for the inertial approximation than for the stiffness approximation. This is because the stiffness contribution of each mode depends on the second span-wise derivative of the mode shape at the hub. For the same amplitude of vibration in each mode, the second derivative gives added weight to the higher modes. Also the stiffness contribution depends only on the mode shape at one point at the hub. The inertial contribution depends on the average value of the mode shape, averaged along the span. For the same amplitude of vibration in each mode, span-wise averaging reduces the weight of the higher modes, because the higher modes have more nodes.

Therefore, since the inertial contributions of the higher modes are smaller than the stiffness contributions of the higher modes, at least for excitation frequencies below the second resonance frequency, we would expect the set of inertial approximations to be the better one. Accordingly, the inertial approximation was used in the subsequent calculations. But we will show later that both sets of approximations agree with the experiment.

EXPERIMENT

The experiment has two primary objectives. We want to demonstrate that blade vibration can affect and significantly alter unsteady propeller forces and moments, and we want to show that quite different responses are possible, depending upon the propeller's hydrodynamic damping and mass. And, equally important, we wish to establish a reliable set of experimental results which can be compared with theoretical predictions. For this purpose propeller forces and all controlling variables, such as mode shapes, resonance frequencies and fluid inflow velocities, were carefully measured.

Of the six possible generalized propeller forces, only alternating thrust and torque were measured during the experiment. These two are sufficient to accomplish the main objectives of the study. The measurements were made in a water tunnel using a six-component dynamometer which utilizes semiconductor strain gages as sensing elements [14,6]. A new technique for measuring alternating thrust, using an upstream hydrophone as a sensor, was also explored in this study, however, the method failed to give satisfactory results for reasons to be discussed subsequently.

To generate large measurable alternating thrust and torques, a wake screen, located upstream from the test propeller, was used to produce an angular wake harmonic equal to the number of propeller blades, $m = N_B$. The frequency of the thrust and torque generated was then equal to the number of blades multiplied by the rotational frequency of the propeller shaft. When this loading frequency was near the resonance frequency for the propeller's fundamental mode, large oscillating blade motion was possible, and it was possible to study its effect on unsteady thrust and torque.

In testing for the elastic effect, the test propellers were operated over a range of loading frequencies by spanning the fundamental resonance frequency while keeping the advance ratio constant. This enabled us to observe and record the changes in propeller loading at the different frequencies of the blade vibration.

There are several possible ways to demonstrate the effects of blade vibration. The most direct way is to take two propellers of identical geometries, but different elastic characteristics--one very flexible, having a resonance frequency within the operating range of the facility and one rigid, having a resonance frequency far beyond the operating range--and measure the alternating forces generated by each under identical flow conditions. Then any measured differences are presumed to be due to differences in blade elasticity. Geometrically identical propellers made of aluminum and plastic could accomplish this, with the lighter mass of the plastic propeller further magnifying the effect.

An alternative method is to select a propeller which has a resonance frequency within the tunnel-operating range and to make measurements at a constant advance ratio over a range of shaft frequencies. If the blades were rigid, the unsteady thrust coefficient would be a constant for all shaft frequencies. A rigid condition is approximated when the resonance frequency of the blades is much larger than the loading frequency, and an elastic condition holds for higher loading frequencies. So by keeping the advance ratio constant and measuring alternating forces for successively larger shaft frequencies, any deviation of the unsteady thrust coefficient over those obtained at low shaft frequencies could be presumed due to blade vibration.

Still a third way is to measure alternating forces over a range of operating conditions for a propeller with a resonance frequency much higher than the operating range, then lowering the natural frequency to within the operating range by cutting the blades near their bases. The propeller would then be re-tested under identical conditions as before, but now the blades will respond elastically. This method, however, was not attempted here.

The first and third methods have the advantage that the rigid and flexible propellers operate under identical flow excitation conditions, so that any differences are presumed due solely to elastic blade effects. This is not quite true of the second method since flow similarity is required to exist at a constant advance ratio for a large range of operating conditions and viscosity effects are not distinguished.

Both the first and second methods were used in the present study. For the first method, two geometrically identical 10.04 inch diameter propellers with somewhat narrow blades were selected; one is made of aluminum (DTNSRDC No. 3956) and the other of plastic (DTNSRDC No. 3958). An 11.52 inch diameter aluminum propeller with wide, overlapping blades (DTNSRDC No. 4064) was selected for the second method.

These propellers enabled a wide variation in geometry to be studied They were selected based upon some preliminary calculations of hydrodynamic damping which indicated that the two geometrically different propellers would have quite different responses near their fundamental resonance frequencies; the narrower bladed propeller was expected to exhibit much higher hydrodynamic damping than the wider bladed propeller.

TEST FACILITY

Except for propeller-mode shape measurements, the experiment was done at the 24-inch variable pressure water tunnel, located at the David W. Taylor Naval Ship Research and Development Center (DTNSRDC). The tunnel is approximately 120 feet in length with a diameter which varies from 6 feet, a few feet upstream from the propeller, to 27 inches at the enshrouded propeller section. The tunnel facility is capable of a maximum water speed of 60 fps. The dynamometer overloads for steady torques in excess of 25 ft-lbs; this limits the maximum shaft rotation speed as well as the useful range of mean propeller loading. Also, the tunnel can be pressurized from 2 to 30 psia, the higher pressures being useful in cavitation suppression. A wake screen which produces large unsteady thrust and unsteady torque was located about 30 inches upstream from the propeller. One hydrophone was positioned along the tunnel axis at the honeycomb section and one was placed near the center of the wake screen. The basic configuration is shown in Figure 1.

Numerous unsteady propeller force measurements using the facilities' six-component dynamometer system have been made at this facility over the past 12 years [14,15], and the peculiarities and specifications of the system are well documented elsewhere [6,14]. The propeller is mounted on a six-component dynamometer which is an extension of the propeller shaft. Fluctuating propeller forces and moments create fluctuating strains in a section of the shaft which are sensed by a semiconductor strain-gage bridge and are resolved into six voltages from which forces and moments are determined. The voltages are, in turn, amplified and exit the rotating shaft by way of slip rings. A signal is then analyzed, and in this case, the amplitude and phase of the blade-passing frequency component is recorded. Phase is measured relative to that of a known reference signal. A schematic diagram

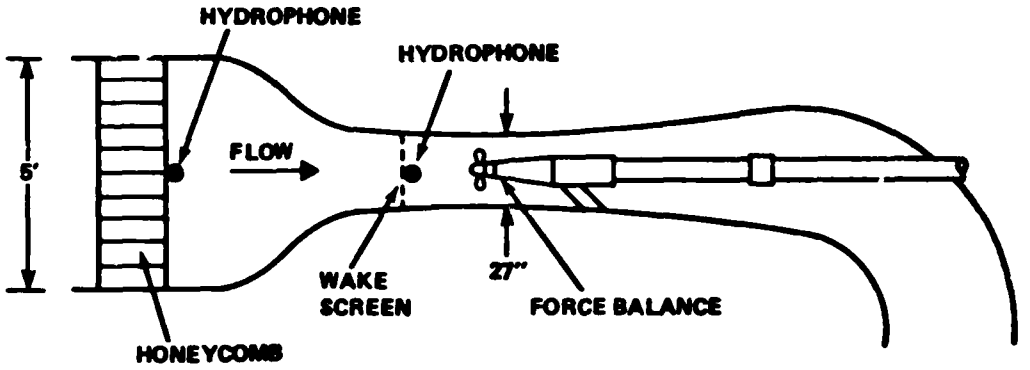

Figure 1 - Test Configuration

of the instrumentation used in measuring alternating thrust and torque is shown in Figure 2a. Forward of the amplifiers, the shaft system has a built-in 2-millivolts (rms), 235-Hz voltage source which was used repeatedly throughout the experiment to calibrate the output voltages from the analyzer. A sketch of the six-component dynamometer system is shown in Figure 2b. (Both Figures 2a and 2b are taken from Reference 6.)

Before the testing started, we calibrated the dynamometer by applying known static thrusts and torques and recording the thrust and torque channel voltages. There was a slight interference between thrust and torque voltages, with the calibration given by

$$F_z = 2.15\ e_F - .070\ e_M \qquad \text{lb/mvolts} \qquad (51a)$$

$$M_z = -\ .189\ e_M \qquad \text{lb-ft/mvolts} \qquad (51b)$$

where F_z is the thrust, M_z is the torque, e_F is the thrust channel voltage, expressed in millivolts, and e_M is the torque channel voltage in millivolts. This static calibration was presumed to hold for all test frequencies. In order to identify any resonances in the system, after the dynamometer was in place and the tunnel filled with water, a waterproofed Wilcoxon F3 electromagnetic shaker with built-in impedance head was attached to a block mass, which replaced the propeller, and driven over a range of frequencies from 25 to 300 Hz. The ratio of thrust to thrust voltage varied only slightly ($\pm$5 percent) over this frequency range. This agrees with the previous experience of Miller [14].

The errors introduced by using this static calibration are probably not significant, at least in the frequency range used in this experiment. As we explained, there seems to be only a small frequency dependence over the frequency range of interest. Also the calibration showed the desired

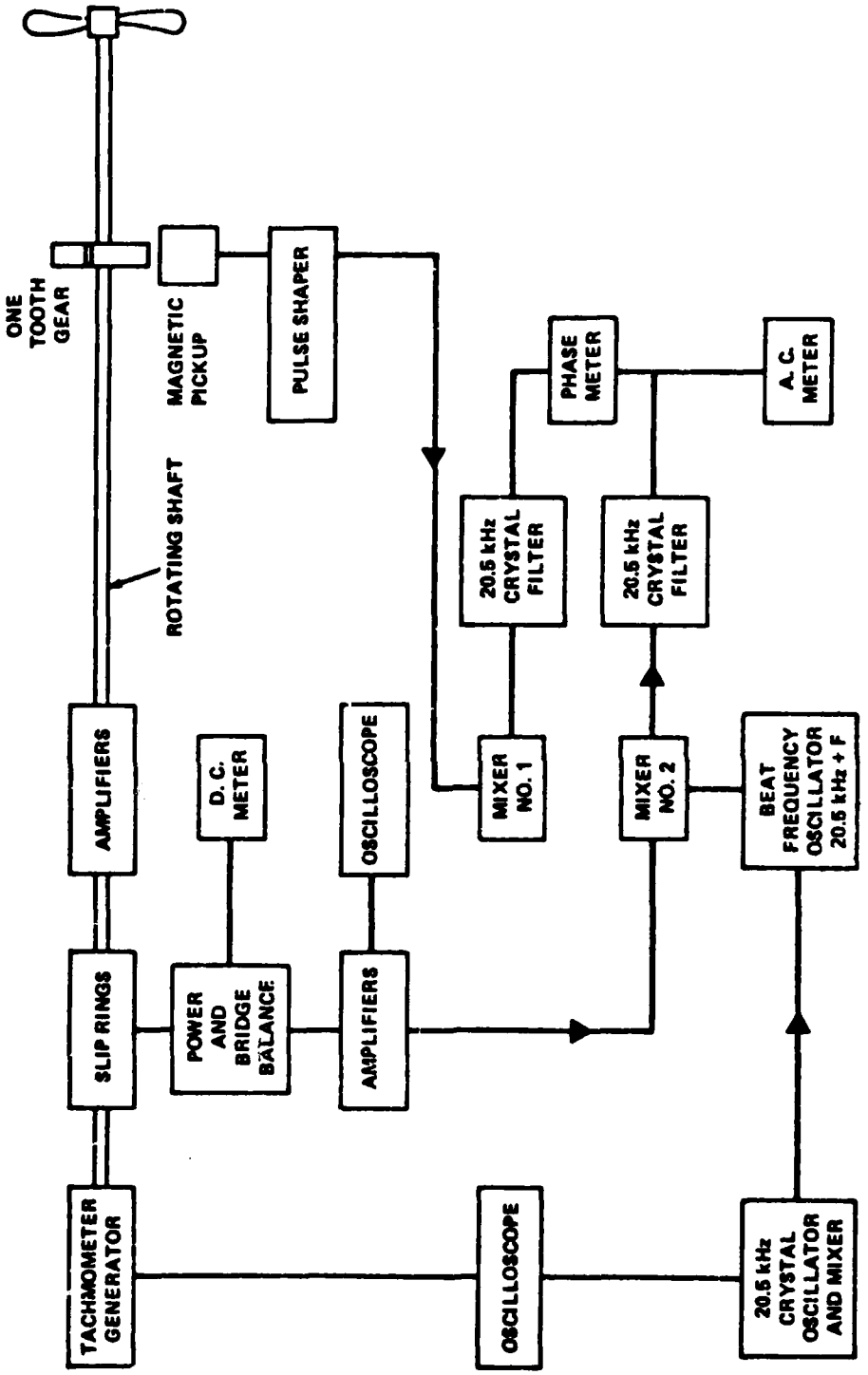

Figure 2a - Schematic Diagram of Instrumentation

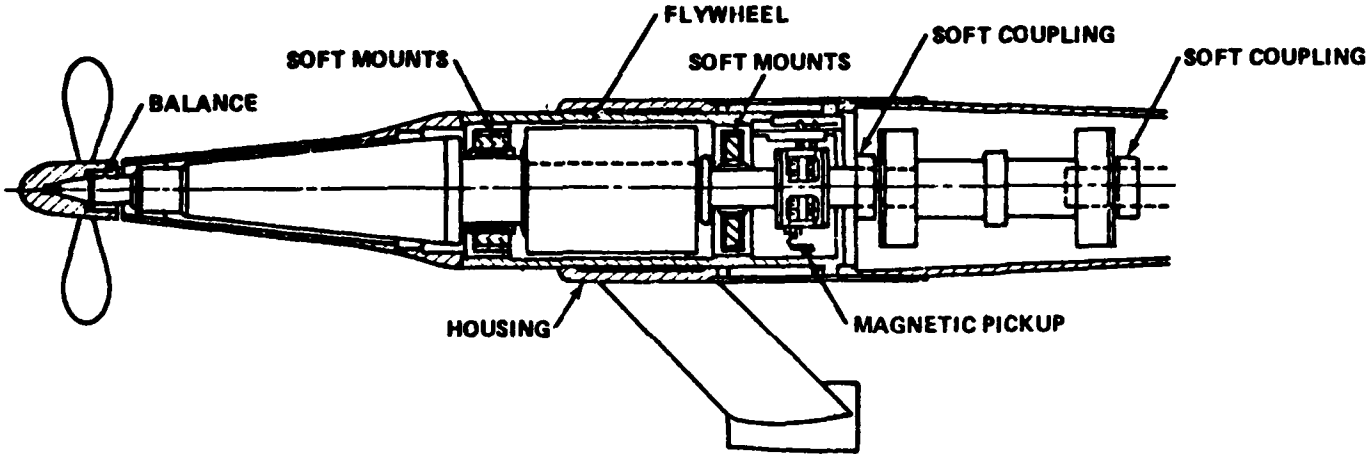

DYNAMOMETER ASSEMBLY

Figure 2b - Six-Component Propeller Dynamometer Assembly

linear dependence of voltage on applied forces, i.e., when we increased the force and moment, the voltage increased proportionally. In addition, the interference between the thrust and torque voltages and the other four voltages is negligible; and the slight interference between thrust and torque voltages is easily accounted for.

PROPELLER MODE SHAPES AND FREQUENCIES

Mode shapes were measured in-air on a laboratory bench. A Wilcoxon F3 shaker with built-in accelerometer and force gage was mounted to the propeller's hub. And a McIntosh 60 watt power amplifier drove the shaker/propeller with a varying sinusoidal excitation until the propeller's resonance frequency was excited. A resonance frequency was identified when the phase of output voltage from the accelerometer was 90 degrees to that of the force gage. Since the propellers used in the test were lightly damped, with a mechanical loss factor of about 0.01 for No. 4064 and about 0.02 for No. 3958, resonance frequencies were easy to identify by this method. They could also be clearly detected by simply listening to the sound from the vibrating blades.

The mode shapes were measured using a Model KD-38 Mechanical Technology Inc. Fotonic Sensor which enables displacements to be measured without loading the blade surfaces. It senses displacements through a needle-like probe containing strands of fiber optics fibers, of which half transmit light and receive the reflected light. The end of the probe is positioned initially about 100 mils from a point on the resonating blade surface. The vibrating surface reflects a fluctuating light intensity which is received and translated into a voltage output signal, whose amplitude and phase are measured using an AC voltmeter and oscilloscope. The mean received light intensity (or DC output voltage) as a function of gap distance (between the probe's end and a point on the mean vibrating surface) is zero when there is no gap,

reaches a maximum at a distance of about 100 mils, and then decreases slowly beyond that. This response curve is linear for gap distances between about 140 to 240 mils; at the midpoint of the linear range, the output DC voltage is approximately 70 percent of its maximum value. Small changes in gap distance, caused by fluctuating surface displacements within this linear range, produce AC voltages which are directly proportional to the slope of the DC response curve. In this range, the AC voltage is insensitive to the exact gap distance.

The procedure for measuring the relative normal displacement for points on the blade surface is to adjust the gap distance until 70 percent of maximum DC voltage is reached, and then record the corresponding AC voltage. This procedure, repeated for a number of points on the surface, maps out the normal component of mode shape $\psi_i \hat{\delta}_i \hat{n}'$ in rapid order. The two inplane components of motion could be resolved by attaching a small perpendicular reflecting surface to a point on the blade and thereby measuring displacements parallel to the local blade surface. This was not done here since the inplane components do not enter into the determination of either the modal forces or the net vector force and moment exerted by the water to the blade surfaces [cf. equation (17), (33), (37)]. For the parts of the theory where a complete description of the mode shape is necessary, we assumed that

$$\psi_i \hat{\delta}_i \simeq \psi_i \hat{n}_i' \tag{52}$$

or, in effect, neglected the in-plane components.* This is probably a good

*The complete mode shape is necessary in the normalization procedure [equation (3a)] and in figuring the blade-mass acceleration contributions [equations (36), (40)]. The approximation also ignores the contributions of modal tangential displacements compared to the modal normal displacements in equation (9).

approximation at these frequencies since the local inplane stiffness is much larger than the local bending stiffness.

The results of the mode shape measurements for propeller No. 3958 and 4064 are listed in Tables 1 and 2. The tabulated values which are along chords of constant radius and normalized to the tip displacement, are for the mode shape on one blade. In the table, chord fraction refers to the local fractional distance along a chord of constant radius; the chord fraction is 0.0 at the trailing edge (T.E.) and 1.0 at the leading edge (L.E.) of the blade. Values on the other blades at rotationally symmetric points differed by as much as ±100 percent in absolute displacement, but only ±10 percent when normalized by their tip displacements.

Measurements of resonance frequencies were made with the propeller in place in the water tunnel. The waterproofed shaker was mounted to the propeller's hub and excited the blades into vibration. The shaft was locked in place which reduced the propeller tendency to rotate when the blades oscillated. Resonances were identified by sweeping the frequency of the input voltage and monitoring the thrust and torque output voltages from the dynamometer. The plastic propeller (No. 3958) has an in-air fundamental resonance frequency of 435 Hz and a second resonance at 940 Hz. In still water this same propeller has a fundamental resonance of 160 Hz and the apparent second resonance is at 400 Hz. The aluminum counterpart (No. 3956) has a fundamental frequency of 800 Hz in air and 360 Hz in still water and for the frequency range of excitation we are interested in, we would expect it to act almost like a rigid propeller. Propeller No. 4064 has a fundamental in-air resonance frequency of 355 Hz and a second resonance at 1050 Hz. In still water the fundamental resonance is 108 Hz and the second resonance is 370 Hz.

TABLE 1

MEASURED FUNDAMENTAL MODE SHAPE FOR PROP. 3958

Radius Inches	Chord Fraction 0.0 (T.E.)	0.5	1.0 (L.E.)
1.512	0.000	0.000	0.000
2.016	.010	.010	.010
2.520	.030	.030	.030
3.024	.100	.100	.100
3.528	.185	.148	.111
4.032	.407	.352	.185
4.536	.704	.630	.519
4.788	.815	.778	.648
5.040		ψ = 1.0 at the blade tip	

TABLE 2

MEASURED FUNDAMENTAL MODE SHAPE FOR PROP. 4064

Radius Inches	Chord Fraction 0.0 (T.E.)	0.33	0.66	1.0 (L.E.)
1.152	0.000	0.000	0.000	0.000
1.728	0.000	0.000	0.000	0.000
2.304	.010	.010	.010	.010
2.880	.010	.010	.010	.010
3.456	.020	.030	.040	.030
4.032	.060	.060	.090	.120
4.608	.210	.390	.550	.390
5.184	.480	.760	.700	.420
5.472	.820	.850	.850	.820
5.760		ψ = 1.0 at the blade tip		

WAKE SURVEY

In order to excite a large, measurable unsteady thrust and torque, an appropriate wake screen was constructed. Three and four-cycle screens which produce wake harmonic velocity amplitudes that are roughly 20 percent of the mean inflow velocity, have been built and tested in the past, and the same construction procedures were followed here [16,6]. A base screen, made of 0.0095 inch diameter 16 mesh stainless steel, is welded to a 27 inch stainless steel support ring. By overlaying sections of 0.016 inch diameter 18 mesh stainless steel screening, a circumferential periodic solidity pattern is produced which matches the number of blades on the test propellers.

The nonuniform flow distribution set up by the wake screen was measured with a pitot tube rake mounted to the shaft in place of the test propeller. Both upstream hydrophones were also in place. Only the longitudinal component of flow was measured; the other components of velocity were presumed to be of secondary importance. The average tunnel speed (as measured by the facilities venturi meter) was set at 10.0 fps and the local dynamic head of water was measured at six radial positions in six degree increments. The local longitudinal velocity was then calculated. Knowing the average velocity $u_o(r)$ at each of the radial positions, the appropriate volume mean velocity $\bar{u}_o$ for each test propeller was estimated by the equation

$$\bar{u}_o = (\pi R_{tip}^2 - \pi R_{hub}^2)^{-1} \int_{R_{hub}}^{R_{tip}} 2\pi\, u_o(r)\, r\, dr \qquad (53)$$

The volume mean velocity was 8.6 fps for propeller No. 3956, 3958 and 8.8 fps for propeller No. 4064.

The inflow velocity (suppressing all but the zero and N_B harmonic) was assumed to be of the form

$$\vec{u} = \vec{u}_o + \vec{u}_m = u_o(r)\,\hat{z} + u_{N_B}(r)\cos\left(N_B \varphi + \varepsilon_{N_B}(r)\right)\hat{z} \qquad (54)$$

where $\hat{z}$ is a longitudinal unit vector (positive in the direction of flow), (r,φ) are the radial and angular coordinates with φ measured from the vertical and positive in the direction of rotation of a right hand propeller ($\varphi=0^\circ$ corresponds to the top of the wake screen) and $\varepsilon_{N_B}(r)$ is the radial distribution of phase of the N_B harmonic. The local velocity $\vec{u}$ was normalized by the appropriate volume mean velocity and this ratio was assumed to be independent of tunnel speed-speeds that ranged from 1.5 fps to 20 fps--throughout the experiment, i.e., $\vec{u}/\bar{u}_o$ is assumed independent of $\bar{u}_o$.

The velocity field was analyzed for its harmonic content [17]. Values of the zero and N_B harmonics are shown as a function of radius r in Figure 3. The harmonic amplitude is very small at radii less than five inches because of the close spacing of the pie sections near the screen's center. Beyond this distance there is only a small amount of mixing and the amplitude flattens out.

HYDROPHONE MEASUREMENTS

An alternative method for measuring unsteady thrust was also investigated in this study. The method depends on establishing a stable, measureable relationship between alternating thrust and the accompanying induced alternating pressure in the water. At distances from the propeller which are much less than one acoustic wavelength, the water behaves as though it were incompressible, and there are two geometric configurations where a simple relation between alternating thrust and alternating pressure exists: one is the incompressible pressure field surrounding an oscillating point force in an infinite fluid and the other is the incompressible pressure field about a point force oscillating in a rigid duct of constant diameter.

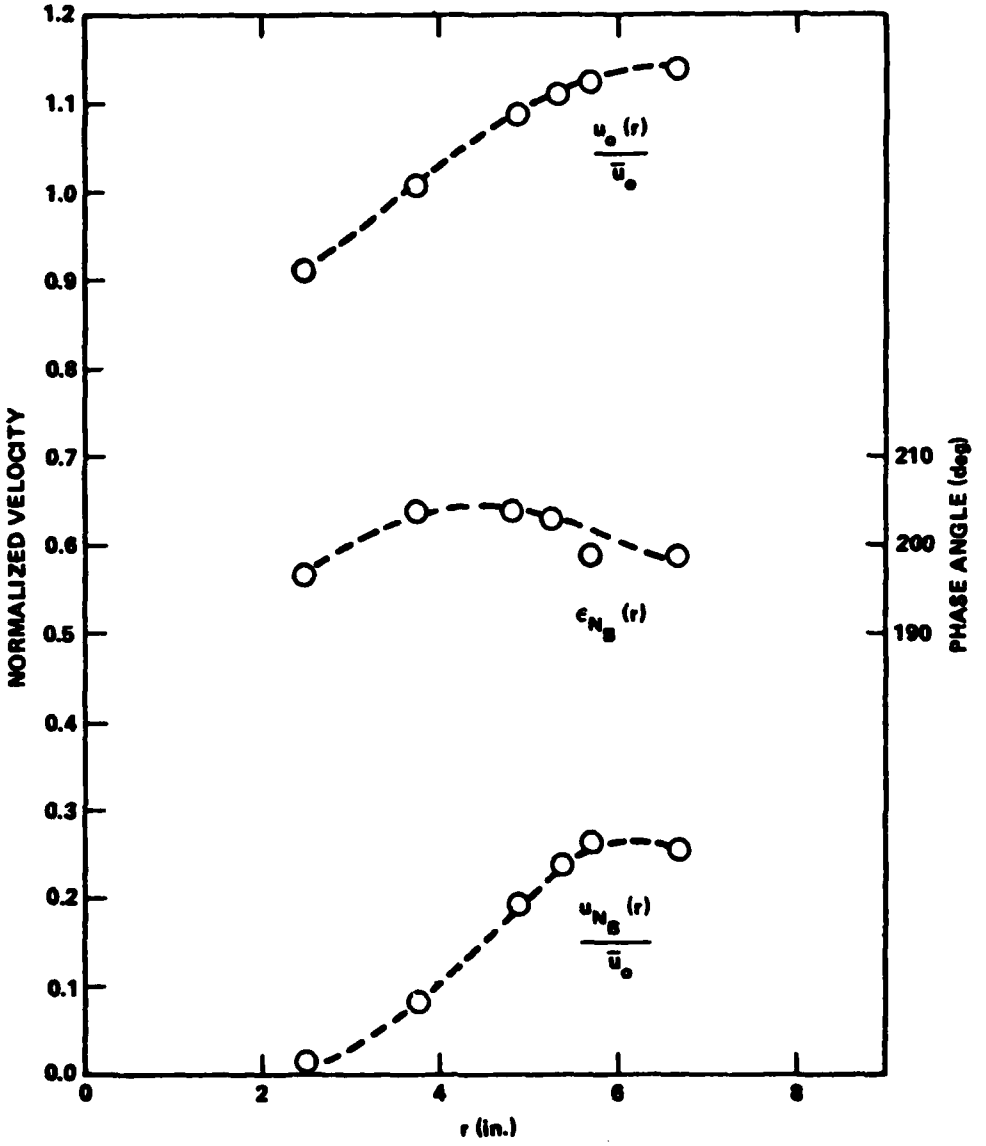

Figure 3 - Harmonic Analysis of Measured Inflow Velocity (Normalization Is Appropriate for Prop. No. 3958). The Phase Angle Is Measured From the Vertical and Is Positive in the Direction of Rotation of a Right Handed Propeller

In the first case the pressure falls off as the square of the distance between the pressure point and the force [18], and in the second the pressure is independent of distance beyond one duct diameter [19]; in both cases the pressure is directly proportional to the force and independent of the frequency of oscillation. In our water tunnel, we have neither of these two idealized situations, but we nevertheless wanted to explore experimentally the existence of a relationship.

To do this, we located two hydrophones upstream from the propeller. The first hydrophone, a UT 103 with a voltage sensitivity of -104 dB re 1 V/μbar, was located about 30 inches from the propeller in the 27-inch diameter section of the tunnel. The other hydrophone, an LC 10 with a sensitivity of -108 dB re 1 V/μbar, was placed about 10 feet upstream from the propeller in the 6-foot diameter section. Both hydrophones were placed along the tunnel axis so that the unwanted portion of pressure at the blade-rate frequency which is due to rotational noise--pressure field generated by the propeller's steady rotating surface pressure--would be minimized. Particular care was taken in mounting the hydrophones to ensure that they did not respond to either structureborne or waterborne vibrations. Under normal operating conditions the first hydrophone was expected to receive the clearest pressure signal. But if the first hydrophone became flow-noise limited at the higher water tunnel speeds, a strong signal might still be received at the second hydrophone since it operates in lower flow speed region.

To calibrate the system and to explore the relationship between pressure and alternating thrust, we suspended an oblate spheroidal disk in place of the propeller. The 12-inch diameter disk had a hollowed-out section which enclosed a Wilcoxon F3 shaker with built-in impedance head. The disk

was shaken in the broadside direction over a range of frequencies. Both the drive-point force and the disk's acceleration (measured on the face opposite the drive point) were monitored. The disk oscillated nearly as a rigid body over the frequency range of interest. Therefore, the force the disk exerts on the water was equal to its added water mass times its axial rigid body acceleration. Alternatively, the oscillating force on the water is equal to the force, as measured by the force gage, less the disk's body force (the disk's mass times its rigid body acceleration). In any event, since the force exerted on the water was known, as was the oscillation frequency and hydrophone pressure, a relationship between alternating thrust and received pressure could be established.

The results of the calibration are shown in Figure 4. These results show a disappointingly strong dependence on frequency. At both hydrophones there was a quasi-periodic structure to the response with local maxima at multiples, roughly, of 25 Hz interspersed with local minima. The response was not very stable, with small deviations in driving frequency resulting in large changes in hydrophone voltage response; neither was the calibration repeatable from test-to-test and from day-to-day.

The source of the instability in the response was never determined for certain. The possibility of a resonance condition in the hydrophone support mounting was investigated carefully and eliminated as a potential source. Some interference effect between the elastic duct and the driving pressure field could be a possible source, as could be the interference between the incident pressure field and the sound field which travels one or more times around the circular-like water tunnel (this would produce a maxima at multiples of 40 Hz).

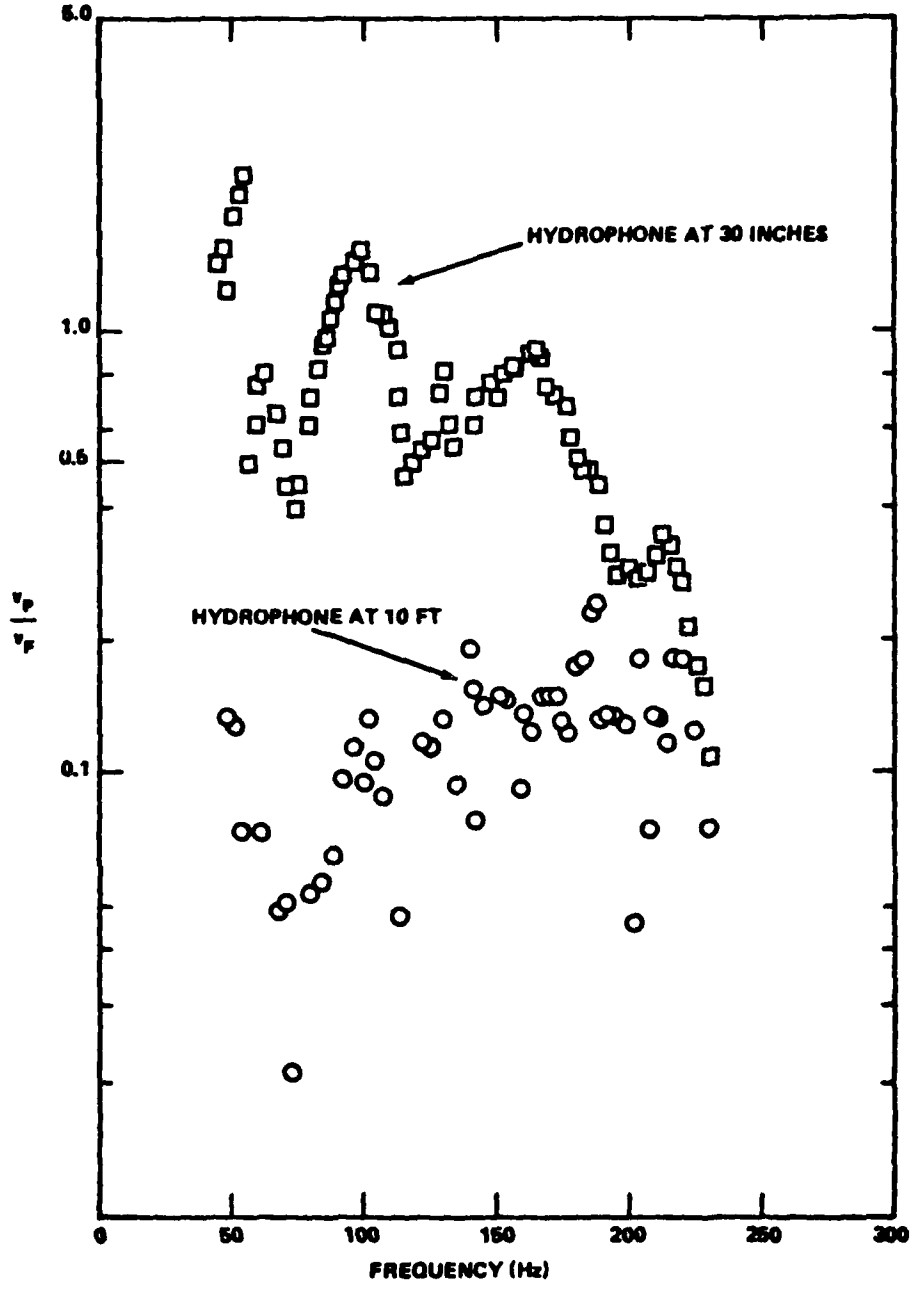

Figure 4 - Calibration of Disk-Hydrophone System. v_p is the (Unamplified) Response Voltage at the Hydrophone, and v_F is the Output Voltage from the Force Gage at the Drive Point (Force Gage Voltage Sensitivity is 1.32 mV/lb)

Nevertheless, the hydrophones were left in place throughout the experiment and measurements were recorded whenever possible. Interpreting the voltage output from the hydrophones was complicated by the presence of gear noise in the water. This is caused by the meshing of gear teeth in the shafting system which causes harmonics of the shaft rotational frequency to be present in the pressure output even when the shaft rotates without a propeller. Since the pressure field induced by the operation of the propeller also has frequencies which are multiples of the shaft frequency, the gear noise acts as noise. During the tests for the two narrow-bladed propellers, the pressure signals from the propellers were judged to be insufficiently above the gear noise to permit proper interpretation. Figure 5 gives a hydrophone output typical of these propellers. The pressure signal induced by the operation of the wide-bladed propeller, however, was above the gear noise, with a typical hydrophone output given in Figure 6.

Figure 7 shows the measured values for $\tilde{K}_T$ at two advance ratios for the wide-bladed propeller; to illustrate the hydrophone response to the force the propeller imparts to the water, a nominal hydrophone response of 0.8 mvolts per pound of propeller force is used here instead of the measure response curve given in Figure 4. The alternating thrust values show a peak near 100 Hz (even when the calibration curve is used) and a decline beyond that. Although this is in general agreement with the strain-gauge measurements, the hydrophone method does not appear to be a dependable alternative method for measuring alternating thrust. It should be noted, however, that if the technique worked, the force calculated from the measured sound pressure would be the force the propeller exerts on the water, which would be somewhat different from the force transmitted through the hub to the dynamometer.

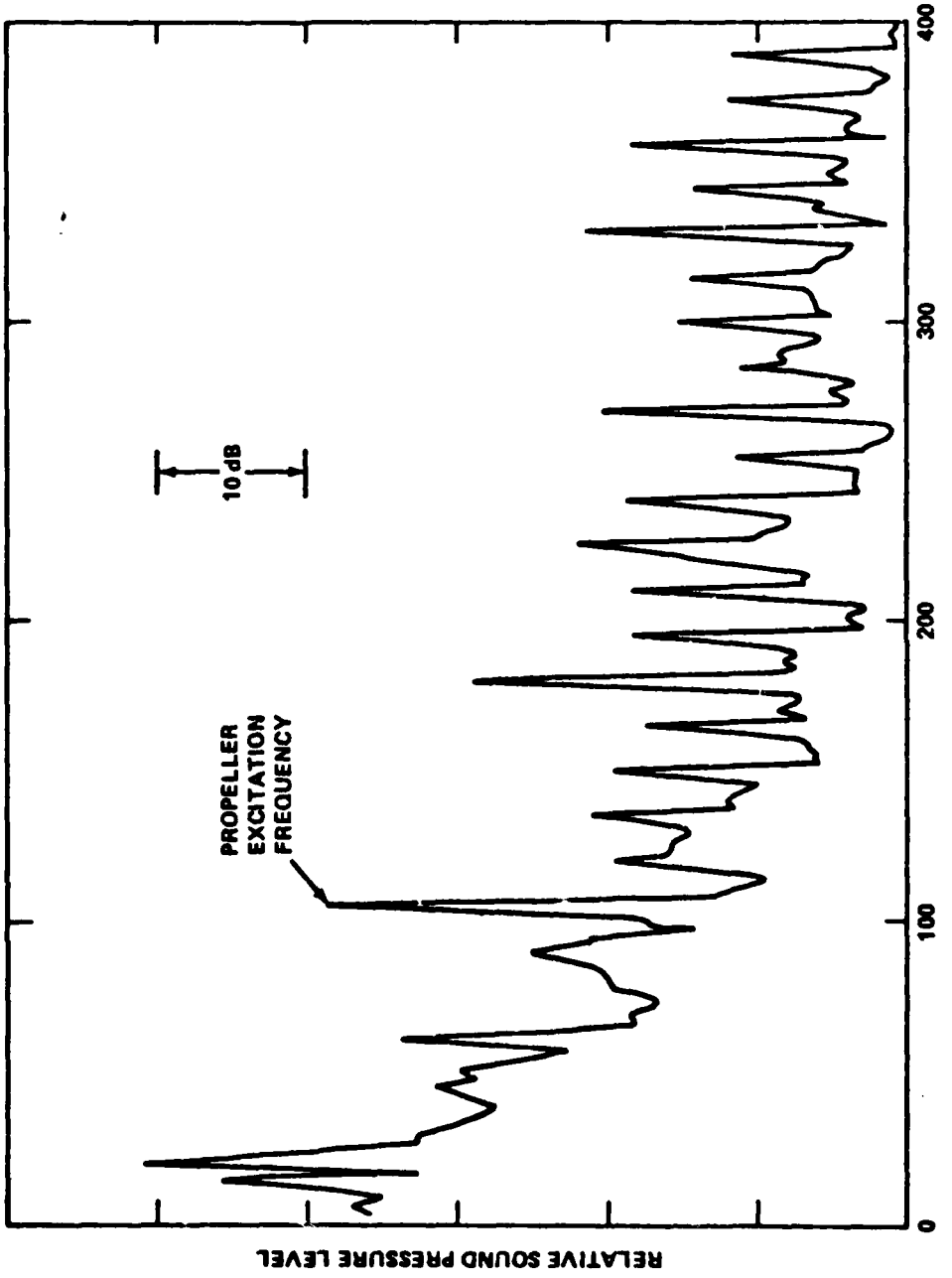

Figure 5a - Typical Pressure Spectrum at the Hydrophone 30 inches from Prop. No. 3956

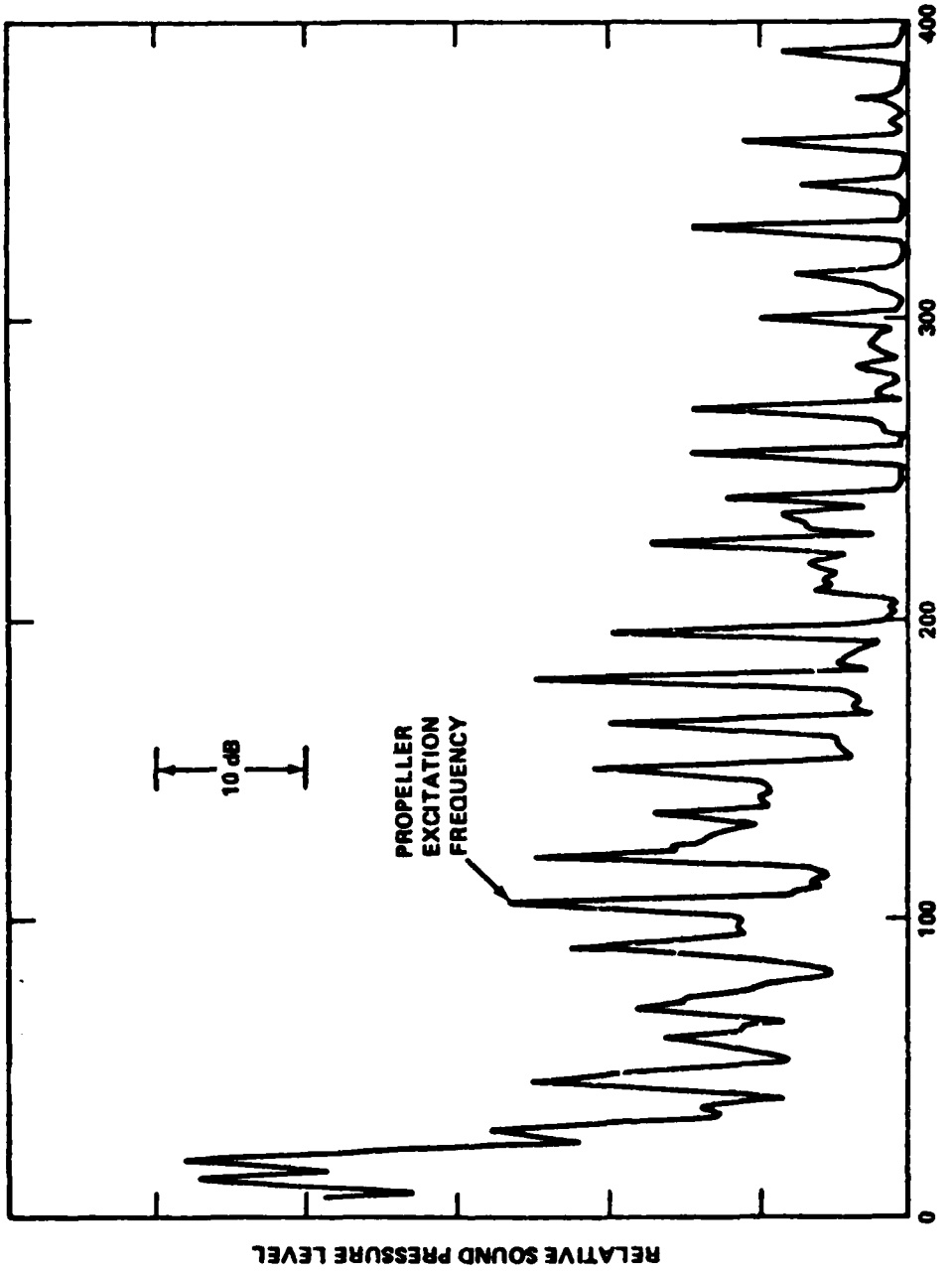

Figure 5b - Typical Pressure Spectrum at the Hydrophone 10 feet from Prop. No. 3956

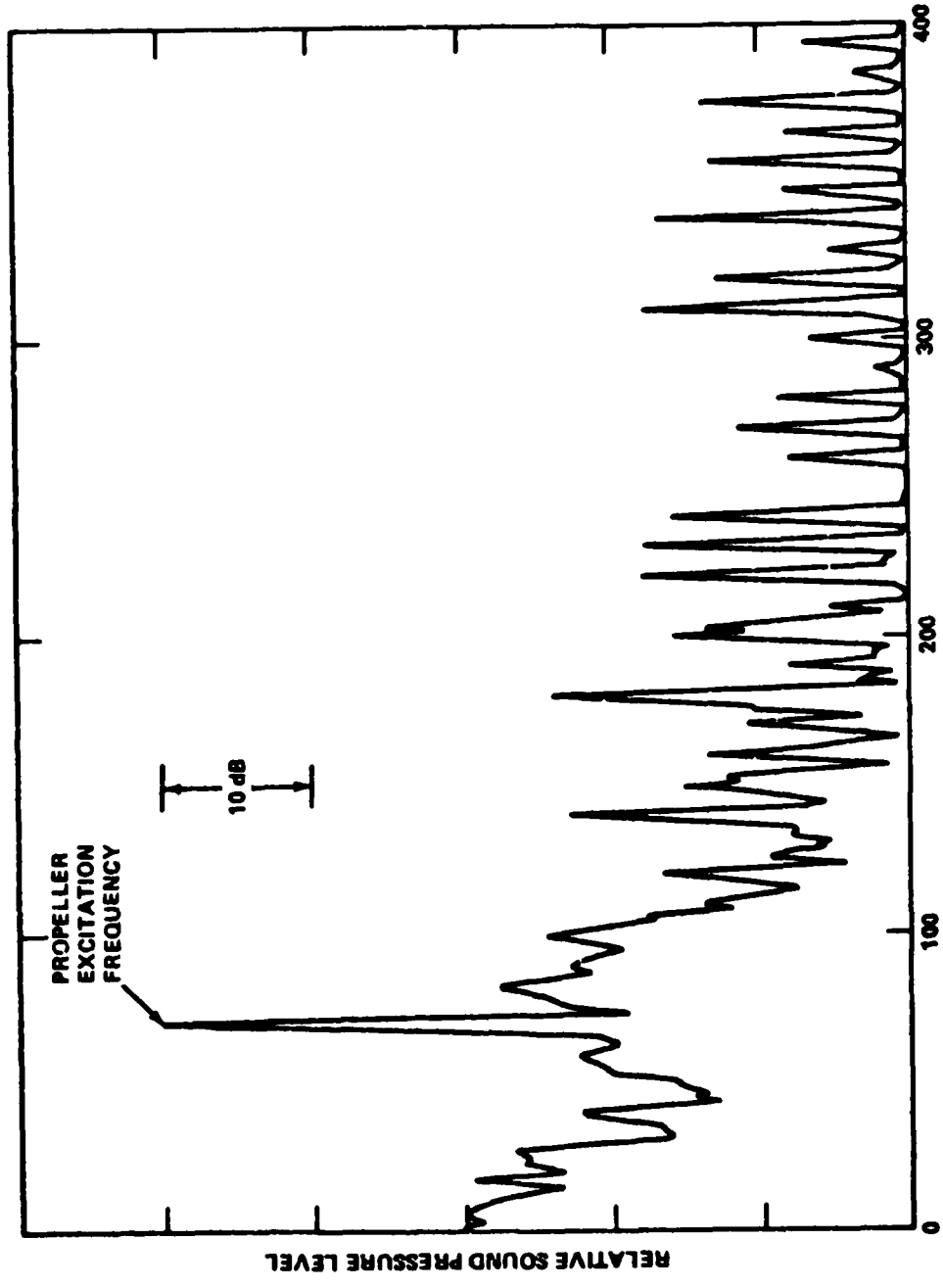

Figure 6 - Typical Pressure Spectrum at the Hydrophone 30 inches from Prop. No. 4064

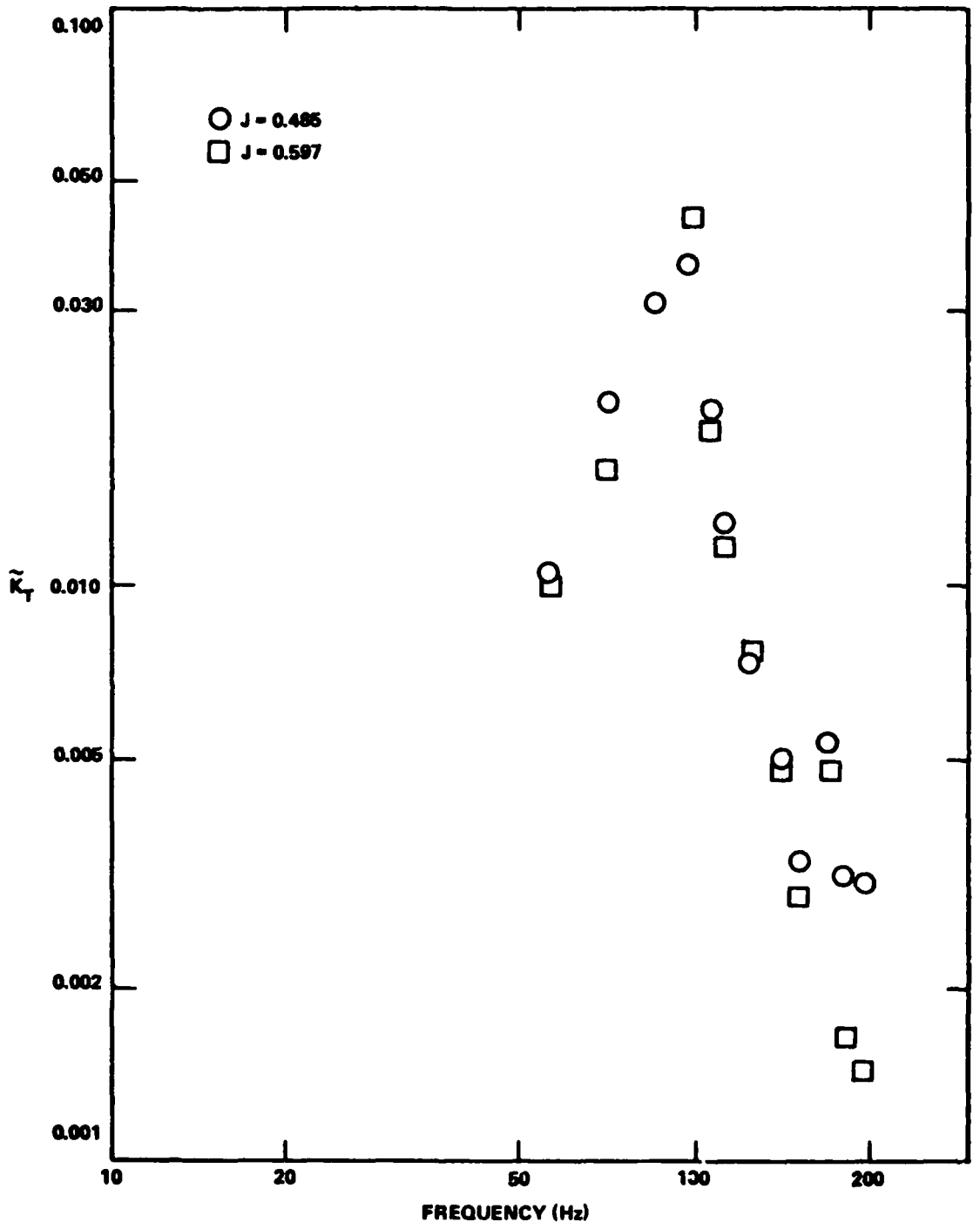

Figure 7 - Nominal Unsteady Thrust Coefficient as Measured by Hydrophone at 30 inches for Prop. No. 4064

TEST FOR NO. 4064 PROPELLER

The DTNSRDC No. 4064 propeller was operated over a large range of shaft rotation frequencies, the upper frequency range of which was limited when the steady torque overloaded the dynamometer. This allowed the exciting frequency to range beyond 200 Hz, spanning the propeller's fundamental resonance frequency. For each shaft frequency, alternating thrust and torque, voltages were measured for two different advance ratios--J=0.597, near zero steady thrust and at J=0.485, where the steady thrust is positive ($\bar{K}_T$=0.05).

With the propeller operating, there is no direct method for measuring the volume mean velocity $\bar{u}_o$. This means there is no direct way for determining the advance ratio, taken here as

$$J = \frac{2\pi \bar{u}_o}{\Omega D} \tag{55}$$

What is commonly done, and was done for this set of tests, is to infer $\bar{u}_o$ from an experimentally determined open water curve relating steady thrust coefficient to advance ratio. This curve is available and is reproduced here as Figure 8. The procedure was to adjust the shaft rotation frequency to the desired value, then slowly vary the water tunnel speed until the measured steady thrust coefficient was zero, to obtain a value J=.597, or until $\bar{K}_T$=.05, to obtain a value J=0.485.

Steady thrust was measured by balancing the forces acting on the shaft against known weights. To separate the portion of the measured force that is due to the action of the propeller blades from those remaining forces acting on the propeller's hub and on the shafting system, a "bladeless propeller", having no blades (but the same hub construction as the test

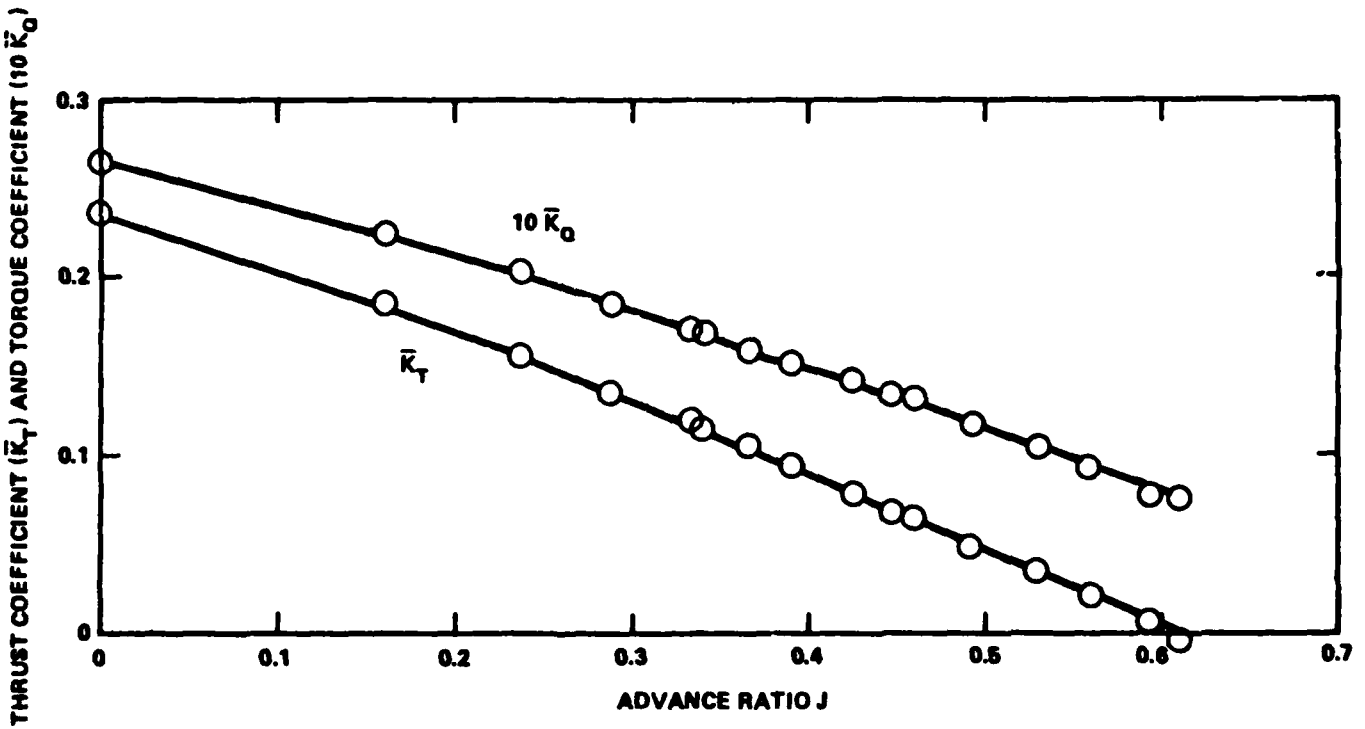

Figure 8 - Open Water Curve for Prop. No. 4064

propeller) was measured under identical flow conditions. This force was then subtracted from the total measured force, giving steady thrust and, therefore, the advance ratio.

Having attained the desired advance ratio, the phase and amplitude of the alternating thrust and torque output voltages were recorded; the signals from the hydrophones were also recorded. Figure 9 gives a typical alternating thrust voltage signal from the dynamometer assembly and its spectrum.

Figure 10 shows the measured unsteady thrust as a function of blade frequency for two advance ratios--J=0.597 where the steady thrust is zero and J=0.485 where the steady thrust coefficient is 0.05. If the blades did not vibrate, the alternating thrust coefficient should be constant, independent of rotational frequency (provided inflow velocity similarity is maintained over all frequencies). Clearly this is not the case here. The thrust coefficient for the J=0.597 case builds up slowly from an apparent low-frequency asymptotic value of about 0.025 to a maximum value of 0.160 at 105 Hz, and then falls off rapidly for higher frequencies. The apparent alternating thrust at the blade resonance frequency is about six times that of a rigid blade. Consequently, the apparent loss factor is about 0.15, much greater than the propeller's measured material loss factor of 0.01, and is presumed to be due to the vibration induced hydrodynamic dissipation discussed in equation (22).

Very similar results were obtained at the lower advance ratio (J=0.485). Unsteady thrust were uniformly smaller over the entire frequency range. Again the maximum thrust coefficient occurred at 105 Hz, but the magnification at the resonance frequency was about 10% greater than that at the higher advance ratio.

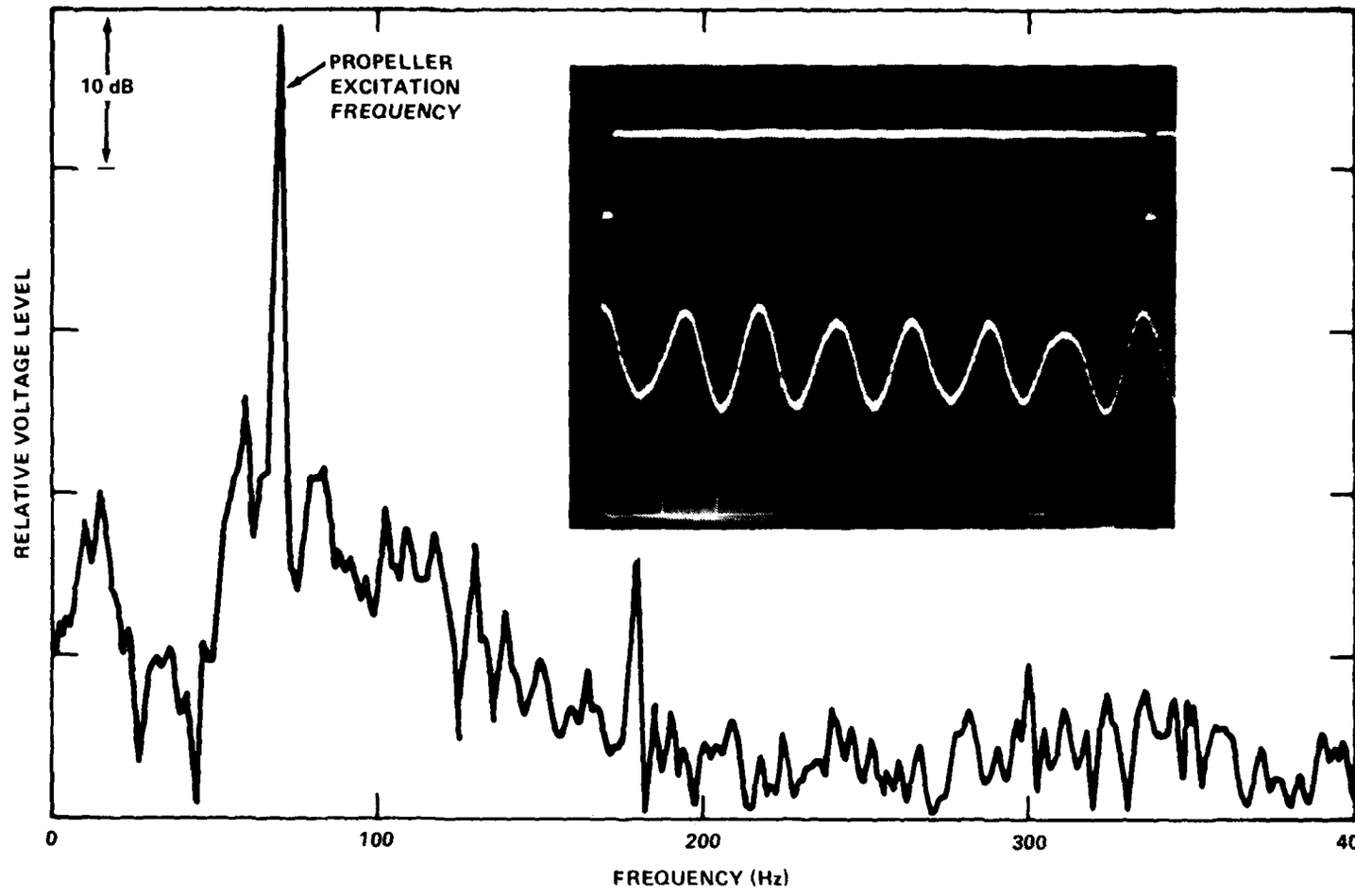

Figure 9 - Typical Alternating Voltage Signal and Its Frequency Spectrum for Prop. No. 4064

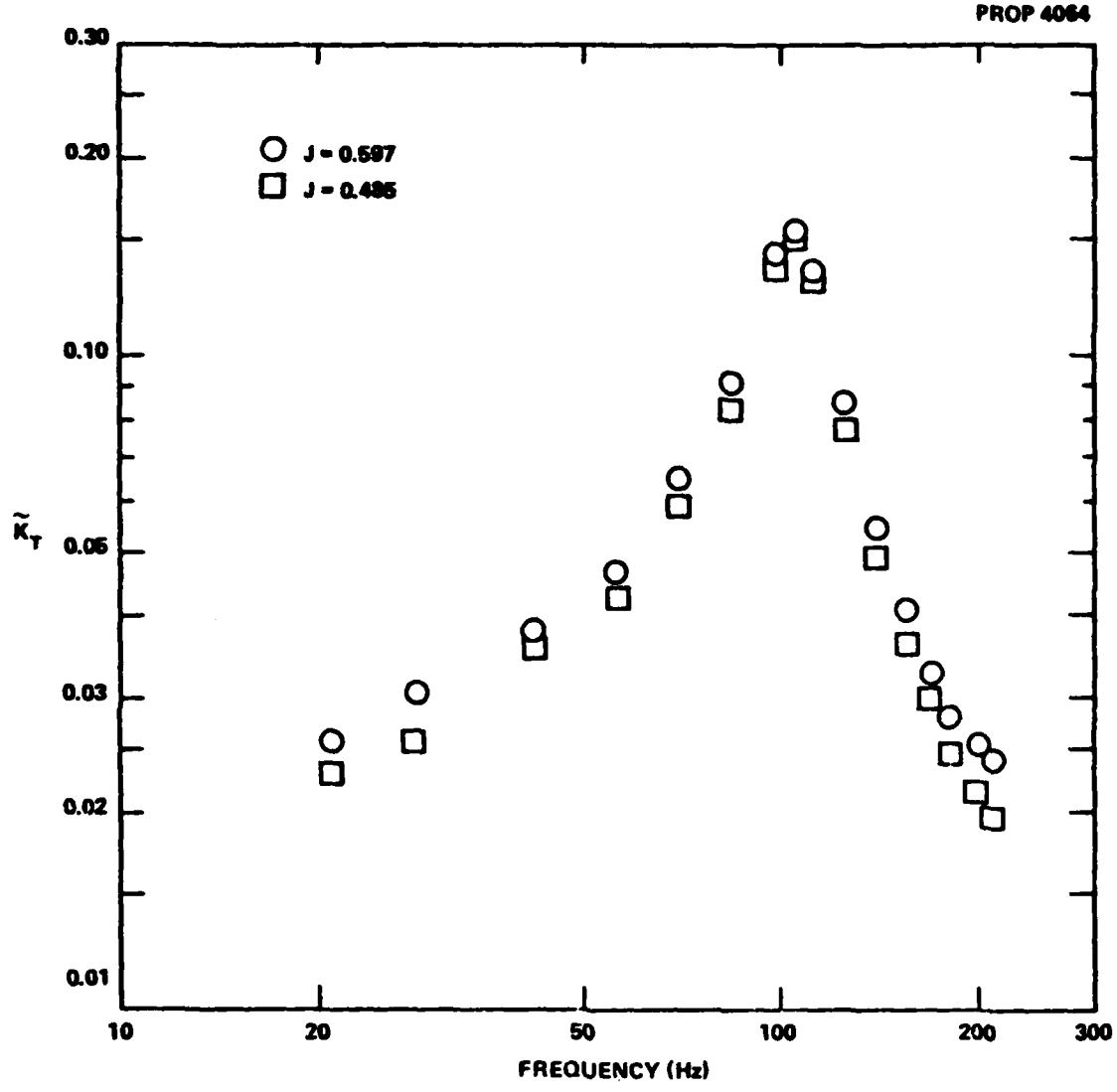

Figure 10 - Measured Unsteady Thrust for Prop. No. 4064

The response curves for unsteady torque were also very similar, as shown in Figure 11. For the J=0.597 case, the unsteady torque coefficient had a maximum value of 0.0175 at 105 Hz and an apparent torque magnification of about 6. For the J=0.485 case, the torques were uniformly smaller and the apparent torque magnification was about 10% greater.

TEST FOR NO. 3956, 3958 PROPELLERS

Both the aluminum (DTNSRDC No. 3956) and the plastic (DTNSRDC No. 3958) propellers operated under identical flow conditions. The excitation frequency ranged up to about 240 Hz. Unsteady thrust and torque were measured, as a function of excitation frequency, for three advance ratios--J=0.76, J=0.67 and J=0.59.

The operating advance ratio could not be determined as it was in the previous test, since there is no available open water curves for either propeller. There is, however, a venturi meter at the water tunnel which measures the difference in pressure (in inches of water ΔH) between two sections of the tunnel with different cross-sectional diameters. This difference is, in turn, a function of the volume mean velocity. What we did was to record ΔH as a function of inferred $\bar{u}_o$ in the test for the No. 4064 propeller. This established a basic relationship between the venturi meter reading and the volume mean velocity into the No. 4064 propeller disk.* To determine the advance ratio, we then assumed that this same relationship held for the two narrow bladed propellers.

---

*The venturi meter was calibrated many years ago by measuring flow velocities with a pitot tube and comparing them to the venturi meter readings. For the same H, the indicated velocities in the present study were 85 percent ($\pm$ 3%) of those indicated by the old calibrations. The lower mean velocities are probably due to the impeding presence of the wake screen.

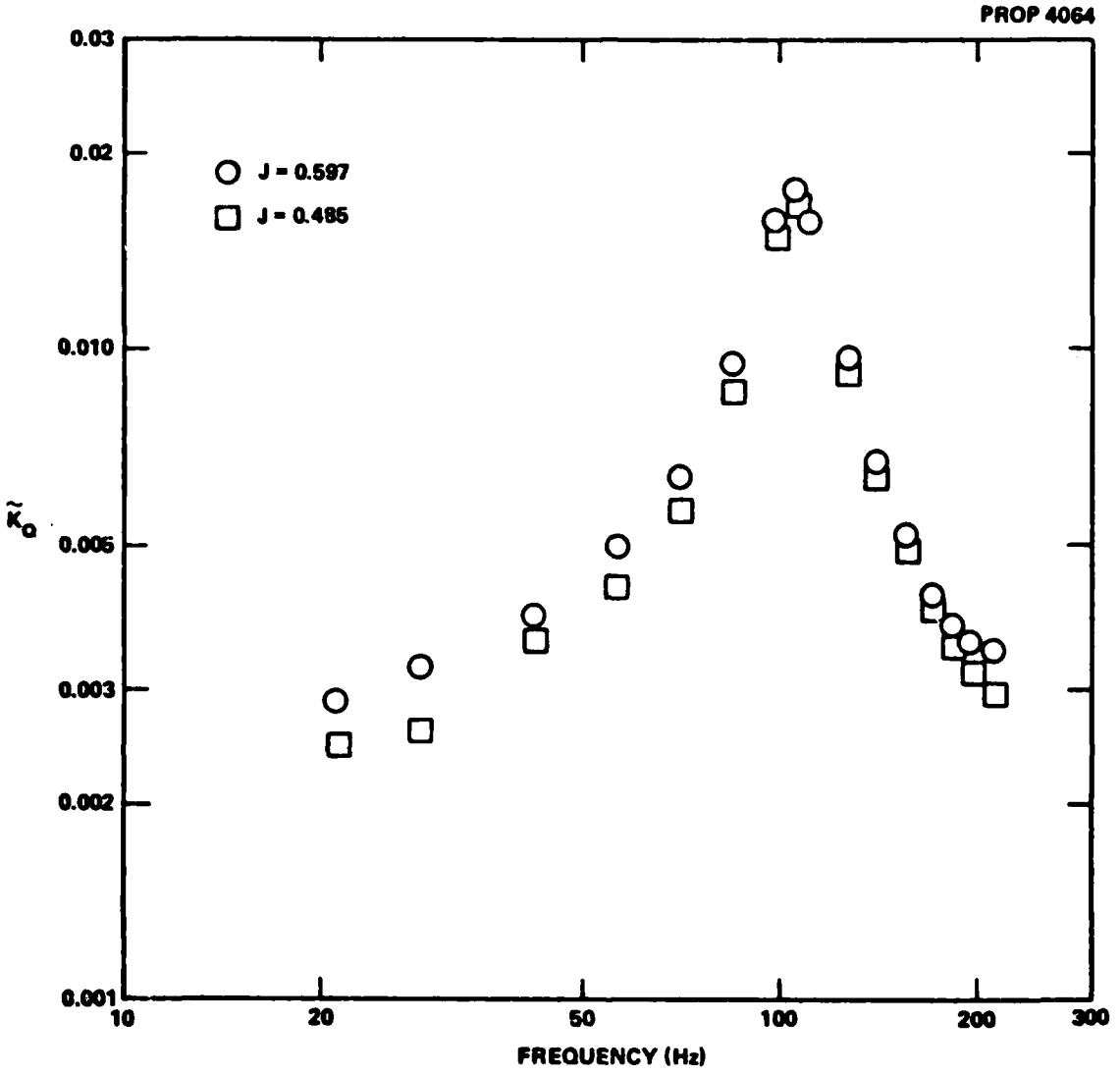

Figure 11 - Measured Unsteady Torque for Prop. No. 4064

The aluminum propeller (No. 3956) was tested first for three different advance ratios, then the plastic propeller (No. 3958) was tested under identical flow conditions. Figure 12 gives the results for J=0.76, a flow condition for which the steady thrust is near zero. Both propellers, as one would expect, have nearly identical unsteady thrusts and torques at the lower frequency end of the response curves. The aluminum propeller, with the much higher resonance frequency, has an almost flat response up to about 150 Hz, and then has a slow increase in both thrust and torque coefficients beyond that point. The plastic propeller exhibits a different response curve. Both the thrust and torque coefficients increase gradually with excitation frequency until about 130 Hz. At this point both the thrust and torques are 42 percent higher than was evidenced by the aluminum propeller. Beyond this frequency the coefficients fall off rapidly; at the highest frequency (196 Hz) they had fallen to 50 percent of the corresponding values for the aluminum propeller.

Results at the two other advance ratios are given in Figures 13 and 14. The response curves are very similar to the J=0.76 case. The unsteady thrust and torque coefficients for the aluminum propeller were fairly constant with frequency, with a slight increase evidenced at the higher frequencies. The alternating thrust and torque coefficients for the plastic propeller increased until they were about 50 percent higher than those for the aluminum propeller, and then decreased dramatically.

Because the necessary flow speeds at these advance ratios are lower than for the J=.76 case, we were able to record the frequency response up to 238 Hz. At this frequency the plastic propeller's unsteady thrust is only 27 percent of that of the aluminum propeller--a marked reduction in unsteady force.

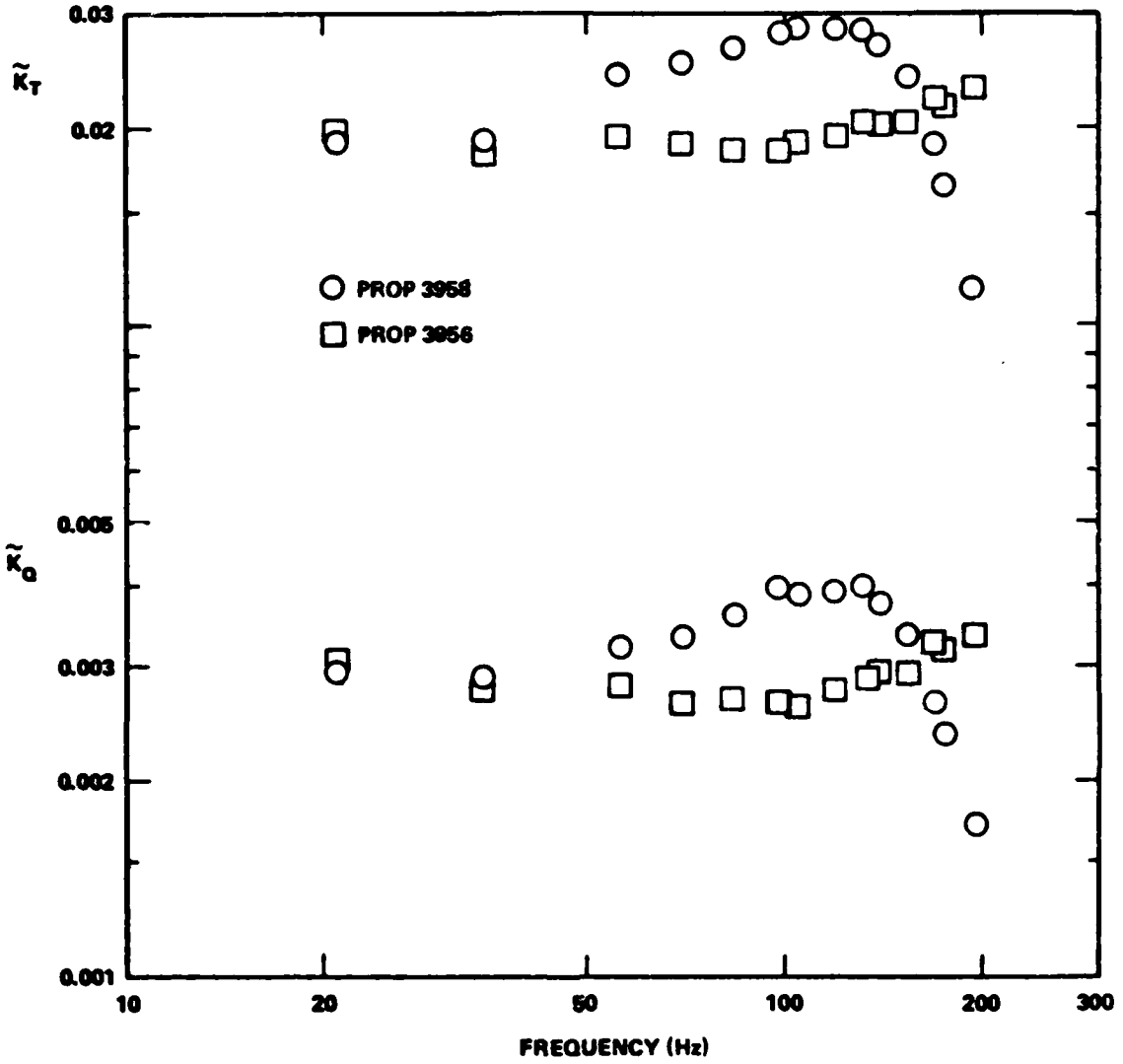

Figure 12 - Measured Alternating Thrust and Torque for Prop. Nos. 3956, 3958, J = 0.76

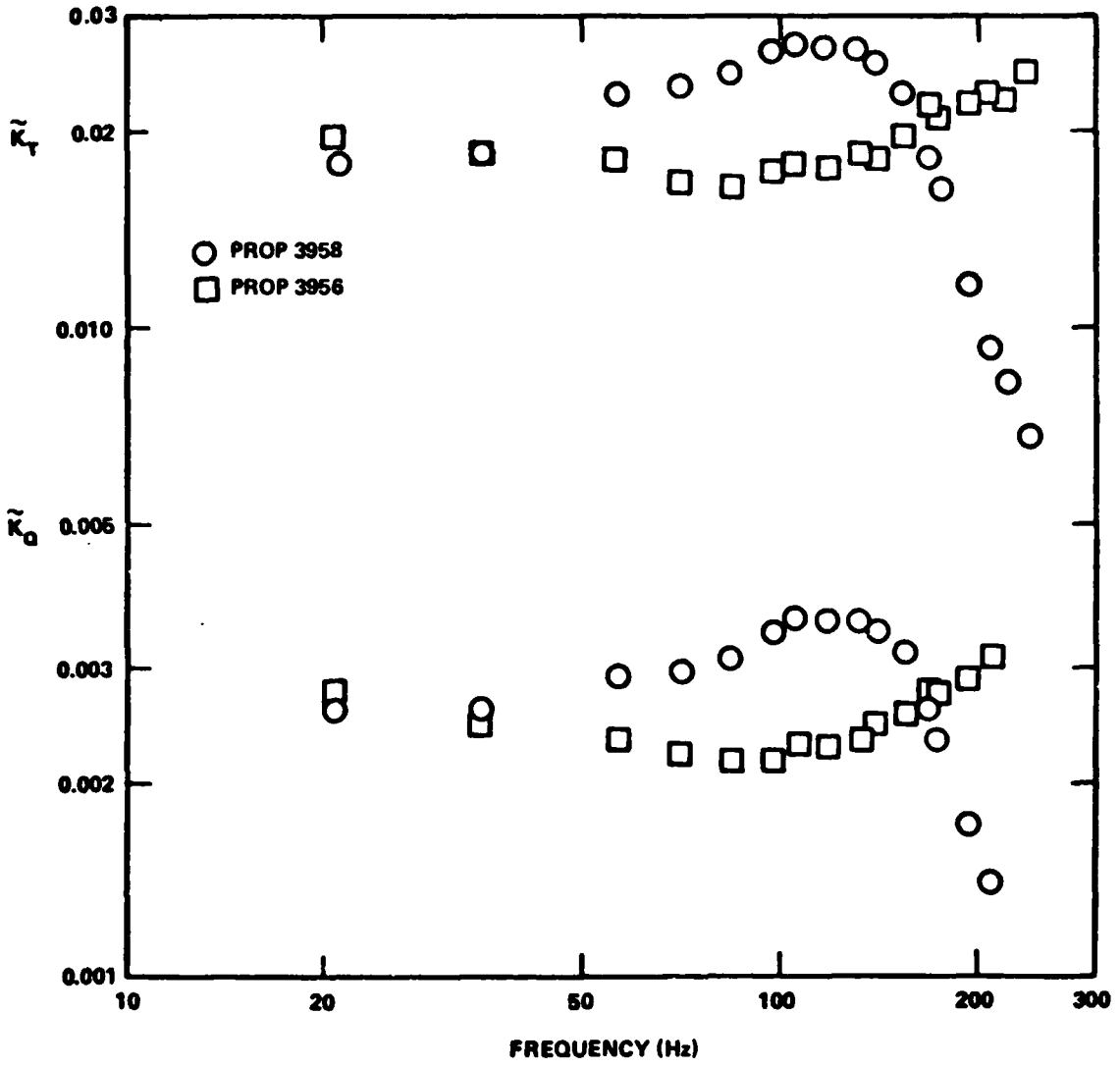

Figure 13 - Measured Alternating Thrust and Torque for Prop. Nos. 3956, 3958, J = 0.67

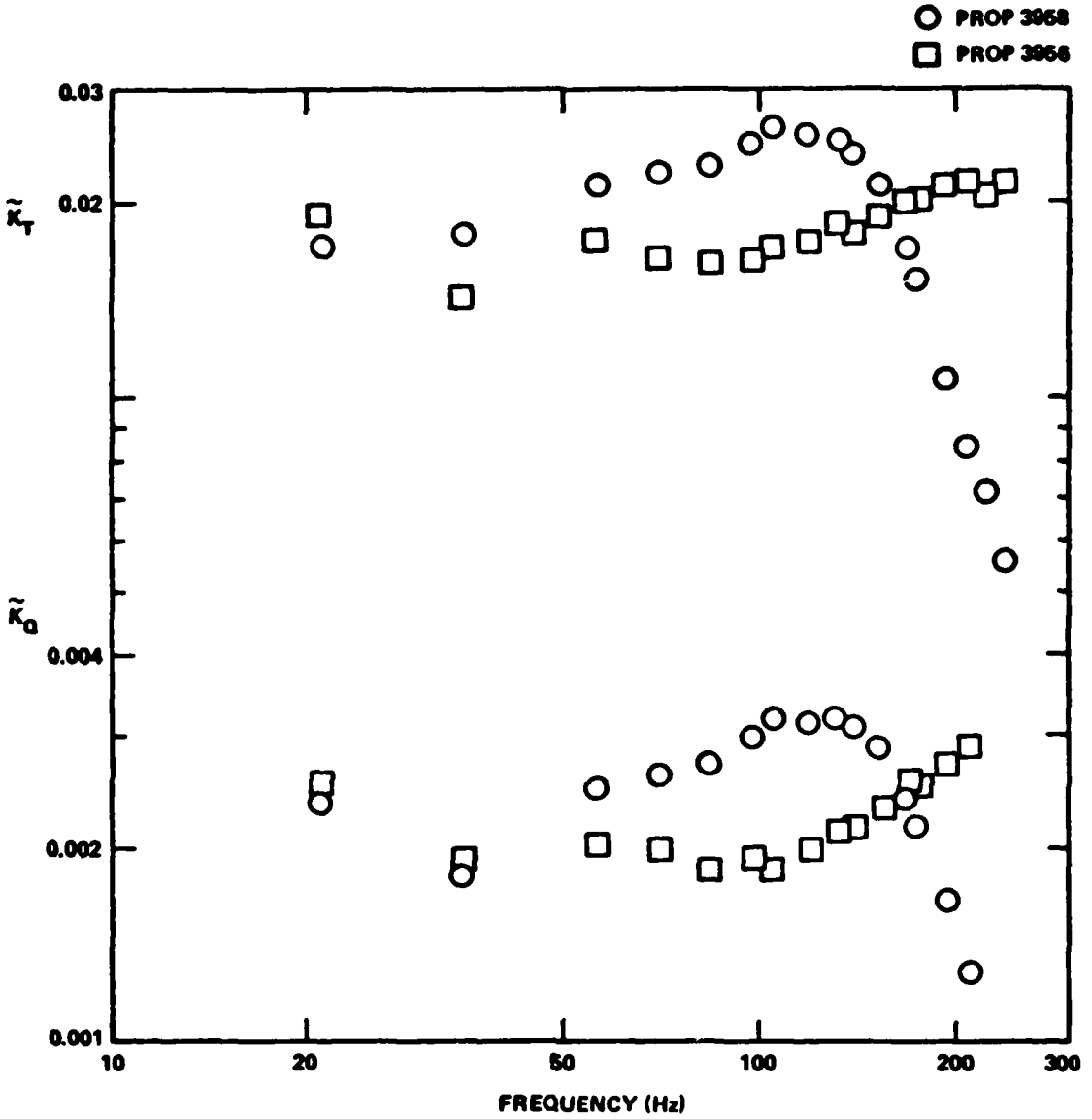

Figure 14 - Measured Alternating Thrust and Torque for Prop. Nos. 3956, 3958, J = 0.59

Before taking the final set of measurements for all three test propellers, certain checkpoint measurements were repeated periodically while the experiment was being "debugged." We noted no more than a ± 5% variation in the day-to-day unsteady thrust and torque readings.

The experimental results for the No. 3958 propeller differed significantly from those of No. 4064. Both evidenced a resonance peak--the wide-blade propeller at 105 Hz and the narrow-bladed propeller at about 130 Hz. But force amplification caused by blade vibration was an order of magnitude larger for the wide-bladed propeller than for the narrow-bladed propeller. The hypothesis is that this response near a propeller's resonance frequency is controlled mainly by the induced hydrodynamic damping factor discussed previously (see equation 26). And that the large difference in force amplification between the two propellers are due to correspondingly large differences ir hydrodynamic damping factors. Calculations in following sections substantiate this hypothesis.

CALCULATION METHOD

Much of the preceding discussion can be summarized by expressing the net vector force (or moment) as a function of its governing variables

$$\vec{F} = \text{func}\left(\text{geometry},\ J,\ \omega,\ \rho_B,\ \omega_{a,i},\ \psi_i,\ p_R,\ \tilde{p}_{V,i}\right) \tag{56}$$

There is no difficulty in specifying the first four functional variables; and the first few in-air mode shapes and resonance frequencies can be measured or estimated separately. The difficulty comes in specifying the hydrodynamic surface pressures. Ruling out direct measurements of these pressures as too difficult a job for most practical applications,* an estimation of the fluctuating surface pressures using propeller theory offers perhaps the best approach. Which one of the many available propeller theories is chosen depends upon the degree of sophistication and accuracy deemed necessary for the particular application, but we should caution that none of even the most encompassing of the existing theories and their accompanying calculation schemes give consistent agreement with experiments.

In the present study both a new three-dimensional propeller theory (described in the next section) and a simpler theory were used to advantage. A simple two-dimensional theory was used initially as a screening device to aid in selecting candidate test propellers. The theory was used to estimate the hydrodynamic damping factor of equation (26). A propeller blade was represented as a long, thin, uncambered wing whose width c was the same as

*Measurements of unsteady surface pressures developed by propeller blades has been recently attempted by Noonan, et al [20].

the propeller's chord at a radius of 70 percent of the blade's tip radius; this wing was given a forward speed of

$$U = \sqrt{(V_a + \bar{u}_o)^2 + (.35\ \Omega D)^2} \tag{57}$$

and it oscillated normally to the forward direction as a rigid body with a frequency $\omega = N_B\Omega$. Then, from a two-dimensional wing theory [2], we can calculate the portion of the unsteady hydrodynamic force which is in phase with the wing's velocity and that which is in phase with its acceleration, and derive the approximation

$$\beta \simeq \frac{2\ \mathrm{Re}\ \{C(\hat{\omega})/\hat{\omega}\}}{\frac{M_B}{M_o} + 1 + 2\ \mathrm{Im}\ \{C(\hat{\omega})/\hat{\omega}\}} \tag{58a}$$

where $\hat{\omega}$ is a reduced frequency $\hat{\omega} = \omega c/2U$ and $C(\hat{\omega})$ is a complex function composed of modified Bessel functions, i.e.,

$$C(\hat{\omega}) = K_1\ (i\hat{\omega})/[K_o\ (i\hat{\omega}) + K_1\ (i\hat{\omega})] \tag{58b}$$

The fraction M_B/M_o is the ratio of blade mass to inertial water mass, where the inertial water mass is $\pi/4\ c^2$ times the length of the blade.

The approximations leading to equation (58) are too crude to be used throughout the present study since they neglect three-dimensional effects, the helical-like geometries of the blade and shed vorticity, interference effects between blades, propeller-blade mode shape, etc. Nevertheless, the equation was useful in selecting two test propellers with a wide variation in hydrodynamic damping factor. Using equation (58), the hydrodynamic damping factor for model propeller No. 3958 was estimated to be quite large ($\beta \simeq 1.1$) and to be much smaller ($\beta \simeq .3$) for model propeller No. 4064. The indication that one propeller has large hydrodynamic damping

and the other small hydrodynamic damping was later confirmed both by the experimental results and calculations based upon a more refined, three-dimensional propeller theory.

As we have illustrated, the propeller-blade vibration theory developed in equations (1) through (40) will accommodate any propeller theory which gives approximate solutions for surface pressures consistent with the boundary conditions of equation (5a) or any of its variations, such as equations (8) and (9). In the following section we briefly outline a new propeller theory developed recently by George Chertock [21]. This theory and its computational scheme were used here to calculate the pressures and forces generated by rigid versions of propellers No. 3958 and 4064 operating in the measured nonuniform inflow velocity fields given in Figure 3. Both were extended to incorporate the propeller-blade vibration theory developed in the present study. The details of these extensions are also included in the discussion below.

CHERTOCK'S PROPELLER THEORY WITH EXTENSION TO BLADE VIBRATION PROBLEMS*

The propeller theory recently developed by Chertock, along with its associate computer program, give the steady and unsteady pressures, forces and moments generated by a rigid marine propeller as it operates in a flow with small spatial variations of axial inflow velocity. An inflow velocity is assumed of the specific form

$$\vec{u} = u_o(r) + u_m(r) \cos(m\varphi + \varepsilon)\,\hat{z} \qquad (59)$$

where $u_m << u_o$, and u_o, u_m, and ε can all vary with radius. The propeller can have arbitrary pitch, chord, skew, camber, thickness and number of blades.

The theory assumes that the induced flow field is inviscid and irrotational for all points outside the propeller and its wake. This allows the induced flow field to be constructed using the mathematical tools of potential flow theory. The boundary condition is that there is no flow into the propeller or into its hub, and that there are no nearby surfaces. An additional condition is imposed on the flow field which is equivalent to a Kutta condition in wing theory. The assumption is that the flow velocity at the trailing edge, relative to an observer on the moving blade, has no component normal to the median surface of the blade. And that each propeller blade sheds a thin, quasi-helicoidal sheet of vorticity which

---

*The material in this section is adapted from a soon-to-be published paper by Chertock and Brooks [21]. The Chertock theory was developed for rigid propellers, but the extension to vibrating blades (or any other condition leading to a linear normal velocity boundary condition) is simple and easily included in a description of his theory.

moves with the mean inflow velocity and does not roll up. This Kutta condition is applied to both unsteady as well as steady flow situations in the theory.

The flow field satisfying these conditions is approximated by assuming the flow induced by the propeller is the same as that from a layer of normal dipoles on the median surface of each blade and a layer of dipoles normal to each blade's wake. These dipoles vary with time and position. In the Chertock theory the induced flow results only from the interaction of the (rigid) propeller and the inflow velocity. This situation is modeled by a single dipole distribution $\mu_R(\vec{S},t)$. To include the additional flow resulting from blade vibration, we need to modify the boundary condition and take two distributions of dipoles. We take $\mu(\vec{S},t)$ as the total instantaneous dipole density on the (time-averaged) median surface, then

$$\mu(\vec{S},t) = \mu_R(\vec{S},t) + \mu_V(\vec{S},t) \tag{60}$$

where μ_V is the dipole distribution resulting from blade vibration. The instantaneous dipole densities μ_R are calculated from the integral equation

$$-\iint \mu_R \, E \, d\sigma = \hat{n}' \cdot [V_a \, \hat{z} - u_o \, \hat{z} + \vec{\Omega} \times \vec{S}' - u_m \cos(m\theta + m\Omega t + \epsilon) \, \hat{z}] \tag{61}$$

which says that the velocity field induced by all the dipole densities is such that, relative to an observer moving with a propeller blade, there is no normal component of fluid velocity at the outer surfaces of the (rigid) propeller blade. In equation (61) the fixed angle φ has been reexpressed in a frame rotating with the blade ($\varphi = \theta + \Omega t$). The right-hand side of

this equation is the component of the inflow velocity at $(\vec{S}',t)$ (relative to a frame rotating with blade) in the $\hat{n}'$ direction normal to the outer surface at $\vec{S}'$. $E(\vec{S}',\hat{n}';\vec{S},\hat{n})$ is the (negative) induced velocity in the $\hat{n}'$ direction at $\vec{S}'$, due to unit dipole density, in $\hat{n}$ direction, over area $d\sigma$ at $\vec{S},t$. The integration is over the median (cambered) surface of each blade and each wake. An integral equation, like (61) is solved for each point $\vec{S}'$.

The kernel function E, which can be interpreted as a Green's function, can be written in a very simple form

$$E = \frac{\partial^2}{\partial n' \partial n}\left(\frac{1}{4\pi D}\right) = \frac{(\hat{n}'\cdot\hat{n}) - 3(\hat{n}\cdot\hat{D})\ (\hat{n}'\cdot\hat{D})}{4\pi D^3} \qquad (62)$$

where $\vec{D} = \vec{S}' - \vec{S}$. Note that E depends critically on the angles between the three directions, $\hat{n}$, $\hat{n}'$, and $\hat{D}$, and varies at $1/D^3$. This means that its numerical value drops off very quickly with distance and changes rapidly with changes in direction. Hence, the average value, averaged over the element $d\sigma$ about the source point, depends critically and in a complicated way on the shape of the source element $d\sigma$.

The instantaneous dipole distribution μ_V is calculated from a similar integral equation.

$$-\iint \mu_V\, E\, d\sigma = \dot{q}_i \psi_i\, \hat{n}'\cdot\hat{\delta}_i$$

$$- q_i\, (\vec{V}_a + \vec{\Omega}\times\vec{S}' - \vec{u}_o)\cdot \nabla_{tan}\, \psi_i\, (\hat{n}'\cdot\hat{\delta}_i) \qquad (63)$$

where the integration is over the time-averaged median surface. Also, following the approximation of equation (52), we ignore the tangential component of displacement.

The linearized boundary conditions from equation (5b), which are incorporated in the integral equations (61) and (63), can be written as a sum of one time-independent part and four time-dependent parts

$$g_o(\vec{S}') + g_R^c(\vec{S}') \cos m\Omega t + g_R^s(\vec{S}') \sin m\Omega t + g_V^c(\vec{S}') \cos(m\Omega t + \phi) + g_V^s(\vec{S}') \sin(m\Omega t + \phi) \tag{64}$$

Since the integral equations are linear, it is convenient to take $\mu(\vec{S},t)$ in five parts

$$\mu(S,t) = \mu_o + \mu_R^c \cos m\Omega t - \mu_R^s \sin m\Omega t + \mu_V^c \cos(m\Omega t + \phi) - \mu_V^s \sin(m\Omega t + \phi) \tag{65}$$

and to solve five integral equations for five parts μ_o, μ_R^c, μ_R^s, μ_V^c, μ_V^s at every field point $\vec{S}'$ on every blade and on every point in the wake of every blade.

$$\iint \mu_o E \, d\sigma = n' \cdot [\hat{z} u_o - \hat{z} V_a - \vec{\Omega} \times \vec{S}'] \tag{66}$$

$$\iint \mu_R^c E \, d\sigma = (\hat{n}' \cdot \hat{z}) u_m \cos(m\theta + \varepsilon) \tag{67}$$

$$\iint \mu_R^s E \, d\sigma = (\hat{n}' \cdot \hat{z}) u_m \sin(m\theta + \varepsilon) \tag{68}$$

$$\iint \mu_V^c E \, d\sigma = q_{o,i}(V_a \hat{z} - u_o \hat{z} + \vec{\Omega} \times \vec{S}') \nabla_{tan} \psi_i (\hat{n}' \cdot \hat{\delta}_i) \tag{69}$$

$$\iint \mu_V^s E \, d\sigma = - m\Omega \, q_{o,i} \psi_i (\hat{n}' \cdot \hat{\delta}_i) \tag{70}$$

The integral equations need only be solved on one blade and along the beginning of the wake adjacent to the trailing edge of one blade, since the dipole density at the remaining points are determined by symmetry and conservation arguments. The dipole distribution μ_R is completely specified by equations (64), (65) and (66). Equations (69) and (70) are solved taking $q_{o,i}$ equal to unity. The dipole distribution μ_V then requires knowing the modal displacement amplitude $q_{o,i}$ and the modal phase angle ϕ.

The instantaneous linearized pressure difference across the propeller blade at each station is constructed from the difference in velocity potential $\nu(\vec{S},t)$ across the blade. The difference in velocity potential is approximated by

$$\nu(\vec{S},t) = \nu_o + \nu_R^c \cos m\Omega t - \nu_R^s \sin m\Omega t$$

$$+ \nu_V^c \cos (m\Omega t + \phi) - {}^{s}_{V} \sin (m\Omega t + \phi) \qquad (71)$$

where

$$\nu_o \simeq \mu_o - 2h\, g_o$$

$$\nu_R^c \simeq \mu_R^c - 2h\, g_R^c \qquad \nu_V^c \simeq \mu_V^c - 2h\, g_V^c$$

$$\nu_R \simeq \mu_R - 2h\, g_R^s \qquad \nu_V^s \simeq \mu_V^s - 2h\, g_V^s \qquad (72)$$

and where 2h is the local blade thickness. The expression for the pressure comes from a particular version of Bernoulli's equation. This requires differentiation of the difference in velocity potential in the chordwise and spanwise directions at every station on one blade do get the difference in tangential velocity across the blade.

The difference in pressure across the blade is taken as the sum of a steady and four time-dependent parts

$$\Delta p = \Delta p_o + \Delta p_R^c \cos m\Omega t - \Delta p_R^s \sin m\Omega t$$

$$+ q_{o,i} \Delta \hat{p}_V^c \cos (m\Omega t + \phi) - q_{o,i} \Delta \hat{p}_V^s (m\Omega t + \phi) \qquad (73)$$

The modal quanities $q_{o,i}$ and ϕ are calculated after the pressure distributions on the rigid blade Δp_R^c and Δp_S^s are calculated [c.f. eqs. (28), (29) and (30)].

The steady component of the pressure difference is

$$\Delta p_o = \rho[V_a \hat{z} - u_o \hat{z} + \vec{\Omega}\times\vec{S}]\cdot\nabla_{tan} \nu_o \qquad (74)$$

which depends on the difference in the steady induced tangential components of velocity.

The unsteady (rigid) components are in phase with either cos $m\Omega t$ or sin $m\Omega t$, and each has an integral part proportional to a local "added mass" and a part dependent upon the differences in steady and unsteady induced tangential velocities,

$$\Delta p_R^c = \rho m\Omega \nu_R^s + \rho (V_a \hat{z} - u_o \hat{z} + \vec{\Omega}\times\vec{S})\cdot\nabla \nu_R^c$$

$$- \rho u_m \cos (m\theta + \varepsilon)\cdot\nabla \nu_o \qquad (75)$$

$$\Delta p_R^s = - \rho m\Omega \nu_R^c + \rho (V_a \hat{z} - u_o \hat{z} + \vec{\Omega}\times\vec{S})\cdot\nabla \nu_R^s$$

$$- \rho u_m \sin (m\theta + \varepsilon)\cdot\nabla \nu_o \qquad (76)$$

The unsteady (blade vibration) components are in phase with either cos ($m\Omega t+\phi$) or sin ($m\Omega t+\phi$) and have similar "added mass" and unsteady induced tangential velocity contributions,

$$q_{o,i}\ \Delta\hat{p}_v^{nc} = \rho m\Omega\ \nu_V^s + \rho(V_a\ \hat{z} - u_o\ \hat{z} + \vec{\Omega}\times\vec{S})\cdot\nabla\ \nu_V^c \tag{77}$$

$$q_{o,i}\ \Delta\hat{p}_v^{ns} = -\rho m\Omega\ \nu_V^c + \rho(V_a\ \hat{z} - u_o\ \hat{z} + \vec{\Omega}\times\vec{S})\cdot\nabla\ \nu_V^s \tag{78}$$

The net vector force on one blade due to the total induced pressure field is then

$$\vec{F} = \iint \Delta p\hat{\zeta}d\sigma_{median} = \vec{F}_o + \vec{F}_c\ \cos m\Omega t + \vec{F}_s\ \sin m\Omega t \tag{79}$$

where the integration extends over the median surface of one blade and $\hat{\zeta}$ is the local unit normal at the median surface. And the net vector moment on one blade from the induced total pressure field is

$$\vec{M} = \iint \Delta p\ (\vec{S}\times\hat{\zeta})\ d\sigma_{median} = \vec{M}_o + \vec{M}_c\ \cos m\Omega t + \vec{M}_s\ \sin m\Omega t \tag{80}$$

Both the force and moment have a steady component and two time-dependent components in phase with either cos $m\Omega t$ or sin $m\Omega t$. To get the net axial force and torque on all blades, the axial force and torques on one blade are multiplied by the number of blades. And to get side forces and moments they are multiplied by half the number of blades.

The Chertock theory, in previous studies, was used to calculate the added mass of elliptical and rectangular disks in ideal potential flow, without circulation, and shows agreement within, say, one percent with exact calculations or other numerical calculations [22]. Such problems are solved by computer program by treating the disks as specially shaped propellers,

omitting the vortex wake that accounts for the circulation forces and using an appropriate inflow velocity distribution. The program was also used to calculate the non-circulating potential flow about two model propellers [23]. But a systematic comparison of the complete Chertock theory with experimental measurements, where they exist, is not complete as yet.

SYNOPSIS OF NUMERICAL METHOD*

To solve these integral equations with their troublesome singular kernels and geometric complications, finite element-type methods are used. Typically, 150 stations are selected on the median surface of each blade, with an additional 10 to 20 stations per blade to cancel flow into the hub. From 200 to 400 stations are selected on the trailing wake which extends downstream as a semi-infinite helicoid. The propeller median surface and a portion of the wake region, roughly one propeller radius in width, are divided into compact areas about their included stations. The dipole densities are assumed to be constant over each element of area. And, after accounting for all the symmetries in the problem, the set of integral equations is converted into a set of matrix equations of 1000 equations with 1000 unknowns. The area elements are taken to be regular hexagons, of equal area, except around the blade's leading and trailing edge. At the border of the blade, the elements are irregular polygons which are sections of regular hexagons. The remainder of the wake is divided into semi-infinite helical strips, each having 8 to 16 stations spaced according to a Laguerre integration scheme. Figure 15 shows a mapping of these hexagon locations in a mathematical plane representing the expanded median surface of the blade.

---

*Details of the numerical method and computer program are in a soon-to-be published paper by Chertock & Brooks [21].

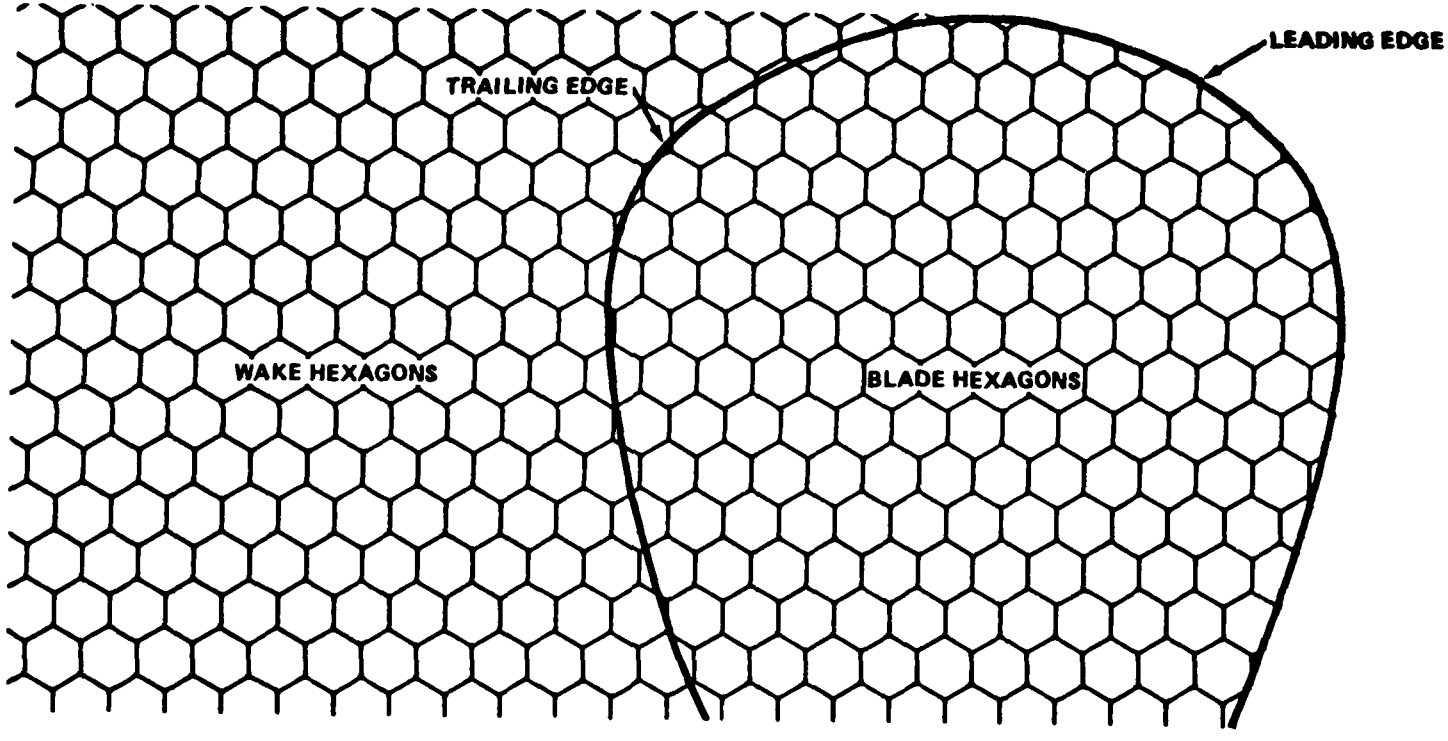

Figure 15 - Hexagon Mapping of Prop. No. 4064 Expanded Blade Midsurface

Breaking the blade's median surface and its adjacent wake region into regular hexagons is only one of several ways to partition these surfaces. Hexagons are advantageous because they "almost" fill all space on the median surface of the blade without overlapping. Also, very simple formulas for calculating the E function coefficients in the matrix are obtained when the source element is a hexagon, and these formulas are virtually independent of direction for all practical orientations. In addition, for the partial hexagon elements at the blade boundaries, very good approximations for E are obtained by replacing these elements by circles of equal area and a further approximation which depends on the closeness to the boundary.

Integration, such as that in equation (79), is done by summation over all blade stations, adding the product of station pressure difference and vector area ($\hat{\zeta}d\sigma$). Differentiation, as in equations (63) and (74-78), is done in two (spanwise and chordwise) directions using 3 or 5 point numerical differentiation formulas for each direction.

The input data for the calculation are the same small set of numerical specifications for pitch, camber, thickness, chord length, skew, and rake that are used to prepare the construction drawings of the propeller. Also required are the specified values for the advance coefficient and the mean and periodic components of the inflow velocity at, say, 5 to 10 different radii. Hence, the preparation of the input data requires only a matter of minutes. Otherwise, all calculations of the position, size, and inclination of each hexagon and the detailed inflow velocity to each hexagon are done automatically. The matrix equations are solved by iteration rather than by a direct method. The solutions converge to within 0.1 percent in 10 to 30 iterations depending on the square of the number of elements, and normally there is no problem with stability. The time for a

complete calculation with, say, 2800 stations on the CDC 6700 System is 8 or 10 minutes, but it would take less than a quarter of this time to make a complete calculation for an additional set of inflow velocities on the same propeller. These times vary principally as the square of the number of elements of area.

In a typical calculation sequence, a calculation for no circulation is made first. The calculaton is made for the same inflow conditions and advance ratio as measured during the experiment, using the same procedures as the full calculation with circulation, except that contributions from shed vorticity are neglected. Alternating thrust, alternating torque and other hydrodynamic quantities are calculated for this case by taking the propeller to be first rigid and then flexible. It is advisable to refine and gain confidence in this calculation before proceeding to the full calculation, which includes the shed vorticity, because it exercises most of the calculation procedures, allowing input and execution errors to be spotted in a cheaper and simpler format. Also, the sensitivity of calculated forces to the size and details of the hexagon grid is easier to assess in this case.

After a satisfactory selection of grid size is made and the "bugs" are exorcised from the calculation for no circulation, the full calculation, including the wake vorticity, is made. In the phase, we test the sensitivity of the calculated results to the number and density of integration points in the vortex wake. This issue is resolved and convergence is guaranteed to within one percent for the present propellers by taking a wake strip of complete hexagons equal in length to the propeller's tip radius and then approximating the rest of the infinite wake by 16 Laguerre integration points.

DTNSRDC propeller No. 3958 (and 3956) was modeled by dividing its expanded area into 20 rows along the radius. There were 156 hexagons on a blade of which 23 were incomplete hexagons along the leading edge and 23 along the trailing edge. And each row in the wake had 23 hexagons in the near region and 16 points spaced along the strip subtending one propeller revolution. Because of blade's symmetries and conservation of vorticity in the wake, the total number of unknown dipoles which are solved in one matrix equation reduces to 222.

The wide-bladed propeller (No. 4064) was modeled by dividing its expanded area into 15 rows along the radius (see Figure 15). On a blade, there were 138 complete hexagons, 20 incomplete ones along the leading edge and 19 along the trailing edge. Again in the wake, there were 16 points along a strip extending downstream one propeller revolution, and 18 complete hexagons in wake's near region. One matrix equation contained 228 unknown dipole densities.

CALCULATED RESULTS AND COMPARISON WITH EXPERIMENT

In this section and the following one we present the main body of the calculated results and compare them with experimental measurements wherever possible. Most of the calculations in this section use the one-mode inertial approximation for unsteady thrust and torque given in equations (42) and (43).

PROP NO. 4064

Some of the important calculated hydrodynamic quantities for Prop No. 4064 are listed in Table 3.

TABLE 3. - SOME CALCULATED RESULTS FOR PROP NO 4064

J	M_1/M_B	β_1	$(\tilde{K}_T)_{Rigid}$	$(\tilde{K}_Q)_{Rigid}$
.485	10.7	.208	.0221	.00212
.597	10.7	.210	.0265	.00252

We see that the calculated added water mass for the first mode is more than 10 times the blade mass, resulting in a predicted resonance frequency $f_{w,1} \simeq 104$ Hz, some 4 percent smaller than the measured frequency when the propeller vibrated in still water. The hydrodynamic damping factor, which controls the blade response near resonance, is 30 percent less than that predicted by the simple two-dimensional theory discussed earlier, and decreases slightly with increasing steady thrust (or decreasing J).

We also made two calculations for unsteady thrust and torque for a rigid version of this propeller using the analysis and computer program of Tsakonas [4]. The program is available at DTNSRDC, and since it is presently the most highly regarded calculation method within the naval architectural community, it is desirable to establish a checkpoint by comparing our present calculation for a rigid propeller with the Tsakonas calculation. The Tsakonas calculation was made, for this propeller as well as for Propeller No. 3956, by diving the blade surface into 8 radial strips and approximating the distribution in pressure difference across the surface by a 5 term Birnbaum series which gives a zero pressure difference at the blades' trailing edge and results in a square-root singularity at the leading edge. For J=.485 the Tsakonas calculation has $(\tilde{K}_T)_{Rigid} = 0.0316$ and $(\tilde{K}_Q)_{Rigid} = 0.00325$, 45 and 55 percent higher than that calculated using the Chertock analysis, and also higher than the low-frequency values (approximating a rigid condition) recorded during the experiment. For J=.597 the Tsakonas calculation gives $(\tilde{K}_T)_{Rigid} = 0.0385$ and $(\tilde{K}_Q)_{Rigid} = 0.00408$, also higher than the Chertock calculation and the experimental values by about the same amounts as in the smaller advance ratio case.

The calculated rms vibration velocity

$$v_{rms} = \sqrt{\iiint dV \; q_{o,1}^2 \; \psi_1^2 \omega^2 / V} \tag{81}$$

as a fraction of the mean volume inflow velocity, is shown in Figure 16. Almost identical frequency dependence is evidenced at the two advance ratios. Since the calculated added mass and hydrodynamic damping factor are about the same at the two advance ratios, and since we expect the modal driving force $Q_{oR,1}$ to be approximately proportional to the advance ratio, it is not surprising that, substantially, the same functional relationship

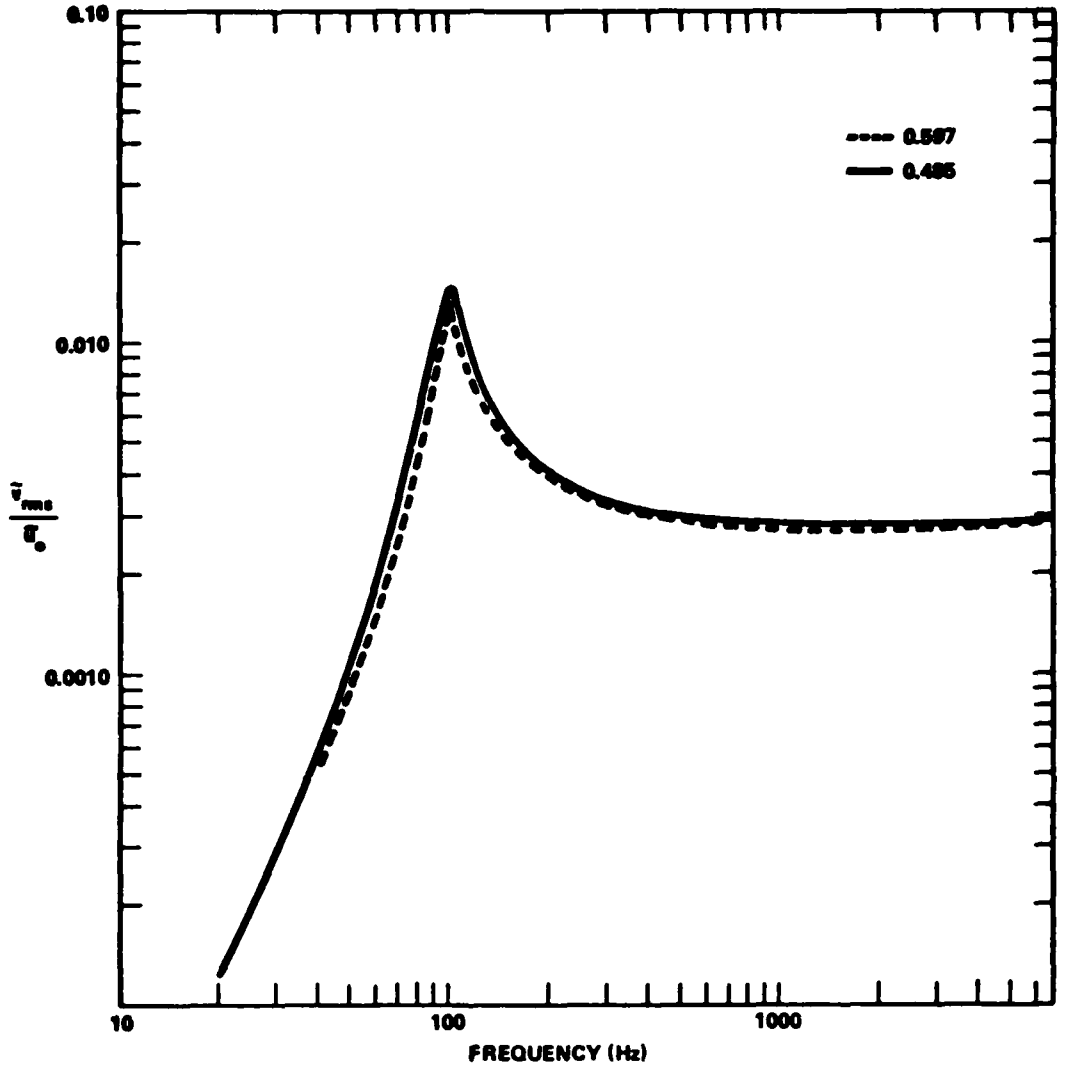

Figure 16 - Calculated Normalized Propeller RMS Vibration Velocity as a Function of Excitation Frequency for Prop. No. 4064. $\bar{v}_{rms}$ Is the Average Root-Mean-Square Vibration Velocity for Mode 1 - Average Over the Blade Volume - and $\bar{u}_o$ Is the Mean Volume Inflow Velocity

is obtained. It is interesting that near resonance the tip vibration velocity $\omega q_{o,1}\psi_1 (R_{tip}) \simeq .196\ \bar{u}_o$ has about the same magnitude as the measured amplitude of the nonuniform inflow velocity produced by the wake screen.

In the next four figures we have the main results--a comparison of calculated and experimental alternating thrust and torque coefficients as a function of excitation frequency, with coefficients calculated by assuming that only the fundamental mode of vibration contributes to the blade vibration. Figure 17 shows the unsteady thrust comparison for the J=.485 case. The calculated unsteady thrust coefficient has a low-frequency value of 0.0221 (approximating a rigid propeller), shows a sharp resonance at 101 Hz where it equals 0.111, then declines smartly beyond this frequency to an asymptotic value of 0.00778, about one-third the low-frequency value. The calculated values are uniformly smaller than the experimental values, although the predicted and measured frequencies of maximum amplification match to within a few percent. The calculated force magnification--over that of a rigid propeller--near resonance is 5.0, about 20 percent smaller than the apparent magnification indicated in the experiment. In the low-frequency (rigid) range the agreement is within 10 or 15 percent. The calculated resonance peak is 66 percent of its experimental counterpart. Both the calculated and experimental values track one another fairly well up to about 150 Hz, with the calculated thrust capturing the main element of the experimental results--the sharp resonance near 105 Hz. However, the one-mode calculation shows that, for sufficiently high excitation frequency, an elastic propeller could have smaller unsteady forces and moments than its rigid counterpart. This effect could not be verified by the experiment because we could not go to high enough frequencies in the experiment.

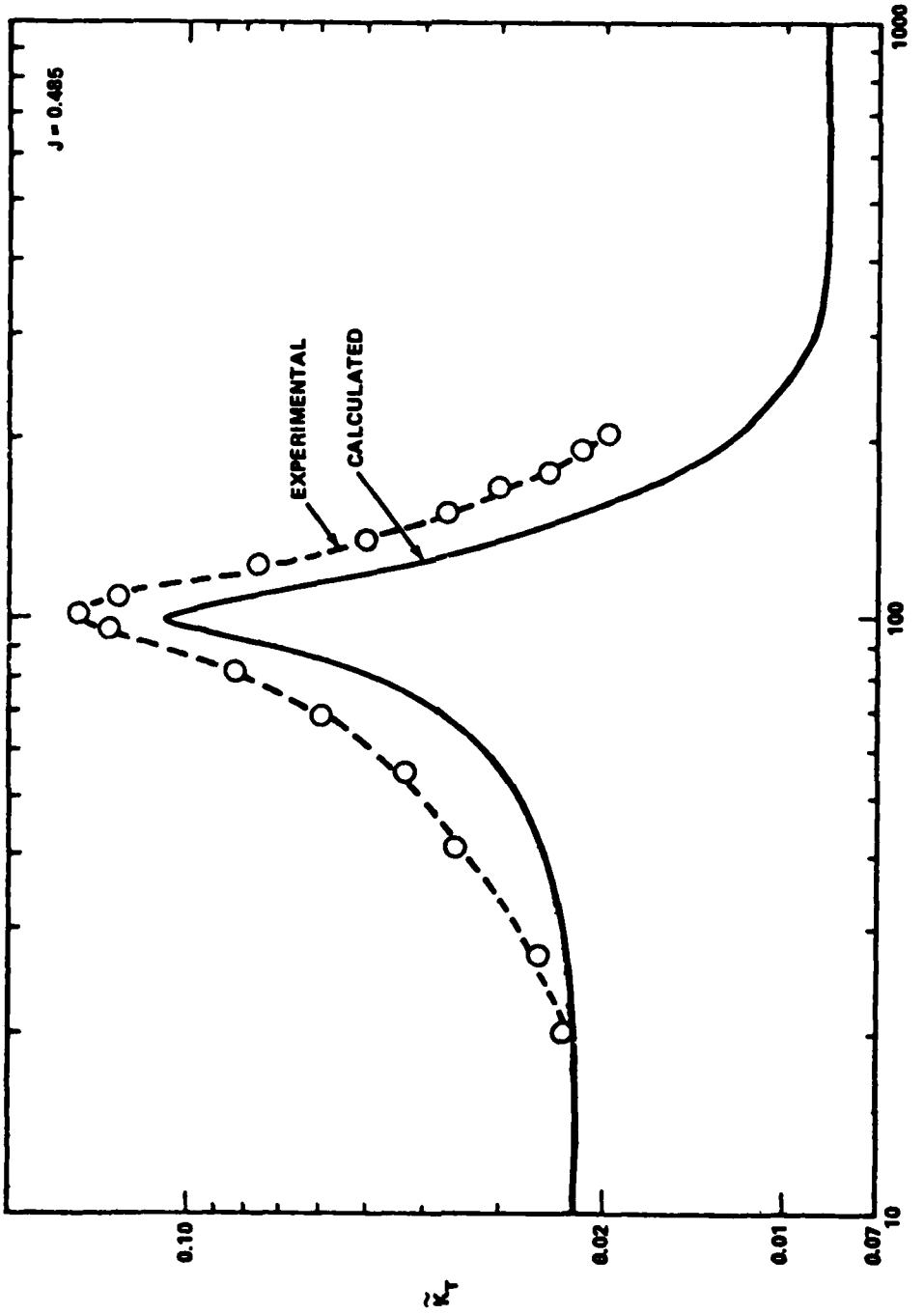

Figure 17 - Comparison of Calculated and Experimental Alternating Thrust for Prop. No. 4064 at J = 0.485

The calculated alternating torque coefficient has a similar behavior with excitation frequency; there is a sharp resonance at 101 Hz with a torque magnification of 5.4 (see Figure 18). This compares favorably with the experimental resonance at 105 Hz and torque magnification of 6.5. The calculated peak value is 70 percent of the experimental peak value. The higher frequency values of the coefficient do not agree as well. The calculated results show that a reduction in alternating thrust (over that for a rigid propeller) is possible at a higher loading frequency, while there is no indication of this in the experiment, again, possibly because of the limitations in the experimental frequencies.

Figure 19 compares calculated and measured unsteady thrust coefficient at J=0.597, where the steady thrust is zero. Overall, the one-mode inertial calculation agrees slightly better with experiment at this advance ratio than at the smaller advance ratio; the calculated peak value is 16 percent smaller than the measured value, and the calculated thrust magnification is 4.9 compared to the apparent experimental magnification of 6.2. Qualitatively, the alternating thrust and torque (shown in Figure 20) have the same overall frequency behavior as the previous advance ratio, and demonstrates similar agreement with the experiment.

PROP NO. 3958 (AND 3956)

A listing of important calculated quantities, similar to those in Table 3, are given in Table 4. We see that, in contrast with our experience with Prop No. 4064, the added mass, as well as the hydrodynamic damping factor for the first mode, increases slightly with advance ratio. The fundamental resonance frequency, as we have defined it in equation (25), occurs at a nominal frequency of 193 Hz, 20 percent larger than the measured or

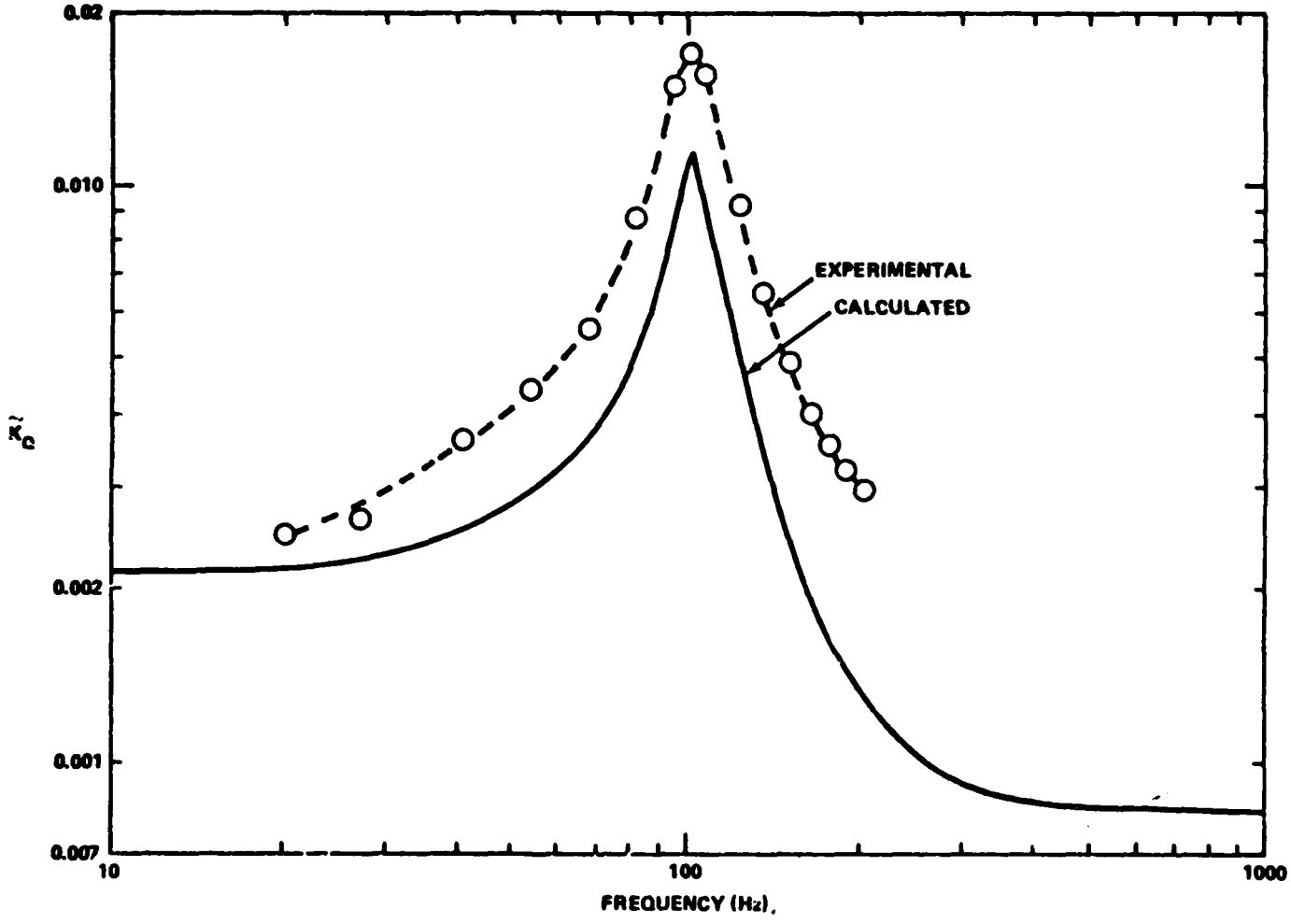

Figure 18 - Comparison of Calculated and Experimental Alternating Torque for Prop. No. 4064 at J = 0.485

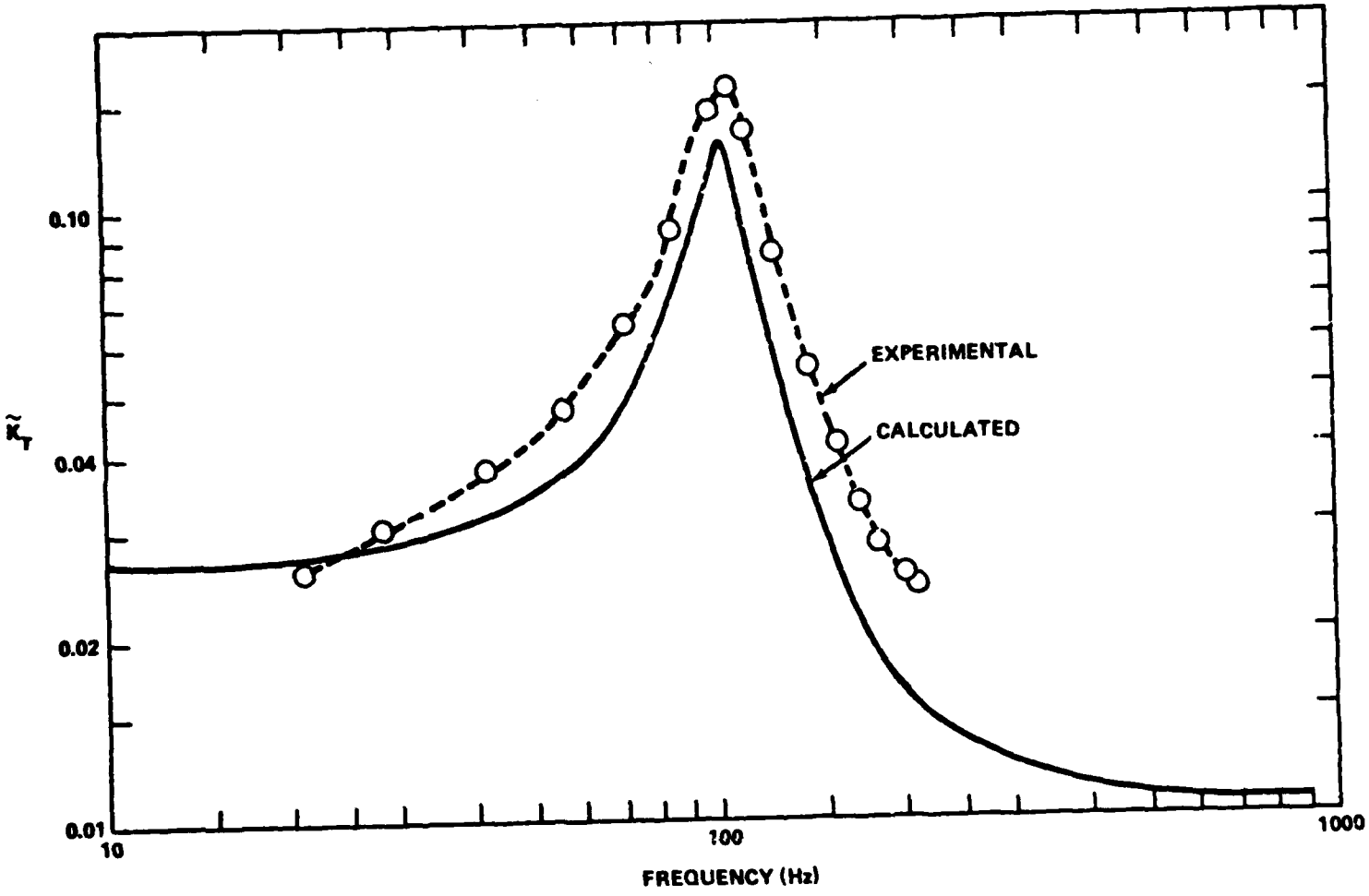

Figure 19 - Comparison of Calculated and Experimental Alternating Thrust for Prop. No. 4064 at J = 0.597

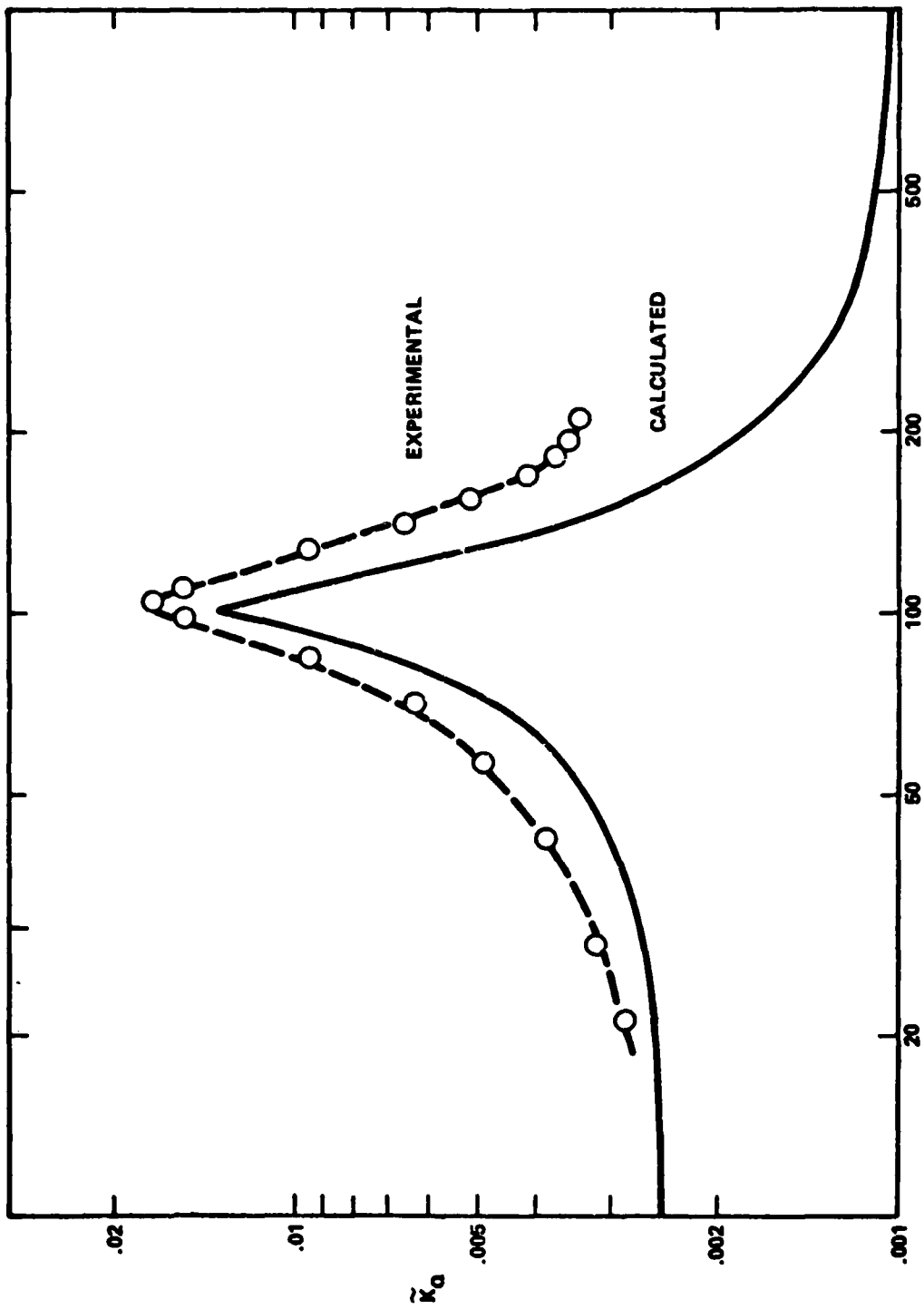

Figure 20 - Comparison of Calculated and Experimental Alternating Torque for Prop. No. 4064 at J = 0.597

calculated still-water frequency. Also the calculated β_1's confirm that the damping is quite large for this propeller, as we estimated by the two-dimensional theory.

TABLE 4. - SOME CALCULATED RESULTS FOR PROP NO 3958

J	M_1/M_B	β_1	$(\tilde{K}_T)_{Rigid}$	$(\tilde{K}_Q)_{Rigid}$
.59	4.03	1.25	.0147	.00195
.67	4.11	1.26	.0178	.00236
.76	4.17	1.28	.0213	.00284

In Figure 21 we present both experimental and calculated values of unsteady thrust and torque as a function of advance ratio for the aluminum (rigid) propeller No. 3956 at a shaft rotation frequency of 15 rps. The calculated thrust coefficient (see Figure 21a) agrees with the experimental results to within 20 percent over the range of advance ratios--the calculated value is 15 percent smaller at J=.59, is 2 percent larger at J=.69 and is 20 percent larger at J=.76. Even though the individual calculated and experimental values agree, the slopes do not. The difference is unexplained except to note that different experimental slopes are possible at other shaft rotational frequencies (see Figures 12, 13, 14). The calculated unsteady torques agree much better with experiment in both amplitude and slope (see Figure 21b)--the calculated unsteady torque coefficients are between 5 and 10 percent than experiment and have the same slope.

Also shown in Figure 21 are the results of the Tsakonas calculation for unsteady thrust and torque. The unsteady thrusts are about 10 percent

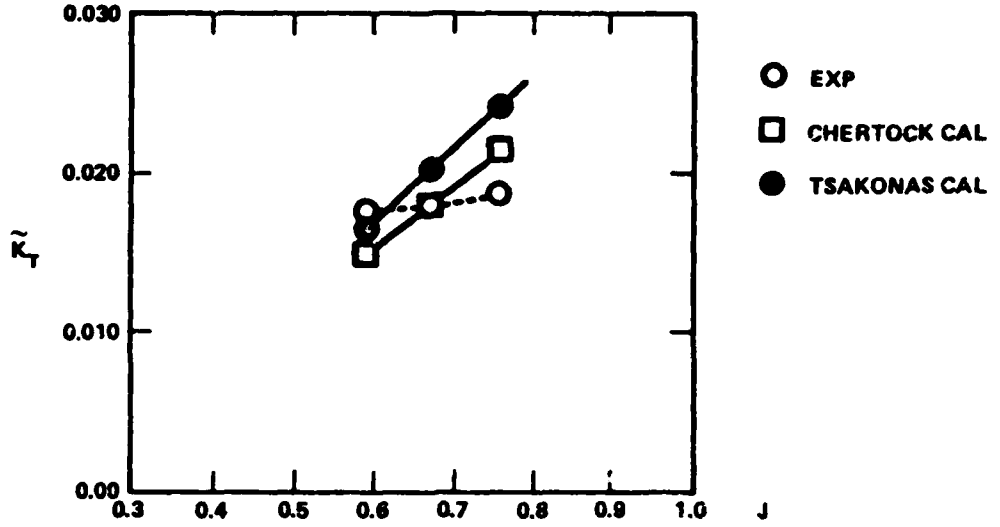

Figure 21a - Comparison of Calculated and Experimental Alternating Thrust for Prop. No. 3956 (Rigid)

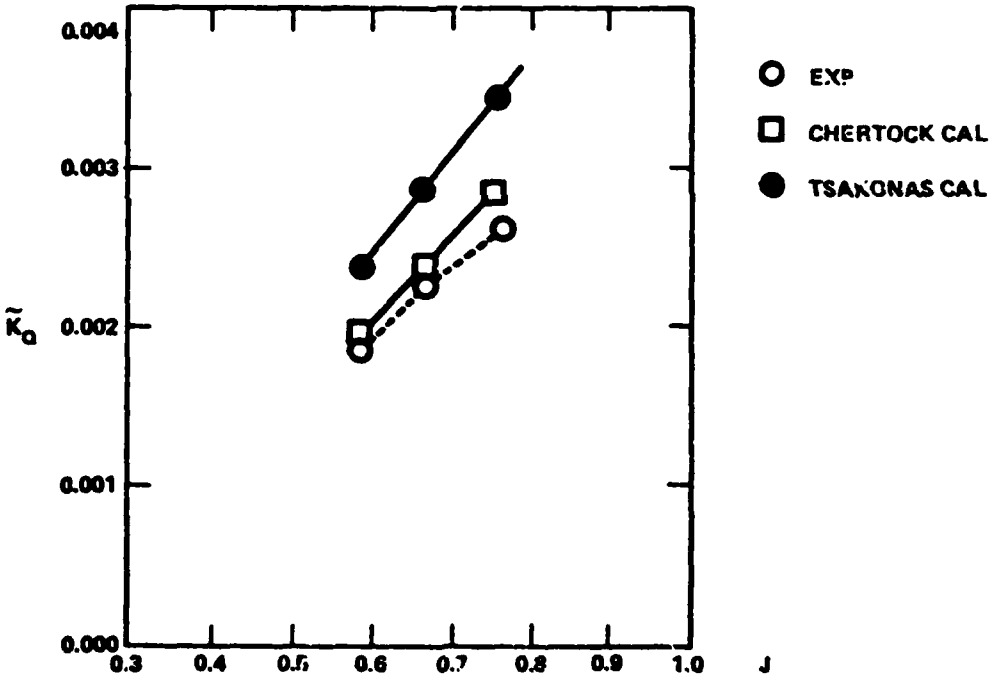

Figure 21b - Comparison of Calculated and Experimental Alternating Torque for Prop. No. 3956 (Rigid)

larger than those from the Chertock analyses, and the unsteady torque are 25 percent larger. The Tsakonas results give the same slope as the present calculation.

The calculated rms vibration velocity, as defined in equation (81), as a fraction of mean volume inflow velocity, is given in Figure 22. As is the case with the wide-bladed propeller, almost identical frequency dependence is obtained at the three calculated advance ratios. Near resonance the normalized tip vibration velocity is 0.126 for J=.76 and slightly smaller at the other two advance ratios. Because of the much larger damping factor, the blade velocities exhibit less peakedness near resonance than is the case for the wide-blade propeller.

A comparison of calculated and measured unsteady thrust and torque coefficients at an advance ratio of 0.76 is given in Figure 23. The results of the one-mode inertial calculation show the coefficients are almost constant with frequency up to about 100 Hz, rapidly decreasing with increasing frequency until about 200 or 250 Hz, and then leveling off to 40 or 50 percent of the low-frequency values. The same basic pattern is repeated at the two other advance ratios (see Figures 24 and 25). Although the calculated unsteady thrusts and torques agree with experiment to within 10 or 15 percent at the low frequency values, and they do confirm the experimental observation that the maximum thrust and moment coefficients are only somewhat larger than those produced by rigid blades, the details of the calculated curve shapes do not agree exactly with experiment. The calculated maximum thrust and torque occur at about 100 to 115 Hz, slightly less than the 120 to 140 Hz range evidenced in the experiment. The maximum calculated alternating thrusts are only about 10 percent greater than their low-frequency values, while in the experiment the force amplification was about

AD-A086 482 DAVID W TAYLOR NAVAL SHIP RESEARCH AND DEVELOPMENT CE--ETC F/G 20/4
VIBRATIONS OF A MARINE PROPELLER OPERATING IN A NONUNIFORM INFL--ETC(U)
APR 80 J E BROOKS
UNCLASSIFIED DTNSRDC-80/056 NL

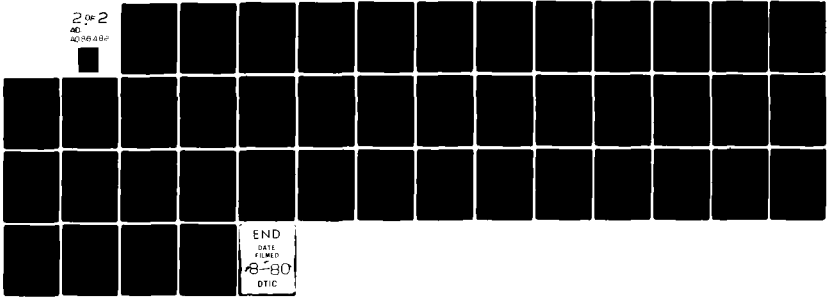

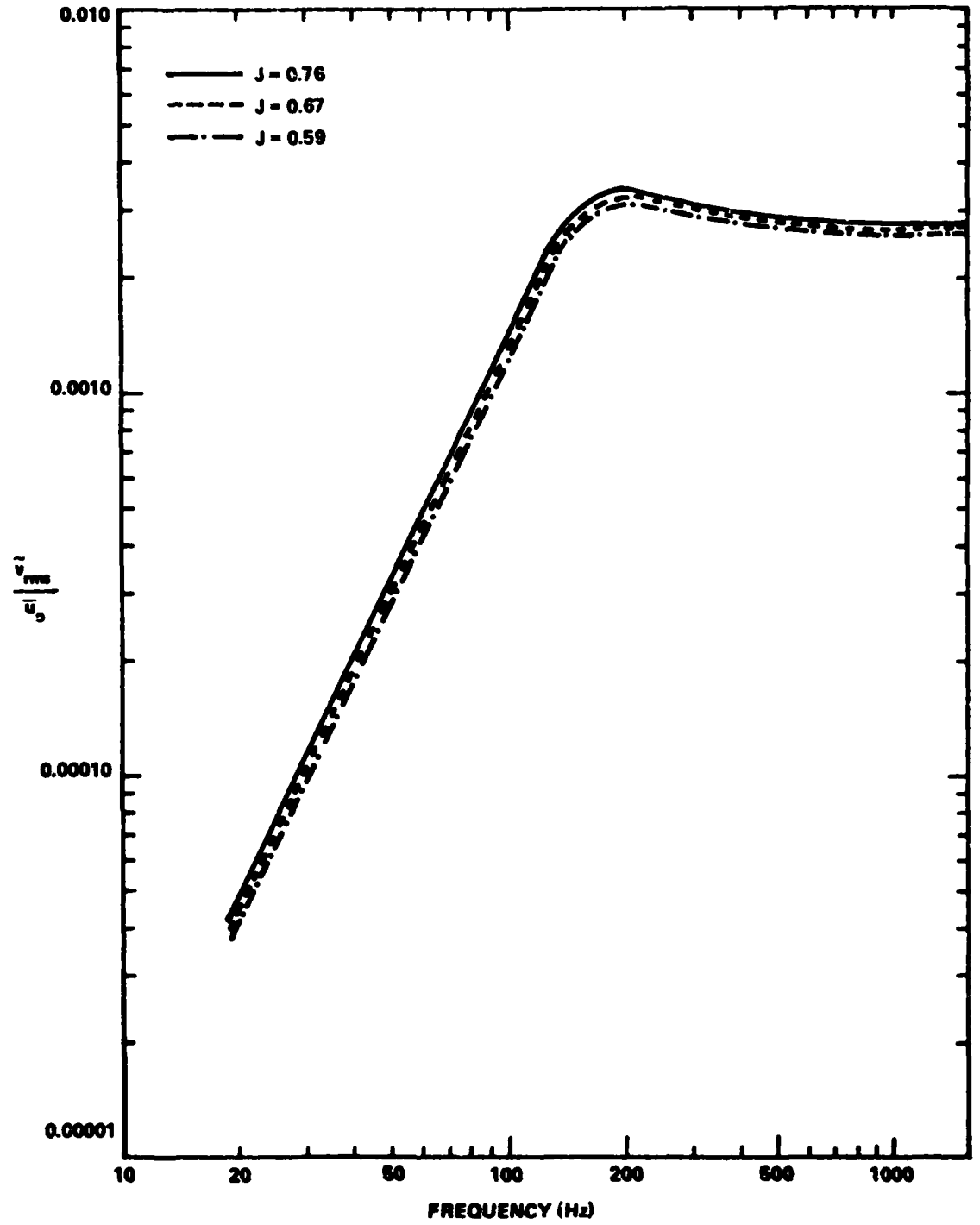

Figure 22 - Calculated Normalized Propeller RMS Vibration Velocity as a Function of Excitation Frequency for Prop. No. 3958

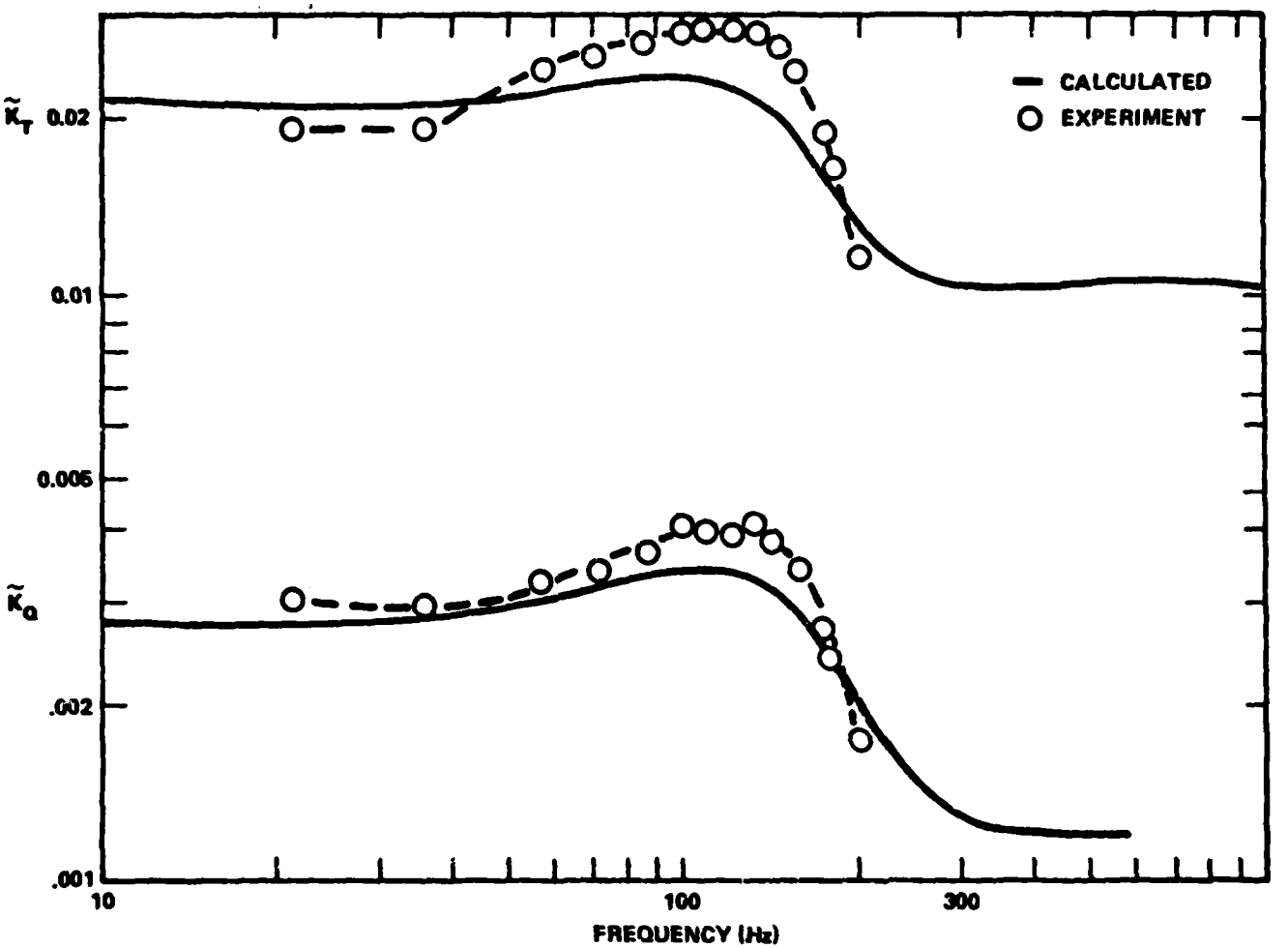

Figure 23 - Comparison of Calculated and Experimental Unsteady Thrust and Torque for Prop. No. 3958 at J = 0.76

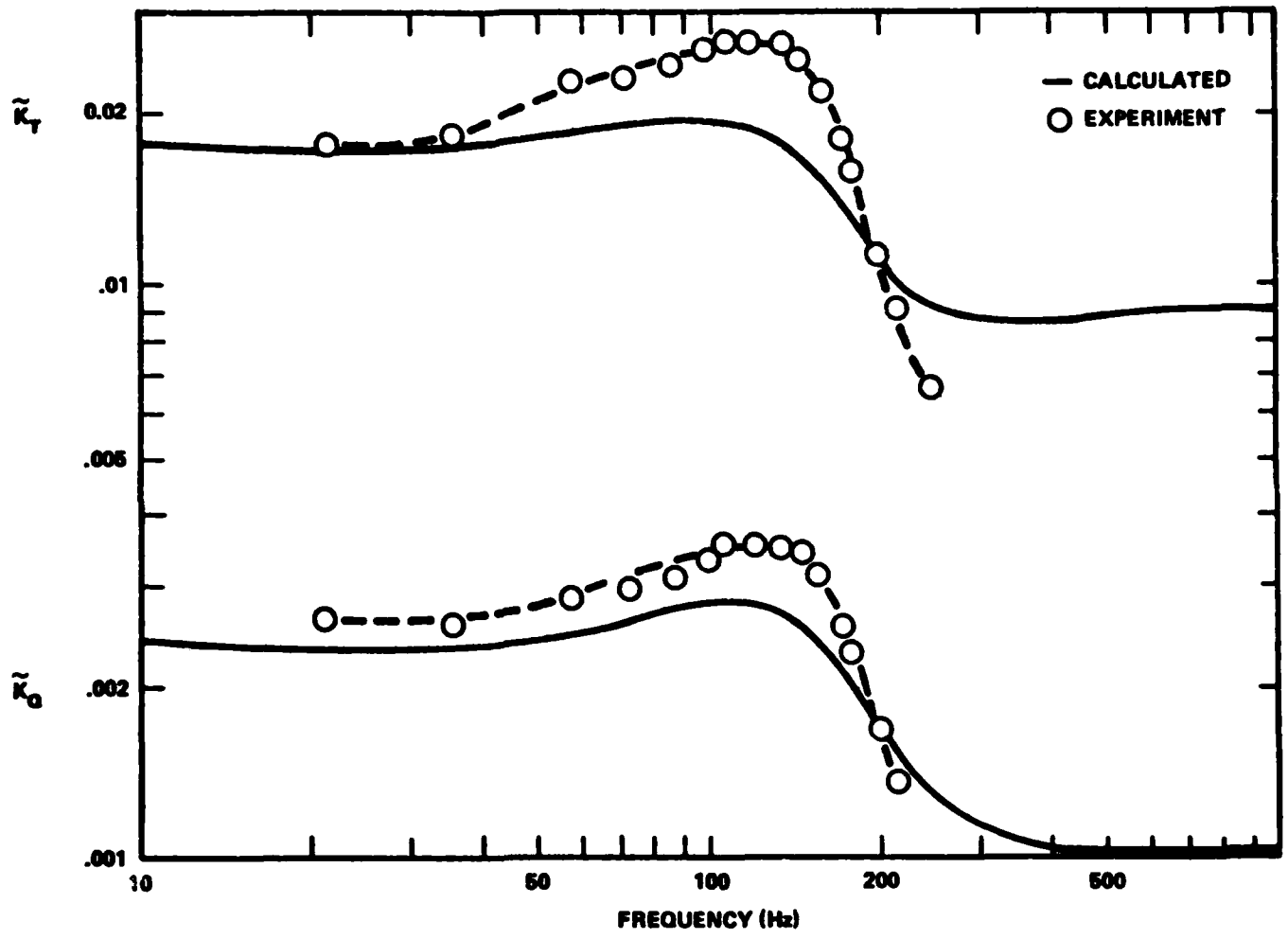

Figure 24 - Comparison of Calculated and Experimental Unsteady Thrust and Torque for Prop. No. 3958 at J = 0.67

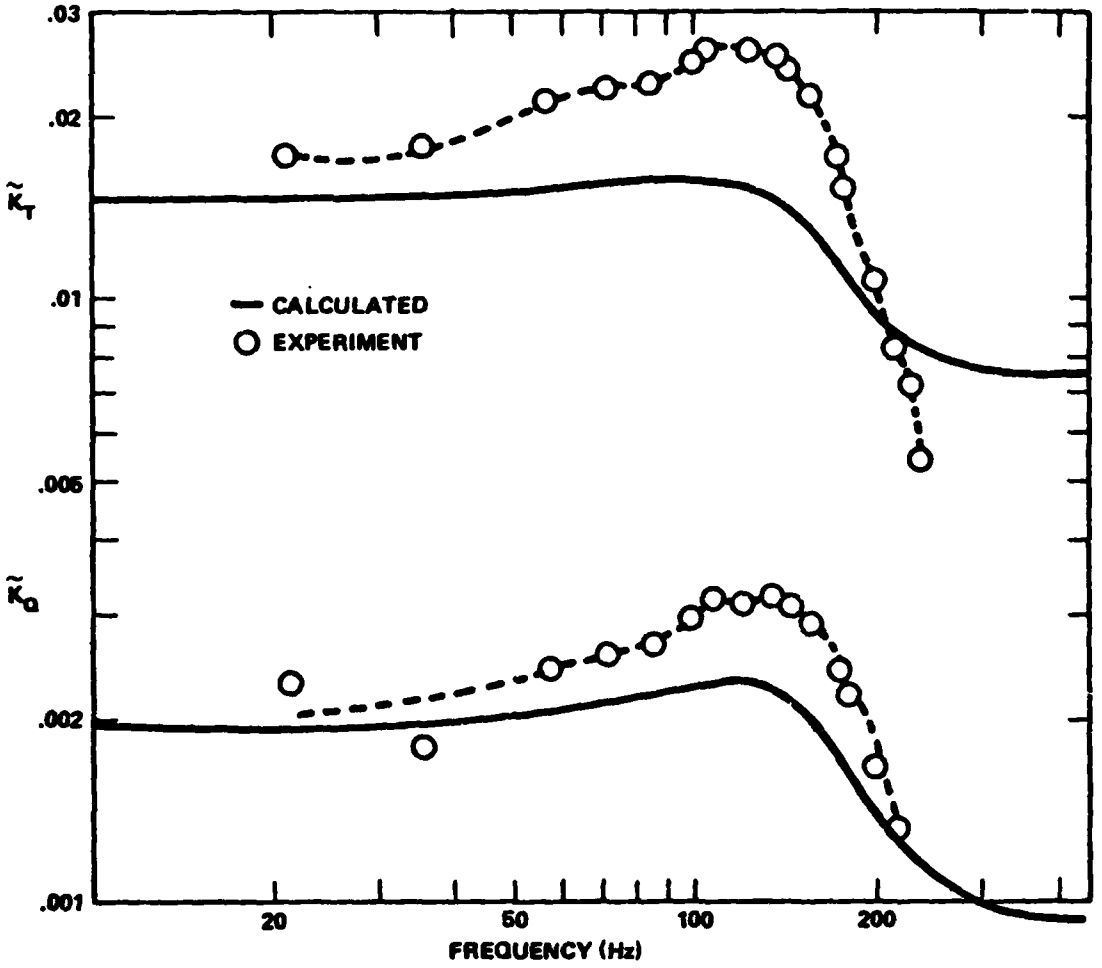

Figure 25 - Comparison of Calculated and Experimental Unsteady Thrust and Torque for Prop. No. 3958 at J = 0.59

1.5 at the three advance ratios; the calculated unsteady torques are about 20 percent greater than the low-frequency values while the experimental torque magnifications are about 1.5 to 1.6. In addition, the experimental results do not show high-frequency asymptotic thrust and torque values as do the calculated results. However, the limitations of the water tunnel facility prevented us from verifying whether a high-frequency asymptote exists at some higher loading frequency.

Nevertheless, the calculations did predict that the frequency response is highly damped. This is in basic agreement with the measurements. It is also significant that measurements show substantial reductions in alternating thrust and torque (over those of a rigid propeller) in the higher frequency range, above 170 Hz. This is also true of the calculated results, although the details of frequency range and reduction levels differ.

COMPARISON OF THE TWO ONE-MODE APPROXIMATIONS

We also made calculations for unsteady thrust and torque using the much simpler one-mode stiffness approximation given in equations (46) and (50). To make this comparison, we have expressed the results in terms of thrust, torque and frequency ratios--$F_z/F_{z,R}$, $M_z/M_{z,R}$ and $\omega/\omega_{w,1}$, respectively.

These approximations are compared in Figure 26 with the one-mode inertial approximation of equations (42) and (43) for Prop No 4064 at its two advance ratios. We see that the two approximation methods agree with ne another to within 25 percent up to a frequency ratio of about 1.4 for)th the thrust and torque ratios; beyond this frequency they diverge pidly, with the stiffness approximation approaching zero as $(\omega_{w,1}/\omega)^2$. We) see that each approximation gives almost identical results at the two

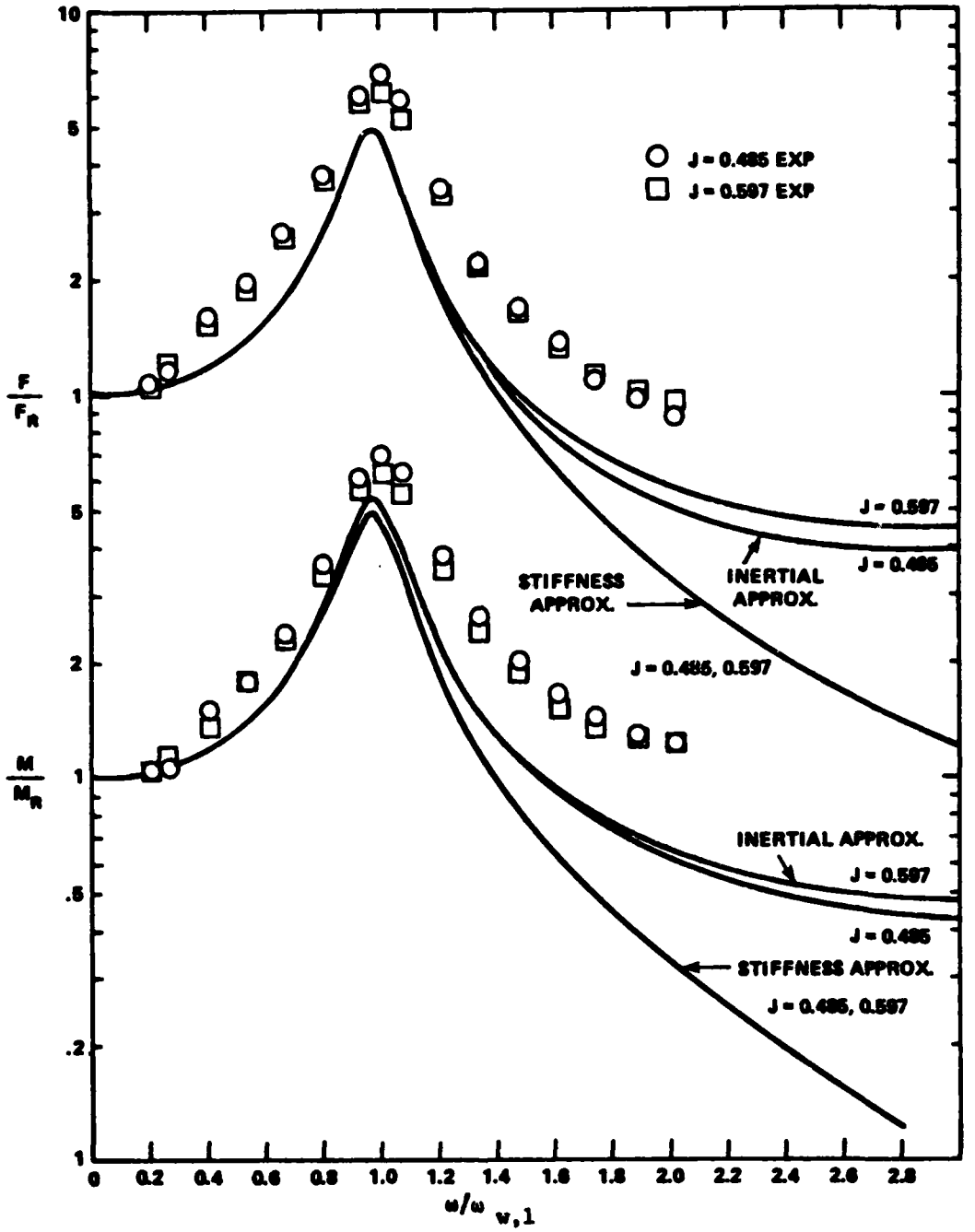

Figure 26 - Comparison of the Two One-Mode Approximations for Prop. No. 4064. In Normalizing the Experimental Results. We Used the Apparent Low-Frequency Asymptotic Values of Thrust and Torque and the Calculated Values of the In-Water Resonance Frequency

advance ratios. This is to be expected since the calculated hydrodynamic damping factors are about the same at the two advance ratios. The experimental results, expressed in terms of these ratios, also give almost identical values at the two advance ratios.

The same type of comparison was made for Prop No 3958, which is shown in Figure 27; for a frequency ratio up to about 1.3 the two approximation methods agree with one another to within 25 percent or better. Again, each approximation method gives an almost identical curve for each advance ratio, as does the experimental results. Although the stiffness approximation presented in equations (46) and (50) are expected to be less accurate than the inertial approximation of equations (42) and (43), it agrees better with the experimental results for both unsteady thrust and torque, especially at the higher frequencies where both the stiffness approximation and the experimental results are decreasing at a rate approximately proportioned to $(\omega_{w,1}/\omega)^2$.

The good agreement which is demonstrated by the two sets of one-mode approximations, at least for these propellers and for a range of excitation frequency up to 1.3 times the fundamental resonance frequency in water, means that the simpler, more physically insightful set of approximations given by equations (46) and (50) can be used to predict unsteady forces and moments.

COMPARISON WITH CALCULATION FOR NO CIRCULATION

Of incidental note is an interesting empirical relationship that seems to exist between the alternating (rigid) thrust and torque for a calculation for no circulation and the same values for a complete (with circulation) calculation, or the experimental values: the values for no circulation are approximately twice the real or experimental values. The following table shows the comparison.

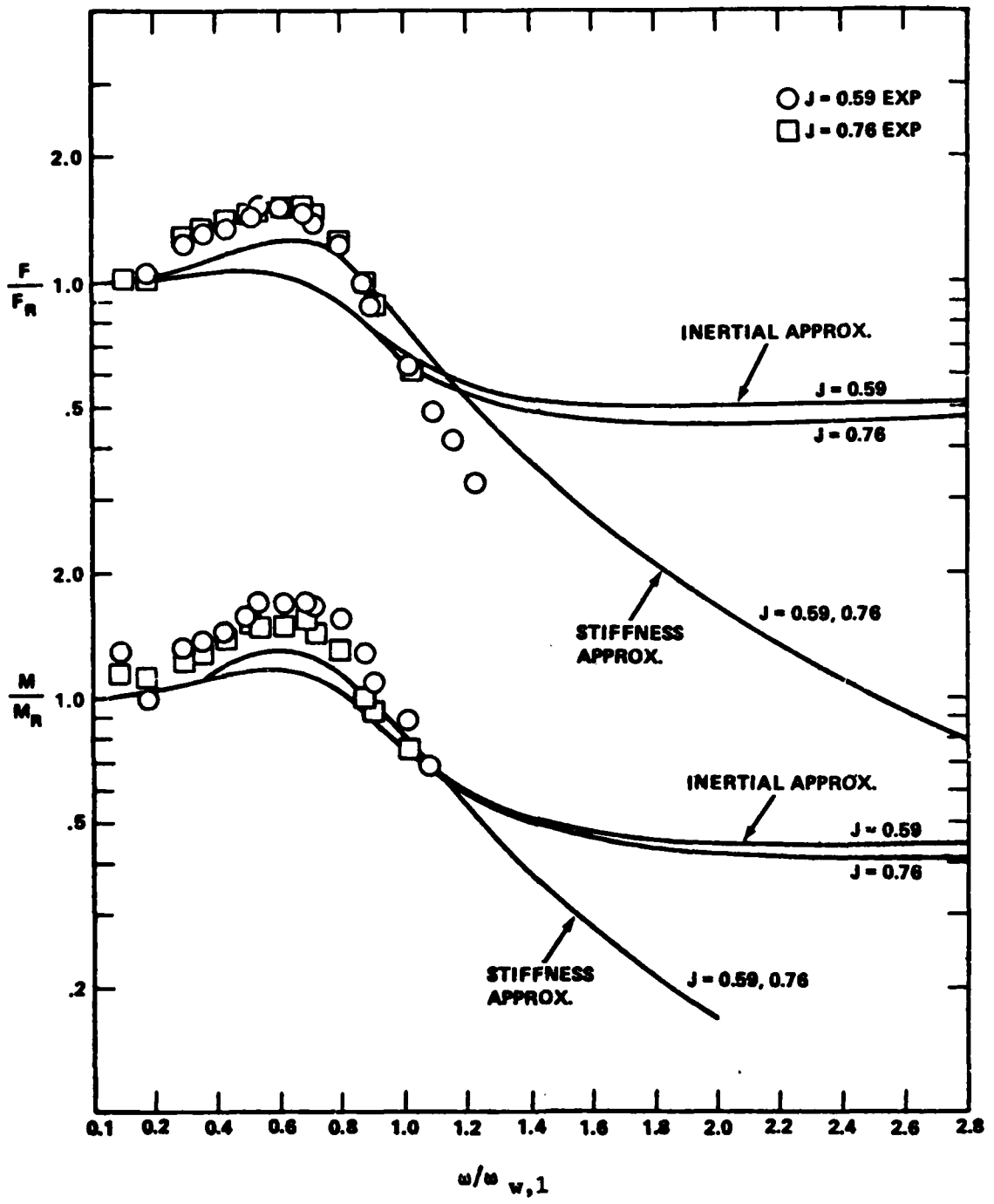

Figure 27 - Comparison of the Two One-Mode Approximations for Prop. No. 3958. In the Normalization of the Experimental Results; the Thrust and Torque Values in Table 4 are Used and the Calculated Resonance Frequencies Are Used

TABLE 5. - NO CIRCULATION, COMPLETE AND EXPERIMENTAL RESULTS

coef\J	Prop No. 3956 .76	.67	.59	Prop No. 4064 (low-freq limit) .597	.485
.5 $(\tilde{K}_T)_{\text{no circ}}$	.0214	.0189	.0166	.0292	.0237
$(\tilde{K}_T)_{\text{complete}}$	.0213	.0178	.0147	.0265	.0221
$(\tilde{K}_T)_{\text{exper}}$	.0188	.0178	.0170	.025	.022
.5 $(\tilde{K}_Q)_{\text{no circ}}$	.00305	.00269	.00237	.00298	.00242
$(\tilde{K}_Q)_{\text{complete}}$	.00284	.00236	.00195	.00252	.00212
$(\tilde{K}_Q)_{\text{exper}}$	.00260	.00228	.00185	.0028	.0024

This relationship has also been noted for other propellers. It is not known whether this is a general result. But if it is, the calculation of unsteady thrust would be considerably simplified since the theory for no circulation and calculation methods based on that theory are on a much firmer foundation than the theory and calculation methods based on the theory with circulation. The no circulation or simple potential theory also very often accomodates simple approximations in terms of independently estimable quantities.*

*For example, we can derive on such simple approximation for the thrust for no circulation in terms of some gross geometric properties of the propeller and the average inflow conditions at the propeller. The approximation assumes that the thrust is the same as that developed by a rigid propeller oscillating in the axial direction. In terms of the thrust coefficient, the approximation is

$$(\tilde{K}_T)_{\text{no circ}} \approx 6.6\ (\text{PAR})^2\ (D/\ell)\ J\ \bar{u}_m/(V_a+\bar{u}_o)$$

where PAR is the propeller's projected area ratio (ratio of projected blade area, projected onto the plane perpendicular to the axis, to the disk area $.25\pi D^2$), ℓ is the perimeter length of one blade and $\bar{u}_m$ is an average inflow velocity (averaged over the projected area A_z of one blade) for the wake harmonic $m=N_B$ defined as

$$\bar{u}_m = \frac{1}{A_z}\sqrt{\{\iint d\sigma_z\ u_m \cos\ (m\theta+\epsilon)\}^2 + \{\iint d\sigma_z\ u_m \sin\ (m\theta+\epsilon)\}^2}$$

where $d\sigma_z$ is an element of the propellers projected area and equal to $d\sigma\ \hat{n}\cdot\hat{z}$. The details of the approximation are given in Appendix B.

DISCUSSION AND CONCLUSIONS

We made several major assumptions in developing the blade-vibration theory, in calculating the propeller forces and moments and in measuring and interpreting the experimental results. We will now review some of the more critical assumptions and assess, where possible, the probable effect of removing the restrictions. And finally we will discuss the main implications of our results and list the significant conclusions.

REVIEW OF ASSUMPTIONS

In developing the equations for blade vibrations we assumed the induced pressures and velocities behave linearly. This is important for then we can make the separation between the field driving the blade motion--i.e., p_R and $\vec{v}_R$--and the field induced by this driving field--p_V and $\vec{v}_V$. The validity of this assumption increases as both the amplitudes of blade-vibration velocity $\dot{q}_i\psi_i$ and the nonuniform inflow velocity u_m become smaller fractions of the mean inflow speed $|\vec{v}_a - \vec{u}_o|$. Near the blade tips of the test propellers the measured amplitudes of the nonuniform inflow were 22 to 25 percent of the mean inflow and the calculated blade-velocity amplitudes were at most 13 to 20 percent of the same mean inflow speed. But perhaps a more representative test for linearity is to compare the mean inflow velocities with the rms velocities (averaged over the blade midsurface), rather than the maximum velocities near the blade tip. Then, for the two test propellers, the rms nonuniform inflow velocities range from 8.8 (for No. 3958) to 11.1 (for No. 4064) percent of the mean inflow velocity, and the maximum rms blade vibration velocities range from 2.7 (for No. 3958) to 5.6 (for No. 4064)

percent. In any event, the neglected nonlinear coupling of the $\vec{v}_R$ and $\vec{v}_V$ fields present in the boundary condition of equation (5a) varies principally as the product of these velocities and is proportional to the local surface gradient of the mode shape, itself a small term since the measured mode shapes vary slowly over the blade surfaces. Based on this sort of reasoning we can argue for the validity of the linearity assumption.

The theory assumes the mode shapes for the propeller operating in water are the same, or effectively the same, as those for a non-rotating propeller vibrating in air. This is probably the most critical assumption in the general theory developed in equations (1) to (40). What counts is not how much the mode shapes change in water, but rather how those changes alter the calculated forces and moments. To determine this, we made additional unsteady thrust calculations using the inertial approximation for widely different mode shapes, although each still resembled a one-noded cantilever mode. It turns out that the measured mode shape in air for propeller No. 3958, at a chord midsection, is proportional, roughly, to the cube of the radial distance from the blade root. Figure 28 shows calculated thrust, as a function of loading frequency, for four perturbations about the original mode shape: one where the mode shape at the midsection of a chord varies as the square of the radial distance from the blade root, another where it varies as the fourth power of that distance, both mode shapes having the same chordwise derivative; in the other two, the radial distribution at the midchord was as the original, and the chordwise derivative was varied--in one we took the derivate as twice that of the original mode shape and in the other as one-half the original. We see that the low-frequency thrust values are the same as the original calculation up to 50 or 60 Hz, and the high-frequency asymptotes above 300 Hz differ by only ±10 percent of the original

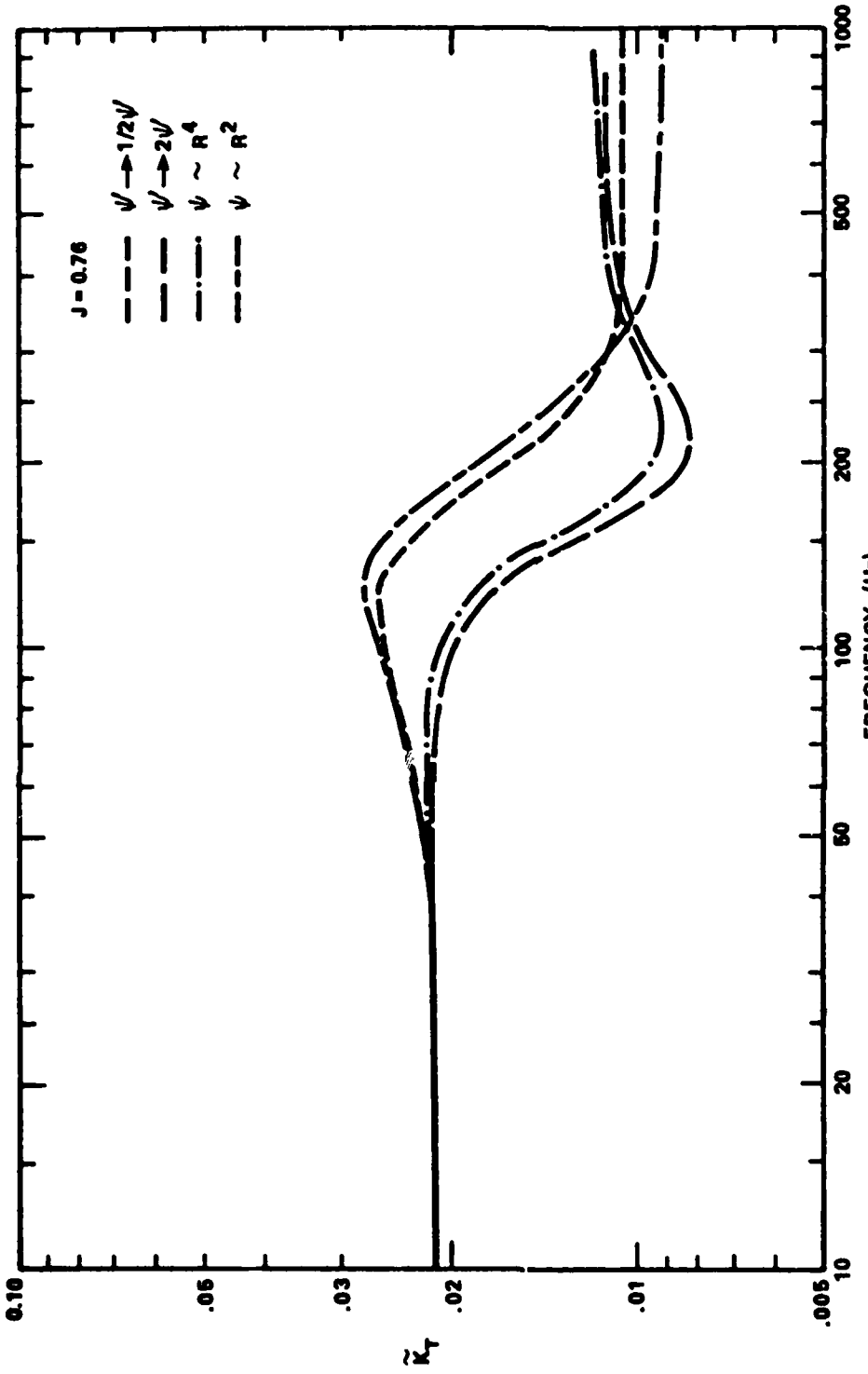

Figure 28 - Calculated Unsteady Thrust for Prop. No. 3958 at J = 0.76 for Four Different Mode Shapes

one. The main difference is in the 60 to 250 Hz range where thrust coefficients differ by as much as 100 percent from the original. Closer examination of the calculations show the calculated hydrodynamic quantities--M_1 and β_1 --are all within $\pm$15 percent of the original calculated ones; and that the differences arise because of the different phase relationship between $\vec{F}_R$ and $\vec{F}_V$ for each mode shape. None of these new calculations, however, agree any better with measured alternating thrust than does the original calculation. The important thing is that the hydrodynamic damping and general functional dependence of unsteady thrust on loading frequency is generally the same for all these various assumed mode shapes.

A similar calculation, shown in Figure 29, was made for the wide-bladed propeller. The various peak values of the alternating thrust coefficients are all within $\pm$30 percent of the original calculation. The calculated coefficients all have similar frequency dependence up until about 170 Hz. The asymptotic values above this frequency are then quite different. Again we see that the general functional dependence on loading frequency is relatively insensitive to the exact details of the assumed mode shape, at least for loading frequencies at or below resonance, and that rough estimates for alternating thrust at or near resonance can be calculated using almost any reasonable mode shape.

In the calculations we assumed that only the first vibration mode contributes to the unsteady thrust and torque. We expect this to be true--at least for these propeller--for two reasons. One is that the second resonance frequency for both the plastic propeller and the wide-bladed propeller are at least two times their fundamental frequencies. Another is that the nonuniform inflow resembles a cantilever mode--i.e., the velocities are small near the root of the blades and increase to a peak value near the blade's tip--

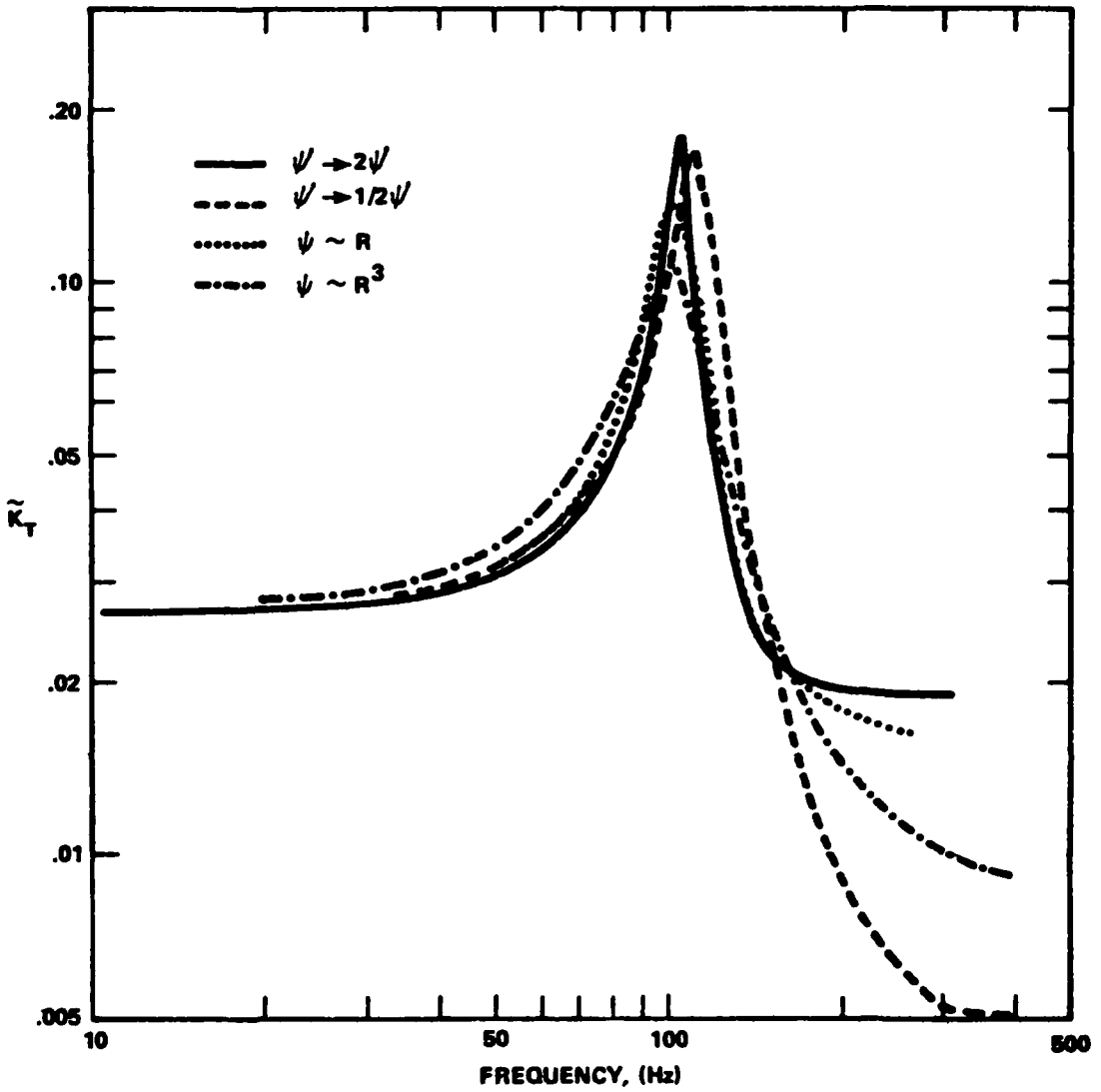

Figure 29 - Calculated Unsteady Thrust for Prop. No. 4064 at J = 0.597 for Four Different Mode Shapes

causing the blade's fundamental cantilever mode to be excited more than some of the higher modes. Therefore, we expect the one--mode inertial approximation to be good for exciting frequencies near or below the propeller's fundamental frequency in water.

For exciting frequencies much beyond the fundamental resonance, we would expect the second mode and higher modes to contribute to the vibration. This may account for some of the differences between calculated and measured thrust and torque in the frequency range above 150 Hz for the wide-bladed propeller, which has its second resonance at 370 Hz. For the plastic propeller, we only measured thrust and torque for exciting frequencies up to 238 Hz, and since the apparent second resonance is near 400 Hz, it is unlikely that additional modal contributions can explain the differences between calculations and experiment.

Nevertheless, we did a calculation to see what the effect might be from the second mode for propeller No. 3958. This was done by using equation (35) and summing contribution from two modes. We assumed that the second mode is the same as that of a uniform cantilever beam. Figure 30 shows how this second mode might affect the transmitted thrust. We see that it contributes at most $\pm$20 percent to the transmitted thrust for loading frequencies from 150 to 300 Hz, and contributes less than 5 percent for frequencies below 150 Hz. This tends to confirm the assumption that the fundamental mode dominates the vibration, at least over the range of measured loading frequencies.

Another assumption in the theory is that all blades vibrate with equal amplitude, and that there is only one one-noded cantilever resonance frequency. Actually, because of slight construction differences in the blades and because of the blade coupling through the common elastic hub and added-mass coupling through the water, there are as many possible one-

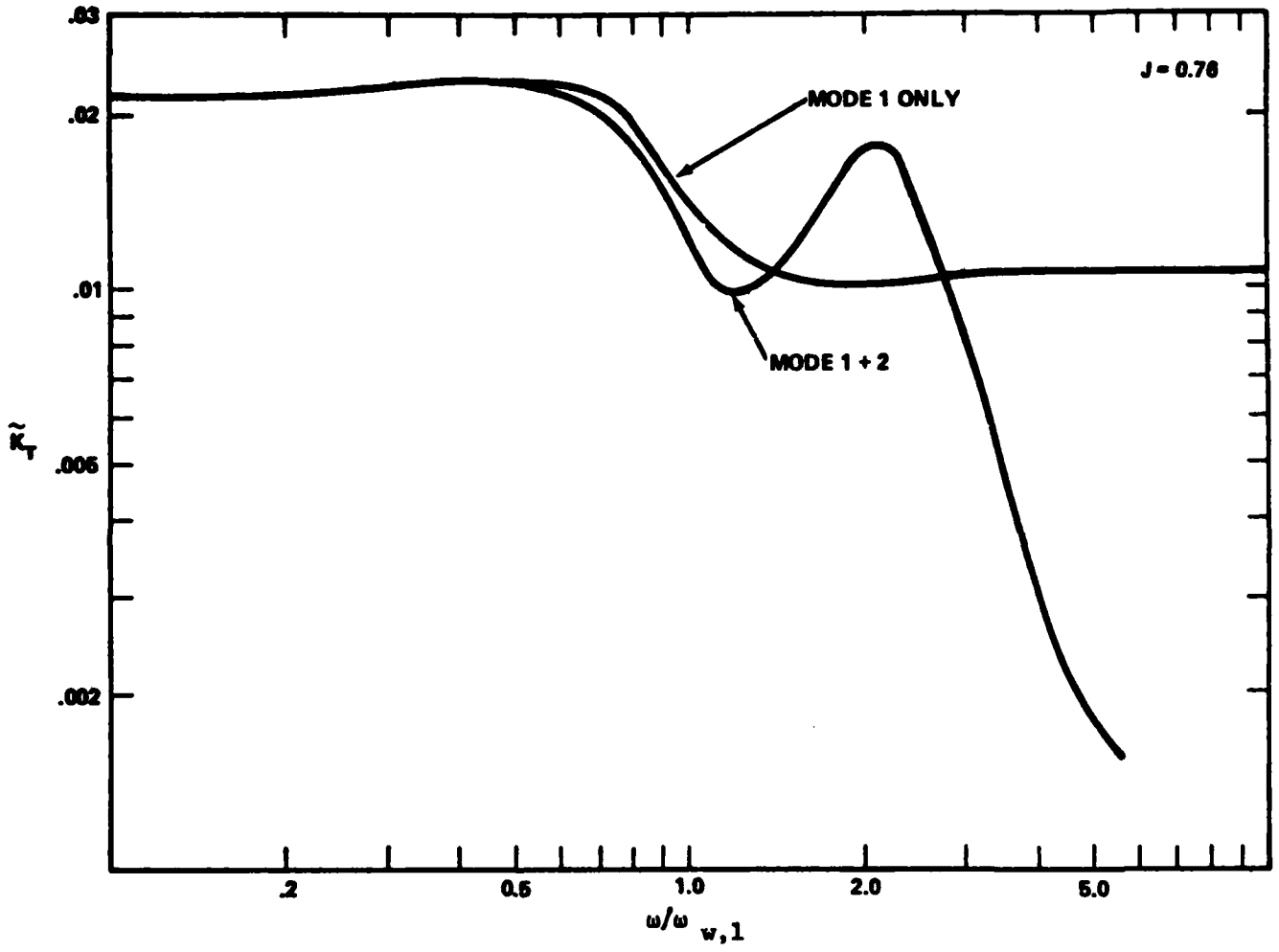

Figure 30 - Calculated Unsteady Thrust Coefficient for Prop. No. 3958 at J = 0.76, Comparing the One-Mode Calculation to a Calculation Using 2 Modes

noded cantilever resonance frequencies as there are blades. These frequencies, N_B in number, will cluster about some central frequency, the width of the clustering dependent upon the amount of mass and stiffness coupling that exists between individual blades. At each of these frequencies the mode shapes on individual blades are probably very similar, although the phase and amplitude at rotationally symmetric points, say at the blade tips, may differ.

We noticed this multi-resonance phenomenon during the in-air mode shape measurements, although by far the dominant resonance occurred when all blades were in phase (at the weaker resonance frequencies the blades had different phase relations). However, when we measured the fundamental resonance frequency for propeller No. 3958 in still water, with the propeller mounted on the dynamometer, we observed only one fundamental resonance frequency (at 160 Hz) through the thrust or torque channels of the strain-gage bridge. But on the side-force channels we recorded a slightly different resonance frequency (at 150 Hz). The same held true for propeller No. 4064--108 Hz on the thrust channel and 102 Hz on the side-force channels. The implication is that a propeller can resonate at more than one fundamental frequency, some producing only thrust components of force, some only side-force components and maybe some producing no net forces at all.

In any case, the blades of the test propellers probably did not vibrate at the loading frequency with equal amplitude as was assumed in the theory. It is also possible that the true unsteady thrust response of the propeller resulted from more than one fundamental resonance frequency. The total effect would be to reduce the calculated force $\vec{F}_V$ in equation (34) and to increase the effective hydrodynamic damping.

In the theory we also neglect the structural damping compared to the hydrodynamic damping. This is justified since the calculated hydrodynamic

damping factors are about 20 times larger than the structural damping factor for the case of propeller No. 4064, and about 50 times larger in the case of propeller No. 3958.

There were also several assumptions made during the experiment which need further examination. We assumed that the local ratio of nonuniform velocity $\vec{u}_m$ to volume mean inflow speed $\bar{u}_o$ remains constant as the tunnel speed increases. This assumption is particularly critical for the test with the wide-blade propeller. One test of the assumption is to measure the unsteady thrust coefficient for a rigid propeller, at a constant J, as a function of tunnel speed. If the velocities scale as we assumed, then the unsteady thrust coefficient should be constant. We have this test for a near-rigid (aluminum) propeller (No. 3956). We see in Figures 12, 13 and 14 that, up to about 200 Hz, the thrust coefficients are nearly constant (deviations from the mean are only $\pm$10 percent). Beyond this frequency, the coefficients increase slowly, possibly an elastic effect since this propeller's first resonance frequency in water is near 360 Hz.

Also we did not consider the steady elastic deformations of the blades in either the theory or the experiment. The effect of the deformation, to a first approximation, is the same as if the propeller geometry were warped to accommodate rake. This effect could distort the comparison of the results for the cases of high steady loading, but would not affect the comparison near zero steady thrust, a case chosen purposefully for each of the test propellers (J=.597 for No. 4064 and J=.76 for No. 3958).

FURTHER DISCUSSION

Although the calculations do not agree with the measurements in all respects, they do capture the most prominent features of the experiment results; the relatively sharp resonant response of the unsteady thrust and torque near 105 Hz for the wide-bladed propeller, and the apparent extraordinarily highly, damped response of the narrower-bladed one. The theory attributes this apparent large difference in damping to a hydrodynamic effect brought about by the relative difference in shed vorticity produced by the two propellers.

We can explain why the two propellers have different hydrodynamic damping by returning to the two-dimensional theory of equation (58). The hydrodynamic damping factor β in this expression decreases monotonically with increasing reduced frequency $\tilde{\omega}$. Since the reduced frequency is proportional to the chord width, the narrower the blade (all other conditions being equal), the higher the hydrodynamic damping. Rephrased, this means that the larger the ratio of shed vorticity wavelength to blade width (or chordwise vibration wavelength), the higher the hydrodynamic damping factor, where near the blade tip

$$\lambda_{\text{shed vorticity}} \simeq \frac{\pi D}{m} \sqrt{1 + .10\ J^2} \tag{82}$$

We can suggest one possible physical explanation for this behavior of the hydrodynamic damping factor β. We know that the force associated with the added water mass depends strongly on the blade width, being approximately proportional to the square of the blade width. The induced hydrodynamic

damping force, however, depends on the amount of circulation set up by the flow off the trailing edge of the blade; it is a function of the details of the blade near the trailing edge and probably not strongly influenced by the width of the blade. Therefore, β, which depends on the ratio of these two types of forces, would tend to decrease with increasing propeller width, provided everything else remains the same. This explains why the narrower-bladed propeller exhibits larger damping than does the wide-bladed one, since otherwise they are roughly the same diameter, have similar resonance frequencies and operate under similar flow conditions.

An interesting feature of the experiment for propeller No. 3958 is that, for frequencies larger than the propeller's resonance frequency in water, the net unsteady thrust and torque is actually smaller than if the blades behaved rigidly. This interesting phenomenon is also substantiated by the calculated results.

To see how this is possible from a theoretical viewpoint, we recall that the total induced pressure acting on the blade's surface is composed of two competing fields: the (rigid) pressure field p_R that exists when the blades do not vibrate and the additional field p_V that exists when they do. They produce separate components of the total propeller force. To understand how these components cancel over a certain frequency range, we refer to Figure 31, a vector diagram showing the calculated phase and amplitude of the two forces $\vec{F}_R$ and $\vec{F}_V$ (nondimensionalized by $\rho\Omega^2D^4/4\pi^2$) as a function of loading frequency. The phase and amplitude of $\vec{F}_R$ are independent of loading frequency at a fixed advance ratio. The $\vec{F}_V$ component's amplitude increases slowly with frequency, reaches a maximum at 191 Hz, then decreases beyond that. At the low-frequency limit, the phase is 97 deg, then it increases slowly to 187 deg at resonance, and has a high-frequency asymptotic value of

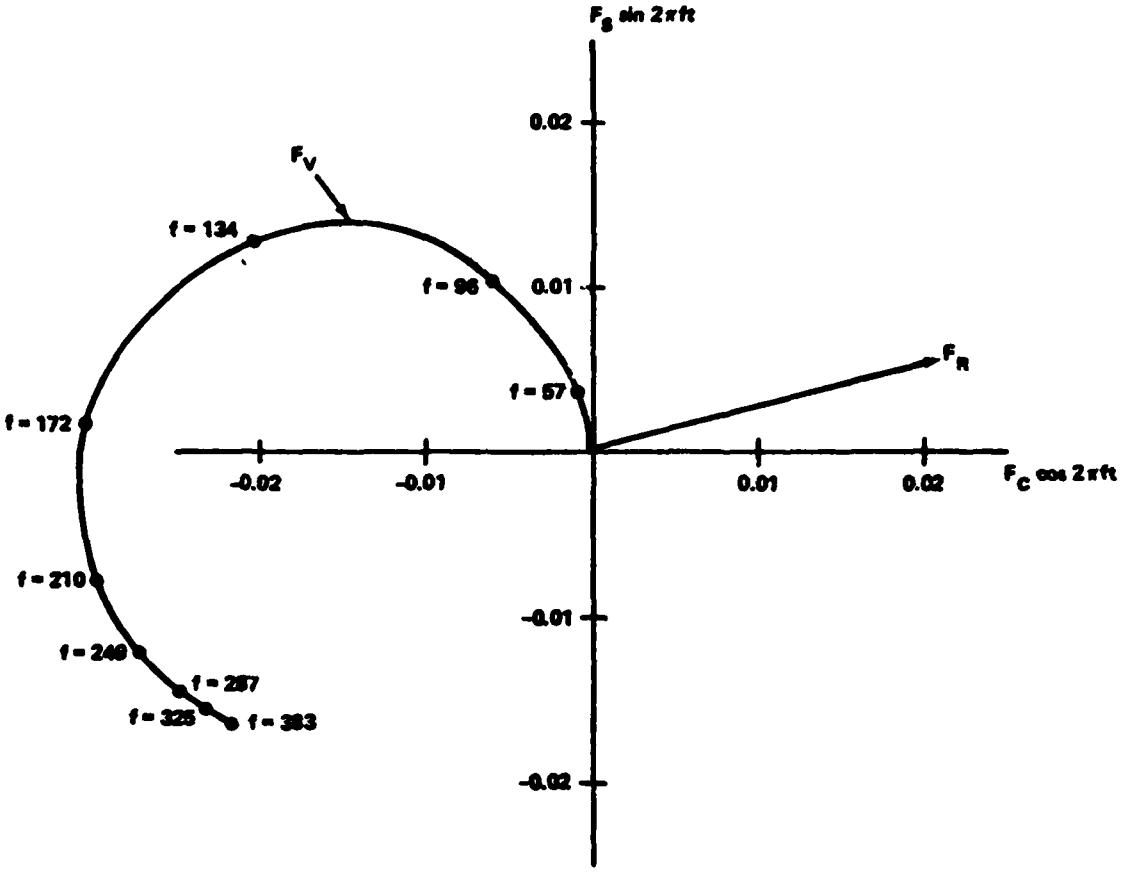

Figure 31 - Amplitude and Phase Diagram for the Two Components of Total Unsteady Thrust for Prop. No. 3958 at J = 0.76

222 deg. For frequencies below 105 Hz the two forces tend to add, that is, they produce a total force whose amplitude is greater than the amplitude of $\vec{F}_R$. In the frequency range above this, the pressure field p_V tends to cancel on the average, the p_R field and produce a net force whose amplitude is smaller than the amplitude of $\vec{F}_R$.

The force cancellation at the hub is also enhanced by the propeller blades acting as a single degree-of-freedom isolation mount, which attenuates transmitted vibrations to the hub from unsteady loads whose frequencies are higher than the resonance frequency of the mounting system. This analogy comes from equation (46), where the applied load is $F_{z,R}$ and the resonance frequency of the mount is $\omega_{w,1}$. From this equation we see that cancellation will always occur for sufficiently large exciting frequencies, provided only the fundamental mode is excited, and will be more pronounced for larger values of hydrodynamic damping β.

Whether or not this phenomenon can be exploited to reduce transmitted unsteady forces and moments in a practical situation is a subject which needs to be studied further. But a partial recipe for the construction of a propeller which would exploit this cancellation phenomenon would require a propeller with (1) narrow blades (i.e., large β), (2) a fundamental resonance frequency in water which is well within the operating range of the ship and (3) a second resonance frequency which is well above the first one. All of this would have to be achieved without degrading the static strength of the blades.

In addition to the effect of blade vibration on propeller forces, the effect of the vibration on stress levels, particularly near the blade root, is also important, since large, sustained unsteady stresses can result in the propeller failing by material fatigue. A full blown study of the stress distribution in the blades, either using a complicated analytical model or a

fully instrumented test propeller, is outside the scope of the present work. But we did make rough estimations for the unsteady stress $\tilde{\sigma}$ as a fraction of the mean or steady propeller stress $\bar{\sigma}_{design}$ developed by the test propellers operating near its design advance ratio.

One way is to assume that the stresses are in the same ratio as the tip deflections. Then if $\tilde{d}$ is the unsteady tip deflection and $\tilde{d}_{design}$ is the steady tip deflection at design J, we have

$$\frac{\tilde{\sigma}}{\bar{\sigma}_{design}} \simeq \frac{\tilde{d}}{\bar{d}_{design}} \tag{83}$$

We have $\tilde{d}$ from the calculation, and the steady tip deflection was estimated by applying a known concentrated force, as measured by a Chatillon (static) force gage, and measuring the resulting tip deflection. Using these bits of information, along with the design J and $\bar{K}_T$, we can estimate the stress ratio for any loading frequency. For the wide-bladed propeller the tip deflected .125 inches under an 18 pound force concentrated at the midchord of a section whose radius is approximately 70 percent of the tip radius; the advance ratio at design is 0.40 and the steady thrust coefficient is 0.15. Taken all together, we estimate that at resonance (104 Hz) the ratio of dynamic stress (for an advance ratio of .597) to design steady stress is 0.60. For the narrow-bladed plastic propeller, the static loading ratio (ratio of tip deflection to static force applied at the 70 percent radius point) was 0.015 inches/pounds; the design point was taken to be a nominal J=.65 and $\bar{K}_T$=0.10. At resonance (193 Hz) the ratio of unsteady stress (at an advance ratio of .76) to design steady stress is calculated, by equation (83), as 0.14, a much smaller ratio than for the wide-bladed propeller.

Another way to estimate the ratio of stresses quickly is to assume

$$\frac{\tilde{\sigma}}{\bar{\sigma}_{design}} \simeq \frac{\tilde{K}_T}{\left(\bar{K}_T\right)_{design}} \tag{84}$$

At resonance this gives the stress ratio for the plastic propeller as .09 (using calculated $\tilde{K}_T$) or .13 (using experimental $\tilde{K}_T$), and approximates the stress ratio for the wide-bladed propeller as .80 (using calculated $\tilde{K}_T$) or 1.0 (using experimental $\tilde{K}_T$).

In any case, the approximations of equation (83) and (84) both indicate a potentially severe fatigue problem if the wide-bladed propeller were to operate near its resonance frequency for long periods of time. On the other hand, the narrower, plastic propeller probably would not fatigue if it operated near its resonance frequency, in fact the dynamic stress is actually reduced because of vibration.

And finally, we have only studied the effect of blade-vibration on unsteady thrust and torque. But the vibration most likely has the same type of effect on side forces and moment, that is, the hydrodynamic damping factors and added masses are probably the same, or nearly the same, as for unsteady thrust; the mode shapes are the same, in both cases so, except for slightly different blade-to-blade interaction producing a slightly different pressure distribution p_v, the hydrodynamic quantities should be about the same. This means that a propeller which exhibits large hydrodynamic damping for unsteady thrust will have large hydrodynamic damping for side forces as well.

CONCLUSIONS

There are many conclusions we can draw from this study, some more important than others. But after distilling the results, three important conclusions emerge.

1. Marine propellers, operating in nonuniform inflows, can develop widely differing unsteady force (and moment) responses for excitation frequencies near the blade's fundamental resonance frequency. A key response determinant is the relative amount of hydrodynamically induced damping developed by the propeller. This damping is, in turn, a function primarily of the blade geometry and the fundamental mode shape of the blade. There is some indication that the narrower the blade chord (everything else being constant), the larger the induced damping and the flatter the forced response near the first blade resonance. For some propellers, as we see in the present study, the hydrodynamic damping can be so large that there is relatively little force amplification near resonance, and, consequently, blade vibration is not a major problem. For other propellers, the force amplifications can become very large indeed and can generate significant propeller vibrations and even cause propeller damage by fatigue.

2. Besides increasing the unsteady propeller forces near resonance, blade vibration can, in some situations and for some propellers, actually reduce propeller forces over a large frequency range. This would occur, typically, for propellers with large hydrodynamic damping and for loading frequencies above the propeller's fundamental resonance frequency.

3. A simple, one-mode approximation is useful in interpreting conclusions (1) and (2):

$$\left(\frac{F}{F_R}\right) \approx \left(\frac{M}{M_R}\right) \approx \left(\frac{\omega_{w,1}}{\omega}\right)^2 \sqrt{\frac{1}{(\omega^2_{w,1}/\omega^2-1)^2 + \beta_1^2}}$$

where the force and moment ratio are ratios of transmitted unsteady force and moment to those that would be transmitted were the blades rigid; the expression applies equally to the transmitted forces from one blade as to the total transmitted force from all blades. It agrees fairly well with the

measured unsteady thrust and torques over the frequency range observed in the experiment, but does not apply for excitation frequencies where the higher vibration modes are important. In that case, to account for the higher modes, the general theory, given in equations (35) and (39), should be used instead.

APPENDIX A

Two surface coordinates - a radial distance r and a helical arc distance c - are sufficient to specify the position and inclination at any point on the time-averaged median or outer surfaces of the propeller blade [21]. If $\vec{S}_o(r,c)$ is a position vector measured from a reference frame rotating and advancing with the propeller to a point on the time-averaged midsurface of the blade, then the instantaneous position $\vec{S}$ of the vibrating midsurface is

$$\vec{S}(r,c,t) = \vec{S}_o(r,c) + q(t)\ \psi_i(r,c)\ \hat{\delta}_i(r,c) \tag{A1}$$

An instantaneous vector normal to the vibrating surface is constructed by taking the vector cross product of two surface tangent vector, i.e.,

$$\vec{n}_{inst} = \left(\frac{\partial \vec{S}}{\partial r}\right)_c \times \left(\frac{\partial \vec{S}}{\partial c}\right)_r \tag{A2}$$

Retaining only linear terms in q, (A2) becomes

$$\vec{n}_{inst} \simeq \vec{n}_o + q\left[\frac{\partial(\psi_i \hat{\delta}_i)}{\partial r} \times \vec{\eta}_o + \vec{\varepsilon}_o \times \frac{\partial(\psi_i \hat{\delta}_i)}{\partial c}\right] \tag{A3}$$

where $\vec{n}_o$ is vector normal to the time-averaged surface and

$$\vec{\varepsilon}_o = \left(\frac{\partial \vec{S}_o}{\partial r}\right)_c,\ \vec{\eta}_o = \left(\frac{\partial \vec{S}_o}{\partial c}\right)_r,\ \vec{n}_o = \vec{\varepsilon}_o \times \vec{\eta}_o \tag{A4}$$

$(\vec{\xi}_o, \vec{\eta}_o)$ form an oblique set of vectors which is tangent to the local midsurface. Reciprocal to this set is another set of surface tangent vectors $(\vec{\xi}_o^*, \vec{\eta}_o^*)$ given by [25]

$$\vec{\xi}_o^* = (\vec{\eta}_o \times \vec{n}_o)/(\vec{\xi}_o \cdot \vec{\eta}_o \times \vec{n}_o) \tag{A5}$$

$$\vec{\eta}_o^* = (\vec{n}_o \times \vec{\xi}_o)/(\vec{\xi}_o \cdot \vec{\eta}_o \times \vec{n}_o) \tag{A6}$$

We can specify a surface gradient operator ∇_{tan} in terms of the reciprocal set as [26]

$$\nabla_{tan} = \left(\frac{\partial}{\partial r}\right)_c \vec{\xi}_o^* + \left(\frac{\partial}{\partial c}\right)_r \vec{\eta}_o^* \tag{A7}$$

Now take $\psi_i \hat{\delta}_i$ in two components: one normal to the time-averaged median surface and one tangent to it, i.e.,

$$\psi_i \hat{\delta}_i = \psi_i (\hat{\delta} \cdot \hat{n}_o)\, \hat{n}_o + \psi_i\, \hat{n}_o \times (\hat{\delta}_i \times \hat{n}_o) \tag{A8}$$

Then if we assume that the normal $\vec{n}_o$ varies much more slowly over the midsurface of the blade than does $\psi_i \hat{\delta}_i$, we can derive the approximation

$$\frac{\partial}{\partial r}\left\{\psi_i (\hat{\delta}_i \cdot \hat{n}_o)\, \hat{n}_o\right\} \times \vec{\eta}_o = \frac{\partial}{\partial r}\left\{\psi_i (\hat{\delta}_i \cdot \hat{n}_o)\right\}\, \hat{n}_o \times \vec{\eta}_o$$

$$= -\frac{\partial}{\partial r}\left\{\psi_i (\hat{\delta}_i \cdot \hat{n}_o)\right\} |\vec{n}_o|\, \vec{\xi}_o^* \tag{A9}$$

and

$$\vec{\xi}_o \times \frac{\partial}{\partial c}\left\{\psi_i(\hat{\delta}_i\cdot\hat{n}_o)\hat{n}_o\right\} = -\frac{\partial}{\partial c}\left\{\psi_i(\hat{\delta}_i\cdot\hat{n}_o)\right\}|\vec{n}_o|\ \vec{\eta}_o^* \tag{A10}$$

so that

$$\frac{\partial}{\partial r}\left\{\psi_i(\hat{\delta}_i\cdot\hat{n}_o)\ \hat{n}_o\right\}\times\vec{\eta}_o + \vec{\xi}_o\times\frac{\partial}{\partial c}\left\{\psi_i(\hat{\delta}_i\cdot\hat{n}_o)\hat{n}_o\right\}$$

$$= -|\vec{n}_o|\ \nabla_{tan}\left\{\psi_i\ \hat{\delta}_i\cdot\hat{n}_o\right\} \tag{A11}$$

Similarly for the tangential component of the mode displacement $\psi_i\hat{\delta}_i$ we have the approximation

$$\frac{\partial}{\partial r}\left\{\psi_i\hat{n}_o\times(\hat{\delta}_o\times\hat{n}_o)\right\}\times\vec{\eta}_o = -\vec{\eta}_o\times\left[\hat{n}_o\times\frac{\partial}{\partial r}\left\{\psi_i\hat{\delta}_i\times\hat{n}_o\right\}\right]$$

$$= -\left[\vec{\eta}_o\cdot\frac{\partial}{\partial r}\left\{\psi_i\ \hat{\delta}_i\times\hat{n}_o\right\}\right]\hat{n}_o$$

$$= \left[\frac{\partial}{\partial r}\left\{\psi_i\hat{\delta}_i\right\}\cdot\vec{\eta}_o\times\hat{n}_o\ \hat{n}_o\right]$$

$$= \frac{\partial}{\partial r}\left\{\psi_i\hat{\delta}_i\right\}\cdot\vec{\xi}^*\ \vec{n}_o \tag{A12}$$

and by similar manipulations

$$\vec{\xi}_o\times\frac{\partial}{\partial c}\left\{\psi_i\ \hat{n}_o\times(\hat{\delta}_i\times\hat{n}_o)\right\} = \frac{\partial}{\partial c}\left\{\psi_i\hat{\delta}_i\right\}\cdot\vec{\eta}_o^*\ \vec{n}_o \tag{A13}$$

or

$$\frac{\partial}{\partial r}\left\{\psi_i \hat{n}_o \times (\hat{\delta}_i \times \hat{n}_o)\right\} \times \vec{\eta}_o + \vec{\xi}_o \times \frac{\partial}{\partial c}\left\{\psi_i \hat{n}_o \times (\hat{\delta}_i \times \hat{n}_o)\right\}$$

$$= \nabla_{tan} \cdot \left\{\psi_i \hat{\delta}_i\right\} \vec{n}_o \qquad \text{(A14)}$$

Then from (A12) and (A14) along with (A3) we have an instantaneous vector normal to the midsurface

$$\vec{n}_{inst} = \hat{n}_o - q\, \nabla_{tan}\left\{\psi_i \hat{\delta}_i \cdot \hat{n}_o\right\} + q\, \hat{n}_o\, \nabla_{tan} \cdot \left\{\psi_i \hat{\delta}_i\right\} \qquad \text{(A15)}$$

To get an approximate instantaneous vector normal to the outer surface of the blade we replace the midsurface unit normal $\hat{n}_o$ by the unit normal $\hat{n}'$ and retain the midsurface gradient operator of equation (A7). This gives Equation (6) in the main text.

APPENDIX B

Here we derive approximations for the unsteady forces developed by a (rigid) marine propeller without circulation when it operates in a nonuniform inflow velocity field. We also give approximate expressions for the forces developed by an elastic propeller without circulation vibrating with a prescribed pattern and operating in a uniform inflow field.

Take a general propeller boundary condition

$$\hat{n}\cdot\vec{v} = g\ (\vec{S},t)\ \hat{n}\cdot\hat{z} \tag{B1}$$

where $g\ (\vec{S},t)\ \hat{n}\cdot\hat{z}$ can stand for the right-hand-side of equation (8) or (9), for example. We also take the propeller thickness equal to zero, so we need only specify boundary conditions on one side of a blade. If $\nu\ (\vec{S},t)$ is the local difference in induced velocity potential across the blade, and if g has a harmonic time dependence with frequency ω, then the alternating thrust amplitude F_z on one blade is

$$F_z = \rho\omega \iint d\sigma\ \nu\ \hat{n}\cdot\hat{z} \tag{B2}$$

where the intergration is over the midsurface of the blade.

The solution set $(\nu,\ g\ \hat{n}\cdot\hat{z})$ can be reinterpreted as the solution for a stationary propeller interacting with a time dependent axial inflow velocity $g\ \hat{z}$. If A_z is the projected area of a blade surface onto the axial plane, we can expand this inflow into a spatially uniform component and a component with zero spatial average (averaged over A_z), i.e.,

$$g = g_o + g_1 \tag{B3}$$

where

$$g_o = \iint \frac{g \, d\sigma \, \hat{n}\cdot\hat{z}}{A_z} \tag{B4}$$

Likewise we can take ν as the sum of the difference of two potentials: $\nu_{o,z}$, induced by the propeller when it oscillates as a rigid body with axial velocity $g_o \hat{z}$ (or equivalently, the difference in velocity potential induced by the nonrotating propeller interacting with a uniform axial inflow g_o); and $\nu_{1,z}$, induced by $g_1 \hat{z}$. Then

$$F_z = \rho\omega \iint d\sigma \, \hat{n}\cdot\hat{z} \, (\nu_{o,z}+\nu_{1,z}) \tag{B5}$$

Rewriting this using Green's Second Theorem

$$F_z = \rho\omega g_o \left[\iint d\sigma \, \hat{n}\cdot\hat{z} \, (\nu_{o,z}/g_o) + \iint d\sigma \, \hat{n}\cdot\hat{z} \, (\nu_{o,z}/g_o) \, (g_1/g_o) \right] \tag{B6}$$

$$= \omega g_o \left[M_{o,z} + M_{1,z} \right] \tag{B7}$$

The unsteady thrust can now be interpreted as an added mass times an average rigid body acceleration ωg_o. $(N_B M_{o,z})$ can be interpreted as the added mass of a propeller oscillating along its axis with unit velocity amplitude, i.e.,

$$M_{o,z} = \iint \rho \, d\sigma \, \hat{n}\cdot\hat{z} \, (\nu_o/g_o) \tag{B8}$$

$M_{1,z}$ is also an added mass, in some generalized sense.

In many situations, we can argue that $M_{1,z}$ will be much smaller than $M_{o,z}$. ν_o is generally all positive (or all negative) at points on the blade midsurface, and g_1 has zero mean value when averaged over the surface A_z. $M_{1,z}$, therefore, tends to have a small value when compared with $M_{o,z}$, particularly if g_o is larger than, say, the average of the absolute value of g_1. Under these conditions wer can ignore $M_{1,z}$ compared to $M_{o,z}$.

Accepting this approximation, but realizing that it may be invalid if g_o is "small", we have the simple result that the alternating thrust developed by a rigid propeller oscillating in the axial direction iwth acceleration amplitude ωg_o,

$$F_z \simeq \omega g_o \, M_{o,z} \tag{B9}$$

Following the same arguments we can approximate the total force acting on a blade as

$$\vec{F} = \omega g_o \left[M_{o,x} \frac{A_z}{A_x} \hat{x} + M_{o,y} \frac{A_z}{A_y} \hat{y} + M_{o,z} \hat{Z} \right] \tag{B10}$$

where

$$M_{o,x} = \iint d\sigma \, \rho \, \hat{n}\cdot\hat{x} \, \nu_{o,x} \tag{B11}$$

$$A_x = \iint d\sigma \, \hat{n} \cdot \hat{x} \tag{B12}$$

and similar expressions for $M_{o,y}$ and A_y.

Chertock [24], a few years ago, noticed an interesting relationship for the added mass M_o of elliptical and rectangular disks in broadside motion,

$$M_o \simeq 1.7 \, \rho \, \frac{A^2}{\ell} \tag{B13}$$

where A is the (one side) area of the disk and ℓ is the disk's perimeter length. The relatonship is exact for elliptical disks of arbitrary length-to-width ratio. It is good to within 8 percent for all rectangular disks -the constant is 1.57 for a long strip and is 1.83 for a square disk. It is also probably a good estimate for the added mass of any arbitrarily, but compactly, shaped disk.

Using the approximation in equation (B13), we can estimate the three propeller masses and rewrite (B10) as

$$\vec{F} \simeq 1.7 \, \rho \, \frac{A_z^2}{\ell} \, \omega g_o \left[\frac{A_x}{A_z} \hat{x} + \frac{A_y}{A_z} \hat{y} + \hat{z} \right] \tag{B14}$$

Then to get the total propeller force, if $\omega = N_B \Omega$ we get the total unsteady thrust

$$(F)_{thrust} \simeq 1.7 \, \rho \, N_B^2 \, \frac{A_z^2}{\ell} \, \Omega \, g_o \tag{B15}$$

and if $\omega = (N_B \pm 1)\Omega$ we get the total side force

$$(F)_{\text{side force}} \simeq .85\rho \; N_B \; (N_B \pm 1) \; g_o \; \Omega \frac{A_z}{\ell} \; \sqrt{A_x^2+A_y^2} \qquad \text{(B16)}$$

We used the approximation (B15) and compared it with the calculation for the two propellers studied in this report. This was done for the rigid propeller operating in the nonuniform inflow and for the propeller vibrating with unit amplitude with prescribed velocity pattern in a uniform inflow. The following table gives the results.

	Rigid (No Circulation)			Vibration (No Circulation)		
Prop	$g_o/\tilde{u}_o$	$(\tilde{K}_T)_R$ Approx	cal	$g_o/\tilde{u}_o$	$(\tilde{K}_T)_v$ approx	cal
3958 (J=.76)	.0436	.0344	.0428	1.28	1.01	1.10
4064 (J=.597)	.0081	.0277	.0584	1.09	3.77	4.08

The approximation agrees with the calculated results to within 25 percent in 3 of the 4 cases. However, it underestimates $(\tilde{K}_T)_R$ for the wide-bladed propeller by 50 percent, probably because the canceling effect of the large blade area results in a rigid body component of the inflow velocity g_o which is "too small" for the approximation in equation (B9) to be valid (evidence also that g_o for the narrow-bladed propeller is 5.5 times that for the wide-bladed one).

REFERENCES

1. Lewis, F. M., "Propeller Vibration," Trans. SNAME, Vol 43, (1935) and Vol. 44 (1936) and "Propeller Vibration Forces," Trans. SNAME Vol. 71 (1963).

2. Sears, W. R., "Some Aspects of Nonstationary Airfoil Theory and Its Practical Application," J. Aeronautical Sciences, Vol. 8, No. 3 (Jan 1941).

3. Hanaoka, T., "Hydrodynamics of an Oscillating Screw Propeller," Fourth Symposium on Naval Hydrodynamics, Office of Naval Research, ACR-92 (1962).

4. Tsakonas, S. et al., "Unsteady Propeller Lifting-Surface Theory," Stevens Institute of Technology, Hoboken, NJ, R-1133 (1966).

5. Brown, N.A., "Periodic Propeller Forces in Nonuniform Flow," MIT, Department of Naval Architecture and Marine Engineering, Report No. 64-7, June 1964.

6. Boswell, R. J., and M. L. Miller, "Unsteady Propeller Loading Measurement, Correlation with Theory, and Parametric Study," Naval Ship Research and Development Center Report 2625 (Oct 1968).

7. von Karman, T. and W. R. Sears, "Airfoil Theory for Nonuniform Motion," J. Aeronautical Sciences, Vol. 5, No. 10 (Aug 1938).

8. Tsushima, H., "Dynamic Response of an Elastic Propeller to a Non-Uniform Inflow," Ph.D. thesis, Dept. of Aerospace Engineering, Pennsylvania State University, University Park, PA (1972).

9. Den Hartog, J. P., Mechanical Vibrations, McGraw-Hill Book Co., Fourth Edition, 1956, p. 272.

10. Chertock, G., "The Flexural Response of a Submerged Solid to a Pulsating Gas Bubble," J. Appl. Physics, Vol. 24 (1953).

11. Lord Rayleigh, The Theory of Sound, Vol. 1, Dover, New York, 1945, p 130.

12. Meirovitch, L., Analytical Methods in Vibrations, The MacMillan Company, New York, 1967, p. 393.

13. Søntvedt, T., "Propeller Blade Stresses, Application of Finite Element Methods, "Computers & Structures, Vol. 4 (1974).

14. Miller, M. L., "Experimental Determination of Unsteady Propeller Forces, " Seventh Symposium on Naval Hydrodynamics, Office of Naval Research (1968).

15. Miller, M. L., "Experimental Determination of Unsteady Forces On Countrarotating Propellers in Uniform Flow," David W. Taylor Naval Ship R&D Center, SPD 65901 (Mar 1976).

16. McCarthy, J. H., "Steady Flow Past Nonuniform Wire Grids," J. of Fluid Mechanics, Vol. 19, Part 4 (1964).

17. Cheng, H. M., "Analysis of Wake Survey of Ship Model Computer Program, AML Problem No. 840-219F, "David Taylor Model Basin Report 1804 (Mar 1964).

18. Sir Horace Lamb, Hydrodynamics, 6th Ed., Dover, 1945, p 123.

19. Levine, P., "Incompressible Potential Flow About Axially Symmetric Bodies in Ducts," J. Aeronautical Sciences, Vol. 25, No. 1, (1958).

20. Noonan, C., et al., "The Barbey Report - An Investigation into Controllable Pitch Propeller Failures from the Standpoint of Full-Scale Underway Propeller Measurements," DTNSRDC Report 77-0080 (Aug 1977).

21. Chertock, G., and J. Brooks, "A Marine Propeller in a Non-Uniform Inflow: Theory," DTNSRDC Report (to-be-published).

22. Brooks, J., "Low Frequency Sound Radiation from Plates," 94th Meeting of Acoustical Society of America, Miami Beach, FL (Dec 1977).

23. Brooks, J., "Added Mass of Marine Propellers in Axial Translation," DTNSRDC Report 76-0079 (Apr 1976).

24. Chertock, G., "Sound Radiated by Low Frequency Vibrations of Slender Bodies," J. Acoustical Society of America, Vol. 57, No. 5 (May 1975).

25. Jeffreys and Jeffreys, Methods of Mathematical Physics, 2nd ed., Cambridge, 1950, p 155.

26. Handbook of Engineering Mechanics, edited by W. Flügge, 1st ed., McGraw-Hill Book Co., 1962, p 6-7.

INITIAL DISTRIBUTION

Copies	
1	ARMY CHIEF OF RES & DEV
1	ARMY ENGR R&D LAB
2	CHONR 1 Code 438 1 Lib
1	NRL
4	ONR BOSTON
4	ONR CHICAGO
4	ONR LONDON, ENGLAND
2	USNA 1 Lib 1 Johnson
1	NAVPGSCOL Lib
1	NROTC & NAVADMINU, MIT
1	NADC
5	NOSC 1 1311 Lib 1 6005 1 13111 Lib 1 2501/Hoyt 1 Nelson
1	NWC
33	NAVSEA 1 SEA 032 1 SEA 0321 1 SEA 03D 1 SEA 052 1 SEA 0521 1 SEA 0522 3 SEA 0524 1 SEA 0525 3 SEA 05D 3 SEA 05H 5 SEA 05R 1 PMS-378
	NAVSEA (Continued) 1 PMS-380 1 PMS-381 1 PMS-383 1 PMS-389 1 PMS-391 1 PMS-392 1 PMS-393 1 PMS-397 1 PMS-399 1 PMS-400 1 Sea Tech Rep Bath, England
1	FAC 032C
1	MILITARY SEALIFT COMMAND (M-4EX)
1	NAVSHIPYD/PTSMH
1	NAVSHIPYD/PHILA
1	NAVSHIPYD/NORVA
1	NAVSHIPYD/CHASN
1	NAVSHIPYD/LBEACH
1	NAVSHIPYD/MARE
1	NAVSHIPYD/PUGET
1	NAVSHIPYD/PEARL
12	DTIC
1	BUSTAND/Klebanoff
2	HQS COGARD
1	US COAST GUARD (G-ENE-4A)
1	LC/SCI & TECH DIV
9	MARAD 1 Div Ship Des 1 Coord Res

Copies	
	MARAD (Continued)
	1 Nachtsheim
	1 Schubert
	1 Falls
	1 Dashnaw
	1 Hammer
	1 Lasky
	1 Siebold
2	MMA
	1 Lib
	1 Maritime Res Cen
2	NASA STIF
	1 Dir Res
1	NSF ENGR DIV LIB
1	DOT LIB
1	U BRIDGEPORT/URAM
2	U CAL BERKELEY/DEPT NAME
	1 Name Lib
	1 Wehausen
1	U CAL SAN DIEGO/ELLIS
2	US SCRIPPS
	1 Pollack
	1 Silverman
1	U MARYLAND/GLEN MARTIN INST
4	CIT
	1 Aero Lib
	1 Acosta
	1 Plesset
	1 Wu
1	CATHOLIC U
1	COLORADO STATE U/Albertson
1	U CONNECTICUT/Scottron
1	CORNELL U/Sears
1	FLORIDA ATLANTIC U OE LIB

Copies	
3	HARVARD U
	1 McKay Lib
	1 Birkoff
	1 Carrier
2	U HAWAII/Bretschneider
1	U ILLINOIS/Robertson
3	U IOWA
	1 Rouse
	1 IHR/Kennedy
	1 IHR/Landweber
2	JOHNS HOPKINS U
	1 Phillips
	1 Inst Coop Res
1	U KANSAS CIV ENGR LIB
1	KANSAS ST U ENGR EXP/Lib
1	LEHIGH U FRITZ ENGR LAB LIB
1	LONG ISLAND U
8	MIT
	1 Ocean Engr/Lib
	2 Ocean Engr/Kerwin
	1 Ocean Engr/Leehey
	1 Ocean Engr/Lyon
	1 Ocean Engr/Newman
	1 Parsons Lab/Ippen
	1 Ocean Engr/Carmichael
1	U MICHIGAN/Nav Arch
3	U MINNESOTA SAFHL
	1 Killen
	1 Song
	1 Wetzel
2	STATE U MARITIME COLL
	S U ARL LIB
	1 Engr Dept
	1 Inst Math Sci
1	NOTRE DAME ENGR LIB

Copies	
5	PENN STATE U ARL 1 Lib 1 Henderson 1 Tsuchima 1 Parkin 1 Thompson
1	PRINCETONU/Mellor
1	RENSSELAER/DEPT MATH
1	STANDFORD U/Ashley
1	STANDFORD RES INST LIB
5	SIT DAVIDSON LAB 1 Lib 1 Breslin 1 Tsakonas 1 Valentine 1 Cox
1	ST JOHNS U
3	SWRI 1 Applied Mech Review 1 Abramson 1 Burnside
1	TEXAS U ARL LIB
1	UTAH STATE U/Jeppson
1	VPI ALDEN HYDRA LAB LIB
2	WEBB INST 1 Ward 1 Hadler
1	ASNE
1	SNAME
1	BOEING ADV MAR SYS DIV
2	BOLT BERANEK AND NEWMAN 1 Brown 1 Jackson
1	BREWER ENGR LAB

Copies	
1	CAMBRIDGE ACOUS/Junger
1	CALSPAN, INC/Ritter
1	EASTERN RES GROUP
1	WHOI OCEAN ENGR DEPT
1	ASME/RES COMM INFO
1	AERO JET-GENERAL/Beckwith
1	ALLIS CHALMERS, YORK, PA
18	ARCTEC, INC/Nelka
1	AVCO LYCOMING
1	BAKER MANUFACTURING
2	BATH IRON WORKS CORP 1 Hansen 1 FFG Project Office
1	BETHLEHEM STEEL SPARROWS
2	BIRD-JOHNSON CO 1 Case 1 Ridley
2	DOUGLAS AIRCRAFT 1 Tech Lib 1 Smith
1	EXXON DES DIV 1 Lib 1 Fitzgerald
1	FRIEDE & GOLDMAN/Michel
1	GEN DYM CONVAIR 1 ASW-Marine Sciences
3	GIBBS & COX 1 Tech Lib 1 Olson 1 CAPT Nelson
1	GRUMMAN AEROSPACE/Carl

Copies	
3	HYDRONAUTICS 1 Etter 1 Scherer 1 Lib
1	INGALLS SHIPBUILDING
1	INST FOR DEFENSE ANAL
1	ITEK VIDYA
1	LIPS, INC.
1	LITTLETON R & ENGR CORP/ Reed
1	LITTON INDUSTRIES
1	LOCKHEED/Waid
2	MARINE VIBRATION ASSOC 1 Bradshaw 1 Vassilopoulis
1	NATIONAL STEEL & SHIPBLDG
1	NEWPORT NEWS SHIPBLDG LIB
1	NIELSEN ENGR/Spangler
1	OCEANICS/Kaplin
1	NAR SPACE/Ujihara
2	ORI, INC 1 Kim 1 Schneider
1	PROPULSION DYNAMICS, INC
1	PROPULSION SYSTEMS, INC
1	K.E. Schoenherr
1	George G. Sharp
1	SPERRY SYS MGMT LIB/ Shapiro

Copies	
3	SUN SHIPBUILDING 1 Pavlik 1 Lib 1 Neilson
1	Robert Taggart
1	TETRA TECH PASADENA/Chapkis
1	TRACOR
1	UA HAMILTON STANDARD/Cornell

CENTER DISTRIBUTION

Copies	Code	Name
1	012.3	Jewell
1	11	Ellsworth
1	1102.1	Nakonechny
1	15	
1	1509	Pollard
1	152	
1	1521	Pien
1	1524	Lin
1	1524	Roddy
1	1524	Reed
1	1532	Dobay
1	154	Cumming
1	1544	Boswell
1	1544	Jessup
1	1544	Lin
1	1552	McCarthy
1	1552	Huang
1	156	Hagen
1	1556	Santore
1	1556	Wisler
1	1556	Jeffers
1	172	Krenzke
1	1720.6	Rockwell

Copies	Code	Name
1	18	
1	184	
1	1843	
1	1844	
1	1844	Henderson
1	1844	Everstine
1	19	
1	1903	
1	194	
1	1942	Armstrong
1	1942	Blake
1	1942	Brown
1	1942	Huang
1	1942	Maga
1	1942	Matthews
1	1942	Paladino
1	196	
1	1962	Branch Head
1	1962	Kilcullen
1	1962	Noonan
1	1962	Perkins
1	1965	Branch Head
15	1965	Brooks
1	1965	Desiderati
1	1965	Liu
1	1965	Solomon
1	2814	Czyryca
1	2823	Macander
10	5211.1	Reports Distribution
1	5221	Lib (C)
1	5222	Lib (A)

DTNSRDC ISSUES THREE TYPES OF REPORTS

1. DTNSRDC REPORTS, A FORMAL SERIES, CONTAIN INFORMATION OF PERMANENT TECHNICAL VALUE. THEY CARRY A CONSECUTIVE NUMERICAL IDENTIFICATION REGARDLESS OF THEIR CLASSIFICATION OR THE ORIGINATING DEPARTMENT.

2. DEPARTMENTAL REPORTS, A SEMIFORMAL SERIES, CONTAIN INFORMATION OF A PRELIMINARY, TEMPORARY, OR PROPRIETARY NATURE OR OF LIMITED INTEREST OR SIGNIFICANCE. THEY CARRY A DEPARTMENTAL ALPHANUMERICAL IDENTIFICATION.

3. TECHNICAL MEMORANDA, AN INFORMAL SERIES, CONTAIN TECHNICAL DOCUMENTATION OF LIMITED USE AND INTEREST. THEY ARE PRIMARILY WORKING PAPERS INTENDED FOR INTERNAL USE. THEY CARRY AN IDENTIFYING NUMBER WHICH INDICATES THEIR TYPE AND THE NUMERICAL CODE OF THE ORIGINATING DEPARTMENT. ANY DISTRIBUTION OUTSIDE DTNSRDC MUST BE APPROVED BY THE HEAD OF THE ORIGINATING DEPARTMENT ON A CASE-BY-CASE BASIS.